Universidad Zaragoza
1542

Trabajo Fin de Grado

"Producción de CH_4 mediante Hidrogenación de CO_2 usando Catalizadores basados en Ni Soportados sobre Carbón Biomórfico"

"Methane Synthesis by CO_2 Hydrogenation Using Ni based Catalysts Supported on Biomorphic Carbon"

Author

Siti Rabiatul Adawiyah Binti Yussop

Director

Dr. Antonio Monzón Bescós

Escuela de Ingeniería y Arquitectura
2018/19

ACKNOWLEDGMENTS

This report means the end of years of work and the end of my degree, however this would not have been possible without the help of many people, so here I would like to thank people who involved in the completion of my project.

First and foremost, I would like to express my deepest gratitude to my research director, Dr. Antonio Monzón Bescós for the inspiration to begin this research. His advices, warm encouragement, attention to all the aspects of works, as well as critique and assessment have led this research to its successful and fruitful results.

My praises and acknowledgement also go to my research supervisor, Ms. Pilar Tarifa for the encouragement to carry on during the hard times. I am immensely grateful for the insights and knowledge she has shared on the subject matter. Thank you both for the technical consultations and productive critics that led to the completion of this project.

Last but not least I would like to express my very profound of gratitude to my parents and my family for providing me with continuous encouragement and unfailing support throughout my years of study and through the process of researching and writing this project. This accomplishment would not have been possible without them.

DECLARATION OF AUTHORSHIP AND ORIGINALITY

TRABAJOS DE FIN DE GRADO / FIN DE MÁSTER

Escuela de Ingeniería y Arquitectura Universidad Zaragoza

DECLARACIÓN DE AUTORÍA Y ORIGINALIDAD

(Este documento debe entregarse en la Secretaría de la EINA, dentro del plazo de depósito del TFG/TFM para su evaluación).

D./Dª. Siti Rabiatul Adawiyah Binti Yussop ,en aplicación de lo dispuesto en el art. 14 (Derechos de autor) del Acuerdo de 11 de septiembre de 2014, del Consejo de Gobierno, por el que se aprueba el Reglamento de los TFG y TFM de la Universidad de Zaragoza, Declaro que el presente Trabajo de Fin de (Grado/Máster) Grado (Título del Trabajo)

Producción de CH4 mediante hidrogenación de CO2 usando catalizadores basados en Ni soportados sobre carbón biomórfico.

es de mi autoría y es original, no habiéndose utilizado fuente sin ser citada debidamente.

Zaragoza, 16 de Septiembre de 2019

Fdo: Siti Rabiatul Adawiyah Binti Yussop

ABSTRACT

CO_2 methanation reaction was investigated over Ni based catalysts modified with the promoters of Mg and/or Ce supported on the biomorphic carbon. These catalysts have been prepared by biomorphic mineralization technique which includes a stage of thermal decomposition in a reductive atmosphere, of cellulose previously impregnated with the metallic (nitrates) precursors. The study on the chemical composition, structure, morphology and texture of the samples have been carried out by different characterization technique such as N_2 physisorption, X-ray diffraction, thermogravimetric analyses by air and transmission electron microscopy. Furthermore, in order to optimize the reaction productivity and selectivity, at high space velocity of 60,000 h^{-1}, the effect of the main operational conditions (reaction temperature and feed composition) has been studied. The catalyst stability test also was performed for 8h on stream at 325 °C. An important fact based on the experimental results obtained was the addition of promoter Ce has increased the BET surface area, microporosity of the catalyst and dispersion of metallic Ni on the surface of carbonaceous support. As a consequence, the performance (the CO_2 conversion, CH_4 selectivity and yield) during the reaction was enhanced. Thus, Ni-MgCe/BC was determined to be the most active for CO_2 methanation at 350 °C with highest CO_2 conversion (up to 68.7%) together with highest values of CH_4 selectivity and yield of 93.5% and 64.2%, respectively.

RESUMEN (SPANISH)

Se ha investigado reacción de metanación de CO_2 sobre catalizadores de Ni modificados Mg y/o Ce, con soportados en carbón biomórfico. Estos catalizadores se han preparado usando una técnica de mineralización biomórfica que incluye una etapa de descomposición térmica en una atmósfera reductora, de celulosa previamente impregnada con los precursores (nitratos) metálicos. El estudio de la composición química, estructura, morfología y textura de las muestras se ha llevado a cabo mediante diferentes técnicas de caracterización como fisisorción de N_2, difracción de rayos X, análisis termogravimétrico con aire y microscopía electrónica de transmisión. Además, para optimizar la productividad y selectividad de la reacción, se ha estudiado el efecto de las principales condiciones de operación (temperatura de la reacción y composición de la alimentación), en condiciones de elevada velocidad espacial (60.000 h^{-1}). Por otro lado, la estabilidad del catalizador se ha medido a lo largo 8h a 325 °C. Un resultado notable obtenido es que la adición del promotor de Ce ha aumentado la superficie BET, la microporosidad del catalizador y la dispersión de Ni sobre la superficie del soporte carbonoso. Como consecuencia, se han mejorado las prestaciones (conversión de CO_2, selectividad a CH_4 y estabilidad) durante la reacción. Se ha obtenido que el catalizador Ni-MgCe/BC es el más activo de CO_2 a 350 °C, alcanzando un 68,7% de conversión de CO_2 y una selectividad de CH_4 del 93,5%, lo que da un rendimiento a CH_4 del 64,2%.

Table of Contents

List of Figures

List of Tables

1 INTRODUCTION

1.1 Renewable power generation

Traditionally fossil fuels have been use as the main resource in the production of energy of developed and developing countries [1]. The generated power and heat is use for transportation, industrial production and private homes in this modern generation [2]. As a result, the global fossil fuel consumption rises tremendously for the past decades. Nearly 15 billion metric tons of fossil fuels are consumed every year. United States, China and India are the largest oil consumer in the world, owing to the fact that about 54% of the world's fossil fuels are consume by these three countries [3].

As the world's fossil fuel consumption rises, so does the risk of global climate change. One of the main factor behind the rise of concentration of CO_2 in the atmosphere and global temperature is the emission of carbon from fossil fuels [4]. According to the U.S. Energy Information Administration (2016), the world energy-related CO_2 emissions are estimated to increase from 32.3 billion metric tons in 2012 to 35.6 billion metric tons in 2020, and reach 43.2 billion metric tons by 2040 [5].

Therefore, ascribable to the negative effect of continued use of fossil fuels on our planet and the depletion of these resources, the utilization of renewable energy sources may necessitate.

The world agreed that a major strategy to mitigate climate change is by using the renewable energy sources. In recent years, the development and utilization of the renewable power generation has been grown rapidly worldwide. Wind power and solar photovoltaics (PV) play an important role in the acceleration of the growth of the renewable power generation as the potential of hydro, biomass or geothermal energy are limited in many countries [6].

According to [7], total renewable energy generation capacity worldwide reached 2,351 GW at the end of 2018, which is around a third of total installed electricity capacity, see Figure 1. The annual increase of 7.9% was bolstered by new addition from solar and wind energy, which accounted for 84% of the growth. In the meantime, non-renewable generation capacity has expanded by about 115 GW per year (on average) since 2000, with no discernible trend upwards or downwards. International Renewable Energy Agency has also reported that, the capacity of non-renewable generation has decreased in Europe, North America and Oceania by about 85 GW since 2010, but has increased in both Asia and the Middle East over the same period.

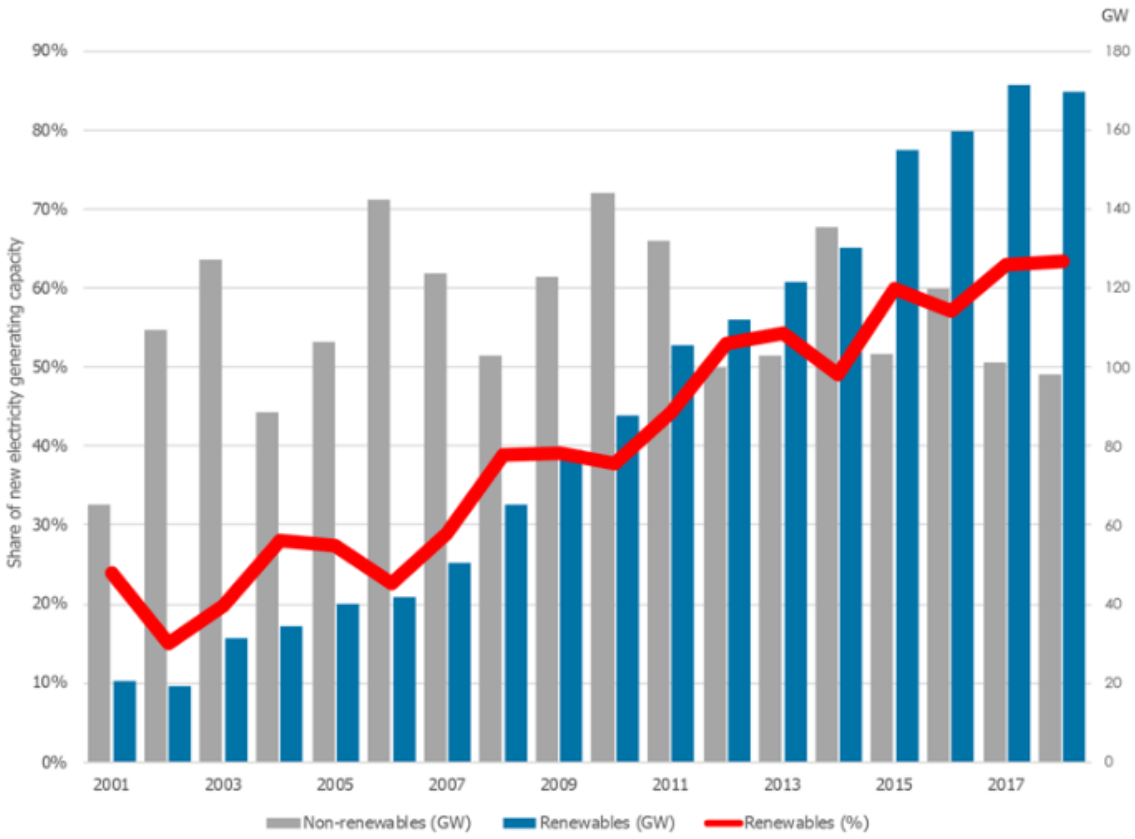

Figure 1. Comparison of the growth in generation capacity of renewable and non-renewable energy. (Source: [7]).

However, a major problem associated to these renewable sources is the mismatch of the load demand and the power supply as the sources influenced by weather conditions, the time of day, season and location. To overcome these difficulties, efficient energy storage technologies are needed [2].

There are various energy storage technologies that come in many different forms. The short-term storage of power is possible only in capacitors and electromagnetic coils. Nevertheless, more economical way to store the power for a long-term is by converting the electrical power to other form of energy with subsequent storage. It seems like the transformation of electrical energy in times of excess power generation by sun or wind into chemical compounds is the most suitable alternative for long-term storage. Therefore, a technically realizable technology that can sort out the aforementioned problem and has been demonstrated in various countries is the power-to-gas technology [8].

1.2 Power-to-gas technology

Power-to-gas technology is an option to convert surplus electricity in form of hydrogen or methane. This technology is considered worthwhile because it is the most cost-efficient long-term storage option for power. In addition, it also supports inter-sectoral decarbonizing and the substitution of fossil energy carries [9].

Methane storage is particularly advantageous due to the large electricity storage at a scale of over 10 GWh and also an existing large-scale infrastructure, which includes pipeline networks, storage facilities and filling stations without additional cost [2,10]. Converting electricity to methane is mostly achieved by combining electrolysis and methanation. Power-to-methane can be divided into three main processes, as shown in the Figure 2.

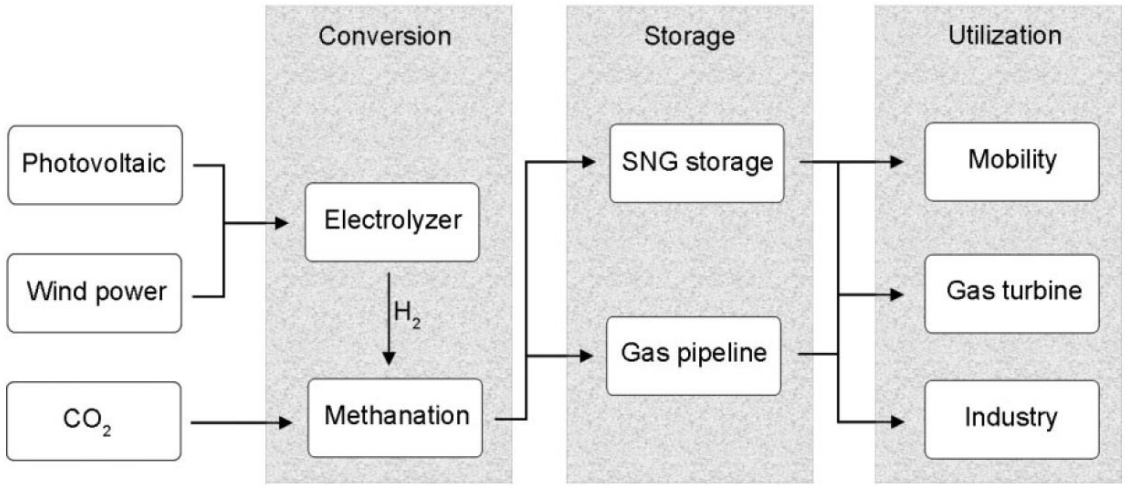

Figure 2. Power-to-methane process flow scheme. (Source: [8]).

The inexhaustible renewable energy resources (mainly wind and solar energy resources) are used to power the electrolyser. This device is used for performing water electrolysis which results in the decomposition of water into hydrogen and oxygen gas [11]. In the second step of the power-to-methane process chain, H_2 reacted with CO_2 to formed CH_4. CO_2 used in this chain process can be attained from biomass plants, power generation plants, industrial processes and ambient air; thus at the same time can contribute to the decrease of greenhouse gas emission [12] The synthetic natural gas (SNG) generated from the methanation process which is similar to natural gas can be injected into the natural gas pipeline without restriction. The process of methanation of CO_2 can be carried out chemically or biologically [13].

The main disadvantage of the power-to-methane concept is the low efficiency owing to the long process chain. Apart from that, the efficiency will further decreases if the heat produced in the process is not used. Nonetheless, power-to-methane promises a long-term storage and is an acceptor of surplus renewable power as it authorizes the possibility to interconnect the electricity market with the heat and fuel markets [8].

1.3 Hydrogenation of CO_2

Catalytic hydrogenation of carbon dioxide to methane, also called the Sabatier reaction, is an important catalytic process of fundamental academic interest with potential commercial application [14,15].

$$CO_2 + 4H_2 \rightarrow CH_4 + 2H_2O \qquad \Delta H_{298K} = -252.9\ kJ\ mol^{-1} \qquad \text{[Eq. 1]}$$

The methanation of CO_2 is exothermic; thermodynamically, the reaction is favoured at low temperature, high pressure and H_2/CO_2 ratios higher than 4. Due to the strong exothermic character of CO_2 methanation, high yield of CH_4 at atmospheric pressure can be achieved at reaction temperature not exceeding 300 °C. This reaction is thermodynamically favourable (ΔG_{298K} = -130.8 kJ/mol); however, the reduction of the fully oxidized CO_2 to methane is an eight-electron process with significant kinetic limitations, which thus required high activity catalysts in order to obtain satisfactory reaction rates and methane selectivity [16].

1.4 Catalysts

In the last decades, various metals have been investigated for the CO_2 methanation. It has been proven that many metals of group VIIIB in the periodic table can catalyse the CO_2 methanation and the metals such as Rh, Ru, Ni and Co were found to be very active for this reaction [17]. However, supported nickel catalysts remain the most widely studied materials due to their low cost and easily availability. Ni catalysts are active only at high temperature, which is within 300 – 450 °C. At the temperature below than 300 °C, interaction between Ni and CO can lead to the formation of mobile nickel subcarbonyls; which is very toxic to the human organism and also at the same time responsible for deactivation of the catalysts [18]. Hence, the performance of Ni catalysts toward CO_2 methanation is depend on various parameters such as the effect of the support, Ni loading, presence of a second metal and the preparation method of the catalyst.

Despite the high activity of Ni catalysts, these kind of catalysts are prone to deactivation by coke deposition and metal sintering at high temperature of reaction [19]. An interesting solution to overcome this problem, that has been widely studied in recent years, is the addition of metal promoters.

Addition of alkaline additives, especially MgO can effectively improve the surface alkalinity by enhancing the capacity of CO_2 adsorption and accelerating the activation of CO_2. In addition, appropriate amount of MgO additive in supported Ni based catalysts was beneficial to the performance of CO_2 methanation due to the increase in Ni species dispersion and effective activation of CO_2 on the surface of MgO [20,21,22]. According to [23], highly dispersed Ni nanoparticles can increase the low temperature activity for CO_2 methanation by facilitating the dissociation of H_2, generating abundant surface-dissociated hydrogen for the removal of surface nickel carbonyls.

Employing suitable metals and/or their oxides as promoters is a common strategy in order to improve the activity and stability of the Ni-based catalysts. Extensive utilization of Ce in the field of catalysis has gained much attention due to its high redox properties [24]. Ceria has good Ce^{4+}/Ce^{3+} reduction-oxidation potential, accompanied by high oxygen storage capacity and the presence of oxygen vacancies [22,25,39]. Recently, studies have found that the addition of CeO_2 containing material to the Ni-based catalyst could effectively promote the adsorption and the activation of CO_2 in the methanation reaction [26]. Furthermore, incorporation of CeO_2 could boost the interaction between support and metal active component and also control the growth of Ni particles, so as a consequence it can greatly enhance the catalytic performance of Ni-based catalysts [27].

1.5 Biomorphic carbonaceous support

The nature of the support has a significant influence on the morphology, dispersion and reducibility of the active phase, and catalytic properties of the catalysts. Over the past several years, attention has been given to carbonaceous materials, a versatile and very environmentally friendly material. Some of this material characteristics such as large specific surface area, high porosity, excellent electron conductivity, presence of a large variety of surface functional groups and relative chemical inertness makes them interesting to be used as catalysts or catalytic supports [28,29]. An advantage of carbonaceous materials is that they can be prepared from biomass wastes, particularly lignocellulosic wastes [30].

The process based in the decomposition of lignocellulosic materials using a reducing or inert atmosphere at high temperature and high heating rates is called biomorphic mineralization. This novel technique is a powerful tool that allows converting structures formed by a biological process, e.g., wood and lignocellulosic biomass to inorganic materials which can be useful in a wide range of applications [31]. Additionally, if the raw material (e.g. cellulose) are previously impregnated with a solution of the metallic precursors, a catalyst is obtained in a single step [32]. Using this technique, the catalyst formed by the metallic nanoparticles highly dispersed on the biomorphic carbonaceous support (BC) can be obtained [33]. This method has proven its versatility whereby different lignocellulose raw materials can be used to synthesize catalyst of large variety of compositions and metal contents [34].

1.6 Objective

The general objective of this final grade thesis has been the study of the catalytic performance of Ni catalysts supported on cellulose derived carbon, modified with the addition of Ce and/or Mg oxides.

In this work, a series of bimetallic catalysts: Ni-Mg and Ni-Ce; and a multi-metallic catalyst: Ni-MgCe supported on cellulose derived carbon, also named as biomorphic carbon, were prepared by the biomorphic mineralization technique, with nominal Ni/Mg or Ce and Ni/Mg/Ce molar ratios of 1/1 and 1/0.5/0.5, respectively. The synthesized catalysts were characterized by nitrogen adsorption isotherm, X-Ray diffraction (XRD), thermogravimetric analyses in air (TGA-Air) and transmission electron microscopy (TEM). CO_2 methanation was investigated in a fixed-bed continuos-flow reactor, at atmospheric pressure, 325 ºC, high space velocity of 60,000 h^{-1} and stoichiometric H_2/CO_2 molar ratio. In order to optimize the results of the CO_2 methanation reaction and the catalysts stability, the effect of the main operational conditions (e.g. reaction temperature and H_2/CO_2 molar ratio) on the catalytic performance of the catalysts were also investigated.

2 EXPERIMENTAL

2.1 Synthesis of catalysts

The Ni-Me/BC catalysts, whereas Me: Mg and/or Ce, were prepared through incipient wetness impregnation of organic material which is cellulose (Sigma-Aldrich) with the aqueous solution of $Ni(NO_3)_2{\cdot}6H_2O$ (Alfa Aesar), $Mg(NO_3)_2{\cdot}6H_2O$ (Sigma-Aldrich) and $Ce(NO_3)_2{\cdot}6H_2O$ (Sigma-Aldrich). Firstly, the cellulose was dried in the stove at 100 °C overnight. Then, an appropriate amounts of the metallic nitrates was dissolved in the distilled water and was added dropwise in the dried cellulose. After impregnation, the Ni-Me/BC was dried at 80 °C for 12h and the impregnated cellulose was thermally decomposed at 600 °C in a reducing atmosphere (50% N_2, 50% H_2) for 3h with the heating rate of 50 °C/min. The catalyst was cooled in a N_2 stream overnight to passivate the catalyst. Lastly, to complete the passivation of catalyst, 50 mL/min of CO_2 and 250 mL/min of N_2 were injected in the furnace at room temperature for 1h. All the catalysts were synthesized with a nominal content of 3.5 %wt of Ni. The detailed calculation for the synthesis of each catalyst can be observed in Annex B.

2.2 Characterization of catalysts

In order to know the physical and chemical characteristics of the catalyst, various characterization techniques were used. Specific areas and porosity of the catalysts were obtained from nitrogen adsorption-desorption isotherms, meanwhile the structural characteristics were analysed by X-ray Diffraction (XRD). The compositions of metal components supported on the biomorphic carbon after the thermal decomposition of cellulose were determined through the thermogravimetric analyses in air (TGA-Air). Lastly, the morphology of synthesized catalyst was investigated using transmission electron microscopy (TEM). The detailed description of each technique can be found in the Annex C.

2.3 Catalytic activity

The methanation of CO_2 was carried out with 0.1 g of catalyst in an 8 mm diameter of fixed-bed continuous-flow reactor. The reactions were performed at atmospheric pressure with a constant flow rate of 700 mL/min, which corresponds to a space velocity of 60,000 h^{-1}. The flow rate of each gas was controlled with a flow rate controller and the reaction temperature was measured by a thermocouple placed in the catalyst bed.

Prior to the reaction, the catalyst was reduced in situ at 500 °C in H_2 (200 mL/min) and N_2 (200 mL/min) for 10 minutes; the heating rate was 10 °C/min. The product gas stream was analysed by parallel gas chromatography (MicroGC 490 of Agilent Technologies). The conversion of CO_2 and H_2, selectivity of CH_4 and carbon yield to CH_4 were calculated using the following equations:

$$CO_2\ conversion\ (\%) = \frac{([CO_2]_{in} - [CO_2]_{out})}{[CO_2]_{in}} \times 100 \quad \text{[Eq. 2]}$$

$$H_2\ conversion\ (\%) = \frac{([H_2]_{in} - [H_2]_{out})}{[H_2]_{in}} \times 100 \quad \text{[Eq. 3]}$$

$$CH_4\ selectivity\ (\%) = \frac{[CH_4]_{out}}{([CO_2]_{in} - [CO_2]_{out})} \times 100 \quad \text{[Eq. 4]}$$

$$Carbon\ yield\ to\ CH_4\ (\%) = \frac{[CH_4]_{out}}{[CO_2]_{in}} \times 100 \quad \text{[Eq. 5]}$$

2.3.1 Conditions of operation

The methanation of CO_2 was performed under the same operational conditions for each catalyst to study their catalytic activity. To investigate the effect of variation of reaction temperature on the catalytic activity of the catalysts, the experiment was carried out within a range of temperature 150 °C to 500 °C with the H_2/CO_2 stoichiometric molar ratio. To study the catalyst stability, the test was carried out at 325 °C with the H_2/CO_2 molar ratio of 4 for 8h. To study the effect of variation feed composition on the catalytic activity of the most active catalyst which is Ni-MgCe/BC, the experiment was carried out with the operational conditions as shown in the Table 1 and Table 2.

Table 1. Variation of the concentration of CO_2 in the feed stream.

Exp.	Temperature (°C)	Molar ratio H_2/CO_2	H_{2in} (mL/min)	CO_{2in} (mL/min)	N_{2in} (mL/min)
1	325	2 – 5.5	400	200 – 73	100 – 227
2	325	2 – 5.5	350	175 – 64	175 – 286
3	325	2 – 5.5	300	150 – 54	250 – 346
4	325	2 – 5.5	250	125 – 45	325 – 405
5	300	2 – 5.5	400	200 – 73	100 – 227
6	350	2 – 5.5	400	200 - 73	100 – 227

Table 2. Variation of the concentration of H_2 in the feed stream.

Exp.	Temperature (°C)	Molar ratio H_2/CO_2	H_{2in} (mL/min)	CO_{2in} (mL/min)	N_{2in} (mL/min)
7	325	2 – 5.5	200 – 550	100	50 – 400
8	325	2 – 5.5	170 – 468	85	148 – 445
9	325	2 – 5.5	144 – 396	72	232 – 484
10	300	2 – 5.5	200 – 550	100	50 – 400
11	350	2 – 5.5	200 - 550	100	50 - 400

3 RESULTS AND DISCUSSION

In this section, the experimental results obtained from the characterization of the catalysts and the study on methanation of CO_2 using 3 different Ni based catalysts supported on biomorphic carbon will be discussed. The objective is to determine the influence of various process variables such as the composition of the catalysts, temperature of the reaction and the composition of the feed stream on the catalytic activity, stability and selectivity of the desired methane.

3.1 Characterization of catalysts

3.1.1 N_2 adsorption-desorption isotherm

The textural effect on the addition of promoters Mg and Ce on the carbonaceous support were studied by N_2 adsorption. Figure 3 shows the N_2 adsorption/desorption isotherm of the Ni-Mg/BC, Ni-Ce/BC and Ni-MgCe/BC synthesized catalysts with a nominal content of 3.5 wt% of Ni with respect to the initial amount of cellulose.

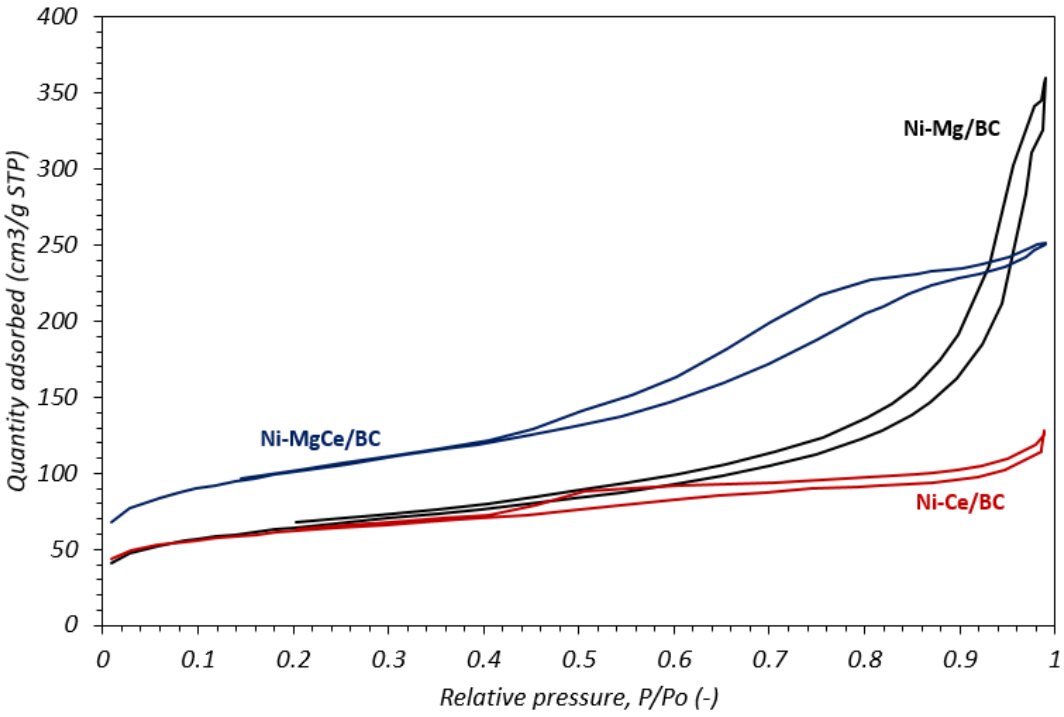

Figure 3. N_2 adsorption/desorption isotherm obtained for Ni-Me/BC catalysts.

According to the IUPAC classification, the isotherm corresponds to the II-type with a hysteresis loop of type H3 or H4. These II-type of isotherm is the result of unrestricted monolayer-multilayer adsorption. At the low relative pressure region, the micropore filling which regarded as a primary physisorption process takes place. In this region, more gradual curvature was seen which indicates there was a significant amount of overlap of monolayer coverage and the onset of multilayer adsorption [35,36].

Meanwhile, the filling of wide mesopores starts to occur at high relative pressure [37]. Behaviour of physisorption in mesopores is distinct from the adsorption phenomena occurring in micropores. The monolayer adsorption and multilayer adsorption that can lead to the pore condensation most probably can occur in mesopores. The thickness of the adsorbed multilayer in mesopores generally increases with relative pressure [36]. In the case of Ni-Mg/BC, the presence of thick adsorbed multilayer was spotted and after the addition of Ce, the catalyst's textural was modified. Formation of less thick adsorbed multilayer can be seen clearly in the Ni-MgCe/BC catalyst. For the case of Ni-Ce/BC catalyst, the thickness of the adsorbed multilayer barely increases with the relative pressure.

The H3- and H4-types of hysteresis loops are typical of disordered materials with distribution of pores size and ill-defined shapes as well as containing aggregates of plate-like particles [35,36]. The more pronounced uptake at low P/P_o as occurred in the isotherm of Ni-Ce/BC catalyst associated with the filling of micropores. The formation of broader hysteresis loops at higher relative pressure of the synthesized catalysts indicates the presence of bigger pores.

In addition, Table 3 shows the values of the BET surface area, total pore volume, micropore volume and average pore diameter of the synthesized catalysts. The BET surface area of Ni-Mg/BC was found to be 228 m^2/g with 21% of micropore volume. On the other hand, the BET surface area for Ni-MgCe/BC and Ni-Ce/BC catalysts were 359 m^2/g and 357 m^2/g with the percentage micropore volume of 46% and 57%, respectively.

Table 3. The textural properties of Ni-Me/BC catalysts.

Catalysts	BET surface area (m^2/g)	Pore volume (cm^3/g)	Micropore volume (cm^3/g)	Average pore diameter (nm)
Ni-Mg/BC	228	0.556	0.116	28.3
Ni-MgCe/BC	359	0.389	0.177	3.3
Ni-Ce/BC	357	0.179	0.102	1.4

After the incorporation of Ce, the BET surface area were enhanced. This effect can be attributed to the formation of small CeO_2 crystallites, which introduce some geometric effect that cause the development of new mesoporous structure. The pore size distribution for Ni-Mg/BC and Ni-MgCe/BC catalysts indicated a mesoporous character (2 – 50 nm, IUPAC classification) meanwhile the Ni-Ce/BC catalyst shows the character of microporous (< 2 nm). Clearly, the addition of the promoter Ce creates more small pores and increase the microporosity of the catalysts. However, the other consequence of the promoter Ce addition leads to the reduction of pore volume. The differences among the pore volume and surface area behaviour were attributed to the fact that metal particles contributed with some additional surface area but not with additional pore volume [40].

According to [38], the larger number of micropores presented on the surface of catalyst means a larger number of CO_2 molecules can be trapped and it has to show the better catalytic activity for CO_2 methanation. Interestingly, the micropore volume and the BET surface area in Ni-MgCe/BC catalyst was found to be the highest, thus this catalyst seems to be the most promising catalyst for the catalytic performance for CO_2 methanation.

3.1.2 X-ray diffraction (XRD)

The XRD patterns of the different catalysts samples of Ni-Mg/BC, Ni-MgCe/BC and Ni-Ce/BC were shown in the Figure 4. The XRD study on the catalyst samples was carried out to determine the crystalline size and to identify the phase of crystalline material presence on the surface layer of catalysts.

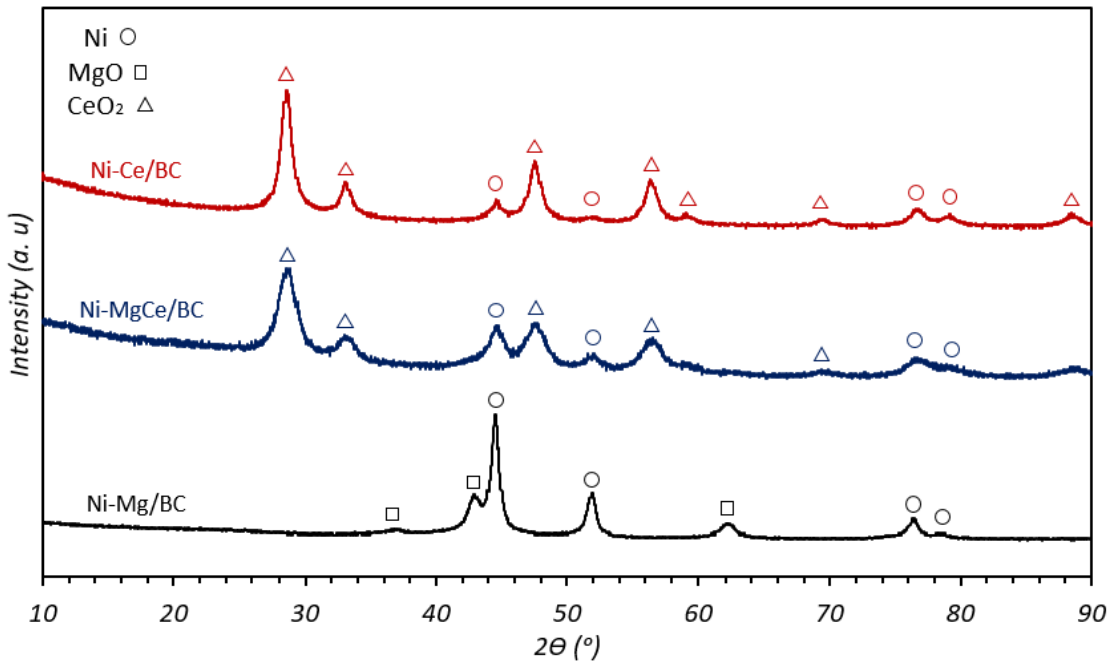

Figure 4. XRD patterns for Ni-Mg/BC, Ni-MgCe/BC and Ni-Ce/BC catalysts.

In all the cases studied, the peaks obtained correspond only to metallic Ni. There were no peaks associated to NiO. The sharp peak of Ni was detected at 2-Theta (2θ) around 44.5° in the Ni-Mg/BC catalyst with average crystallite size of approximately 17 nm. In the Ni-MgCe/BC and Ni-Ce/BC catalysts, the identified peak of Ni was found to be less intense, which indicates less content of Ni presence after the decomposition step during the preparation. The average crystallite size of Ni particles in Ni-MgCe/BC and Ni-Ce/BC catalysts were 8 nm and 10 nm, respectively. As expected, the addition of promoter Ce decreased the average crystallite size of Ni particles.

The XRD patterns show the typical reflection of CeO_2 at 2-Theta (2θ) values of 28.5°, 33.1°, 47.5°, 56.5° and 69.3° in both Ni-MgCe/BC and Ni-Ce/BC catalysts. More intense peak of CeO_2 was seen in Ni-Ce/BC catalyst with average crystallite size of 9 nm while in Ni-MgCe/BC catalyst is equal to 6 nm.

In addition, three diffraction peaks related to MgO were observed in Ni-Mg/BC catalyst with average crystallite size of 8 nm while in Ni-MgCe/BC catalyst no crystal peaks were detected. The particle size of MgO in Ni-MgCe/BC catalyst cannot be estimated, due to the low concentration of these metal oxide that highly dispersed on the catalyst surface and is not detectable by XRD analysis.

Characterization of spent samples was performed to elucidate the reasons why the activity of Ni based catalysts changed during the stability test. The used samples were removed from the experimental setup for characterization by XRD and TEM (see section 3.1.4). The comparison of the XRD patterns of used Ni-Mg/BC, Ni-MgCe/BC and Ni-Ce/BC catalysts with the fresh samples can be observed in the Figure 5.

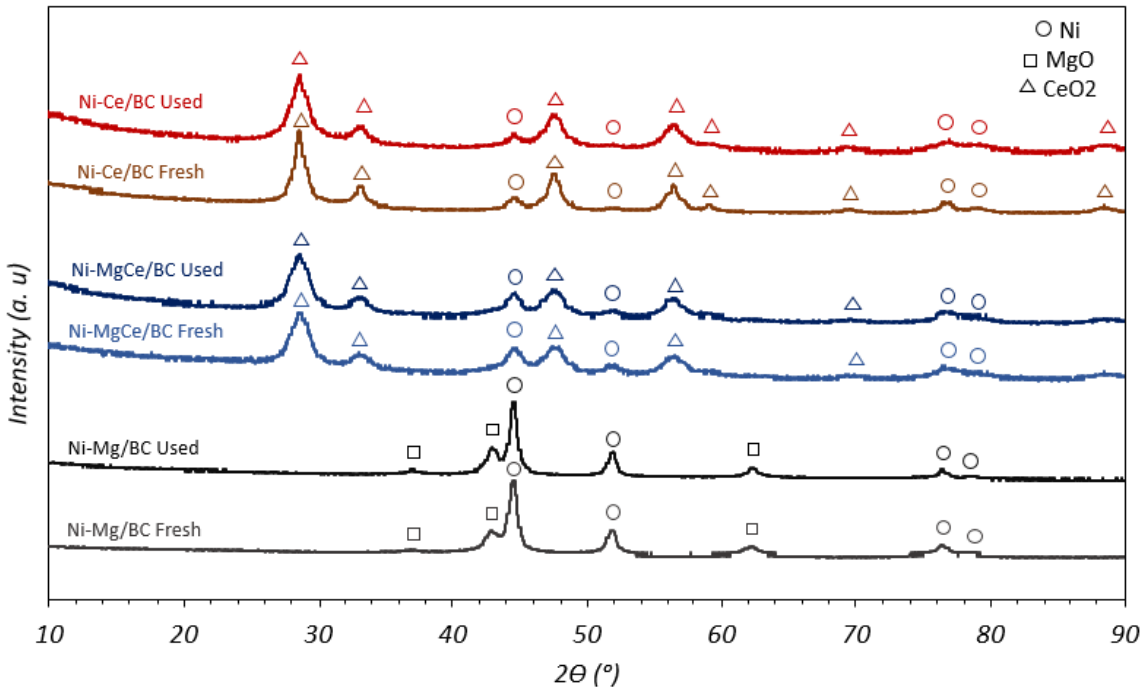

Figure 5. Comparison of XRD pattern for the fresh Ni-Me/BC catalysts and used catalysts in methanation reaction.

Surprisingly, XRD patterns for all synthesized catalysts does not detect the presence of NiO particles, which means no reduction of Ni metal occurs after the methanation reaction. Besides, no noteworthy changes observed in the peaks of each phase of the catalysts after the reaction of CO_2 with hydrogen at 325 °C for 8h. In spite of that, there was a slight changed in the average crystallite size of the particles calculated using Scherrer equation [39] as reported in the Table 4.

Table 4. Estimated crystallite size calculated using Scherrer equation of Ni, MgO and CeO_2 before and after reaction.

	Fresh Catalyst			Used Catalyst		
Catalyst/ dp (nm)	**Ni**	**MgO**	**CeO_2**	**Ni**	**MgO**	**CeO_2**
Ni-Mg/BC	17	9	-	19	11	-
Ni-MgCe/BC	8	-	6	9	-	6
Ni-Ce/BC	10	-	9	12	-	6

The results of Ni, MgO and CeO_2 crystal sizes after the reaction, measured by the Scherrer equation, suggested that the increased in the crystallite sizes were due to the sintering of particles [8]. The presence of both promoters Mg and Ce in the Ni-MgCe/BC catalyst reduced the Ni sintering and probably can lengthen the catalyst lifetime. It is also found that no sintering of CeO_2 particles has occurred. In the case of Ni-Ce/BC catalyst, sintering of Ni particles was occurred and the crystallite size was increased from 10 nm to 12 nm. In contrast, the crystallite size of CeO_2 has decreased from 9 nm to 6 nm.

3.1.3 Thermogravimetric analyses in air (TGA-Air)

Thermogravimetric analyses in air (TGA-Air) is carried out to determine the quantitative composition of metals presence in the supported biomorphic carbon catalysts. Figure 6 shows the TGA-Air curves for the synthesized Ni-Me/BC catalysts.

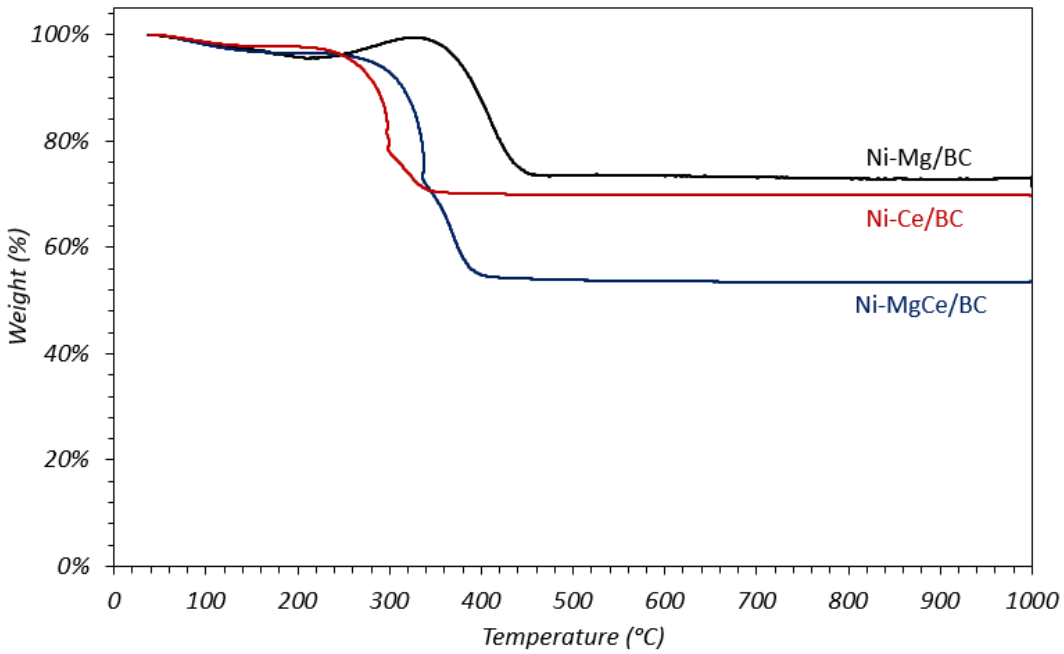

Figure 6. TGA-Air analyses for Ni-Me/BC catalysts.

According to [41,42], the combustion of biomorphic carbon occurs between the interval of temperature 470 °C and 650 °C. As shown in the Figure 6, TGA-Air curve for Ni-Mg/BC catalyst shows a weight loss starting from approximately 345 °C up to 460 °C. Meanwhile, for the Ni-MgCe/BC and Ni-Ce/BC catalysts the combustion peaks appear at temperature of 250 °C and 230 °C respectively. The combustion of biomorphic carbon in these three synthesized catalysts occurred at lower temperature than mentioned in the [41,42] due to the catalytic effect of Ni during the combustion [43]. In addition, between the temperature of 250 °C and 345 °C, noticeable weight increase in the TGA curve of Ni-Mg/BC was spotted. This occurrence is probably attributed to the oxidation of Ni to NiO. No significant weight increase detected in Ni-MgCe/BC and Ni-Ce/BC catalysts due to the less metallic Ni presence in the supported biomorphic carbon compared to in Ni-Mg/BC catalysts as shown in the Table 5.

Table 5. Percentage of Ni, Mg, Ce and BC present in the Ni-Me/BC catalysts.

Catalyst / Compositions (%)	**Ni**	**Mg**	**Ce**	**BC**
Ni-Mg/BC	42%	18%	-	40%
Ni-MgCe/BC	20%	4%	24%	52%
Ni-Ce/BC	19%	-	46%	35%

According to XRD results, after the decomposition step during the preparation, Ni, MgO and CeO_2 particles were found in the corresponding synthesized catalysts. After the oxidation in TGA-Air analyses, the remaining materials found in Ni-Mg/BC were ashes, NiO and MgO; ashes, NiO, MgO and CeO_2 for the case of Ni-MgCe/BC; and ashes, NiO and CeO_2 for the case of Ni-Ce/BC. As expected, the weight percentages of Ni, Mg and Ce were increased in the final catalysts compared to the initial amount on the raw cellulose due to the loss of carbonaceous material in the thermal decomposition stage during the synthesized of catalyst. Indeed, the thermal decomposition is the crucial factor for controlling the final content and dispersion of the metal(s) on the surface of catalyst [44].

3.1.4 Transmission electron microscopy (TEM)

The morphology of the synthesized catalysts was investigated using transmission electron microscopy (TEM). Figure 7 shows the TEM images of the fresh and used Ni-Me/BC catalysts. In addition, the distribution of the metal particles deposited on the carbonaceous support and the average diameter of the particles can be observed in the Figure 8 (Ni-Mg/BC catalyst), Figure 9 (Ni-MgCe/BC) and Figure 10 (Ni-Ce/BC).

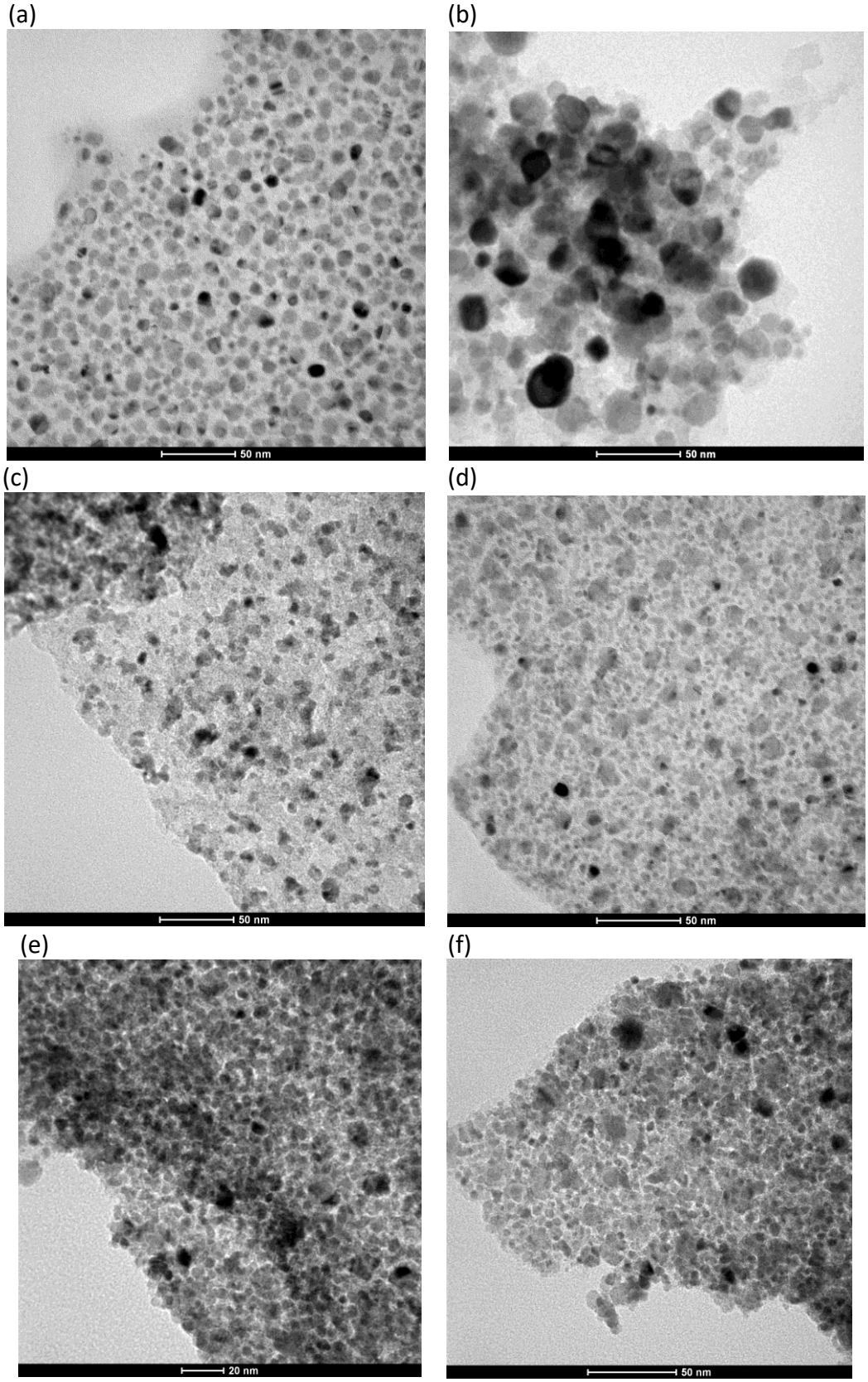

Figure 7. Images obtained by TEM of the Ni-Mg/BC catalyst (a) fresh (b) used, Ni-MgCe/BC catalyst (c) fresh (d) used and Ni-Ce/BC catalyst (e) fresh (f) used.

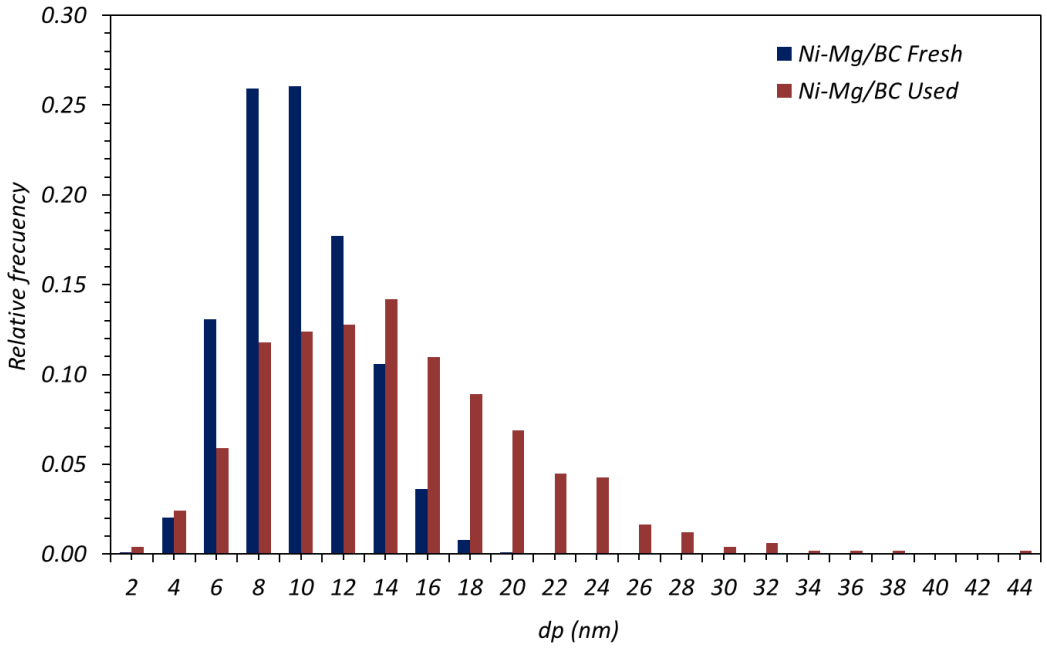

Figure 8. Histogram of the particle size distribution for fresh and used Ni-Mg/BC catalyst.

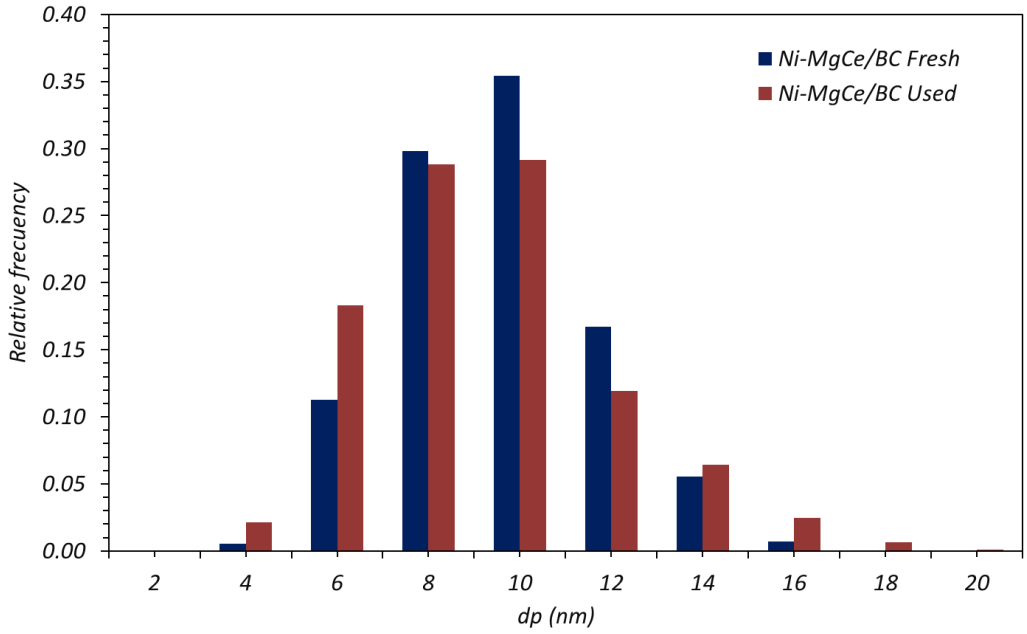

Figure 9. Histogram of the particle size distribution for fresh and used Ni-MgCe/BC catalyst.

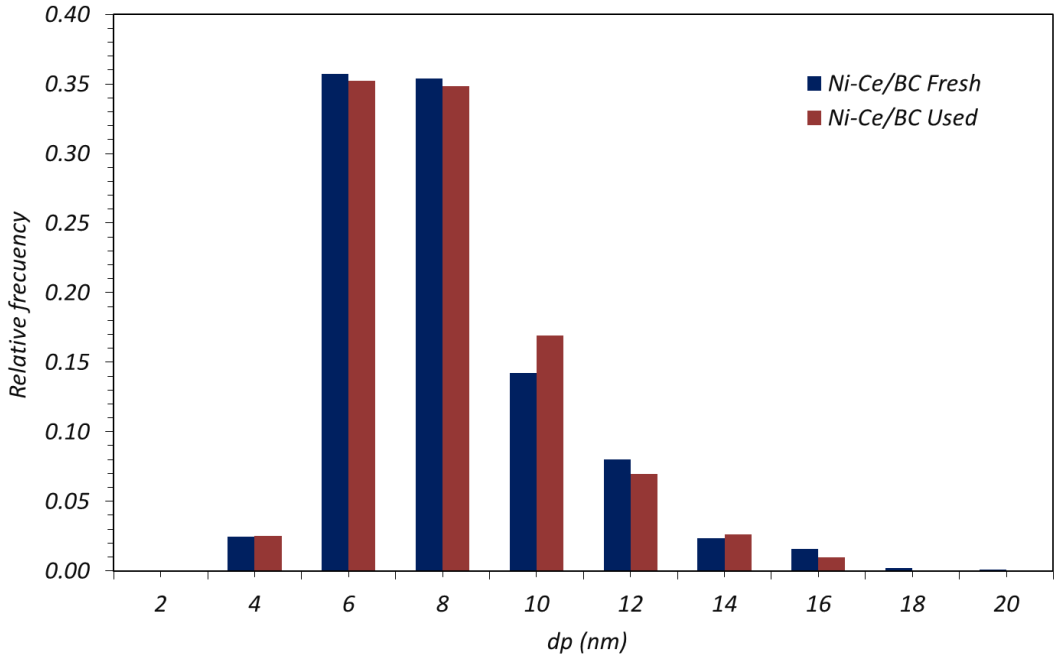

Figure 10. Histogram of the particle size distribution for fresh and used Ni-Ce/BC catalyst.

In the case of fresh Ni-Mg/BC (Figure 7a), Ni-MgCe/BC (Figure 7c) and Ni-Ce/BC (Figure 7e), after the thermal decomposition at 600 °C, all three catalysts seem to have a high dispersion of metals particles on the carbonaceous support, presenting narrow distributions of 10.7 ± 2.8 nm, 9.6 ± 2.1 nm and 8.9 ± 2.3 nm, respectively.

After the reaction of CO_2 with hydrogen for 8h, the particles were remained well dispersed although larger particles were observed. The image of TEM for the Ni-Mg/BC catalyst after the reaction (Figure 7b) shows the aggregation of particles has occurred. In this case, small particles (ca. 4 nm) and also large particles larger than 30 nm were found, see Figure 8. The average particle size is 18.8 ± 6.1 nm.

In the Figure 9, for the case of Ni-MgCe/BC catalyst, a large fraction of Ni-containing nanoparticles before the reaction (ca. 10 nm) has decreased to approximately to 6 nm and some of them increased to 16 nm. However, the average particle size maintained with narrow distribution of 9.9 ± 2.7 nm. As for Ni-Ce/BC catalyst, no significant changes were observed and also even after the reaction, the metal particles remain well dispersed with the average particle size of 8.6 ± 2.2 nm.

The average particle size for the synthesized catalysts determined using TEM technique was shown in the Table 6. Likewise, the estimated size of the particles calculated using the Scherrer equation in XRD method (Table 4) seem to be in a reasonable agreement with the TEMs' results. Hence, from the results obtained for the characterization by XRD and TEM before and after the methanation reaction, the thermal stability of the catalysts decreases in the following order: Ni-MgCe/BC > Ni-Ce/BC > Ni-Mg/BC [45].

Table 6. Average particle size calculated using TEM technique for the fresh and used Ni-Me/BC catalysts.

Catalysts/average dp (nm)	Fresh	Used
Ni-Mg/BC	10.7 ± 2.8	18.8 ± 6.1
Ni-MgCe/BC	9.6 ± 2.1	9.9 ± 2.7
Ni-Ce/BC	8.9 ± 2.3	8.6 ± 2.2

3.2 Study on the catalytic activity

To study the catalytic activity of each catalyst, the analysis on the effect of reaction temperature has been carried out. After the in situ reduction of catalyst for 10 minutes, 700 mL/min of mixed gases with the relation of H_2:CO_2 = 4:1 and the balance N_2 were fed in the reactor for the catalytic evaluation. The steady-state activity data at different temperature were measured for 30 minutes of reaction at each temperature, starting from the highest temperature which is 500 °C and decreased until no more conversion of CO_2 detected.

3.2.1 The effect of reaction temperature on the catalytic performance of synthesized Ni-Mg/BC catalyst

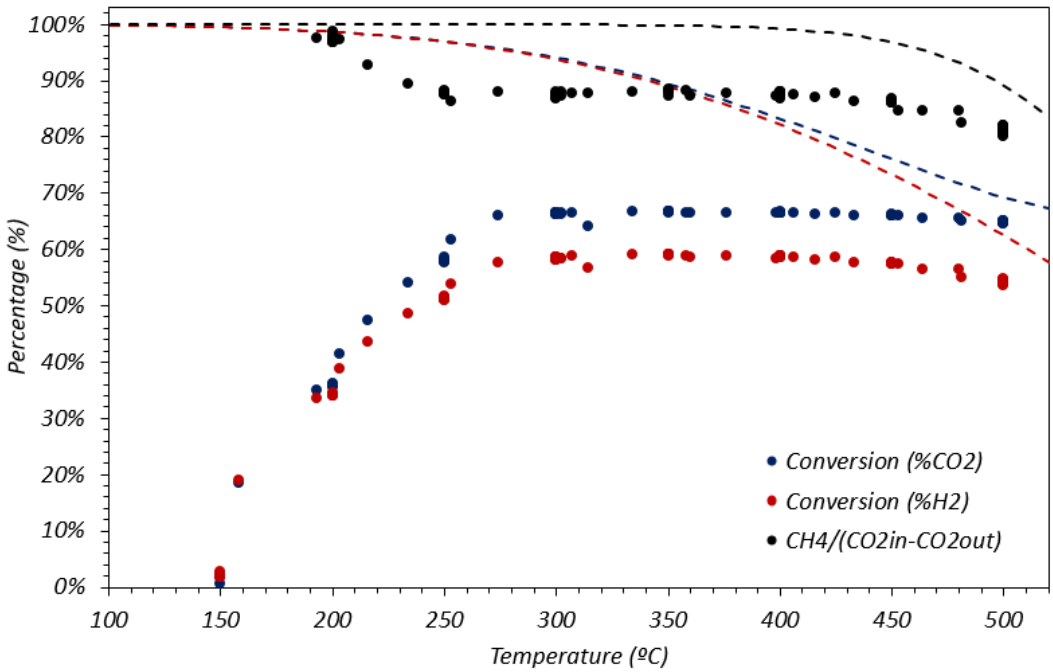

Figure 11. Catalytic performance vs. temperature of Ni-Mg/BC catalyst for CO_2 methanation. Dashed lines represent equilibrium values.

Figure 11 shows the catalytic performance evaluated over Ni-Mg/BC catalyst as a function of temperature of reaction; the equilibrium values are also reported for comparison. From 150 °C to 350 °C both conversion of CO_2 and H_2 rises with temperature and then slightly diminished. Maximum conversion of CO_2 and H_2, as well as selectivity to CH_4 was detected at the temperature of 350 °C. The high value of CH_4 selectivity achieved below the temperature of 250 °C in fact was the consequences of the small value of denominator in the [Eq. 4] which indicates less amount of CO_2 reacted with H_2 to form desired CH_4. The deactivation of this catalyst was occurred at 150 °C.

3.2.2 The effect of reaction temperature on the catalytic performance of synthesized Ni-MgCe/BC catalyst

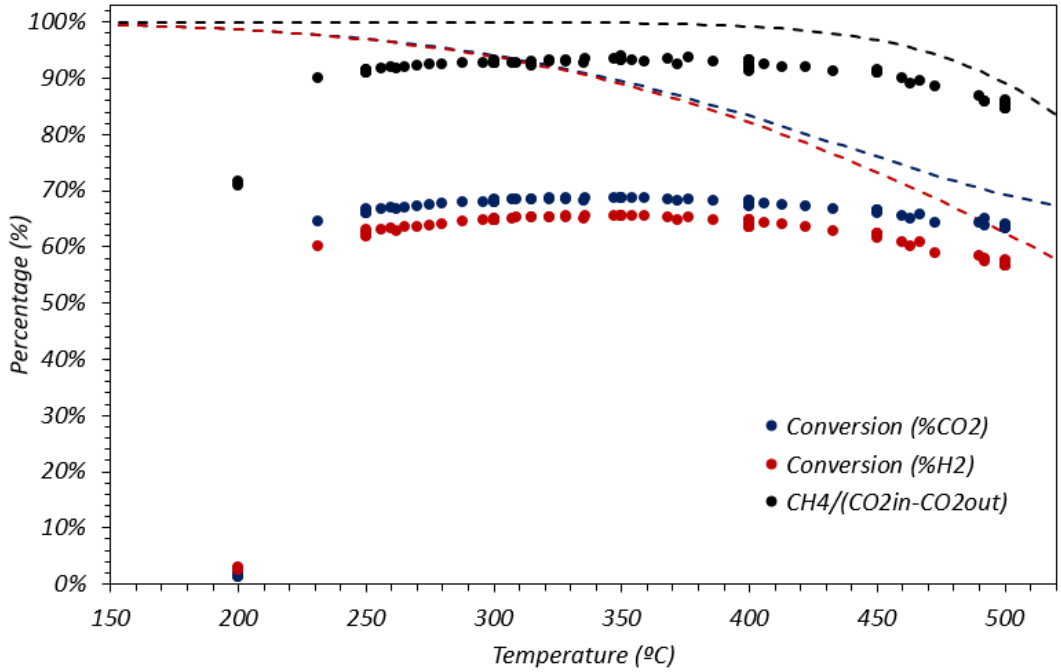

Figure 12. Catalytic performance vs. temperature of Ni-MgCe/BC catalyst for CO_2 methanation. Dashed lines represent equilibrium values.

Figure 12 shows the catalytic performance evaluated over Ni-MgCe/BC catalyst as a function of temperature of reaction for CO_2 methanation. The selectivity of desired CH_4, also the conversion of CO_2 and H_2 increases from 200 °C to 350 °C and then gradually decreases above this temperature in accordance to the thermodynamic limits. Deactivation of both Ni-Mg/BC and Ni-Ce/BC catalysts were occurred at 150 °C, but in contrast this catalyst was found to be inactive at the temperature of 200 °C.

3.2.3 The effect of reaction temperature on the catalytic performance of synthesized Ni-Ce/BC catalyst

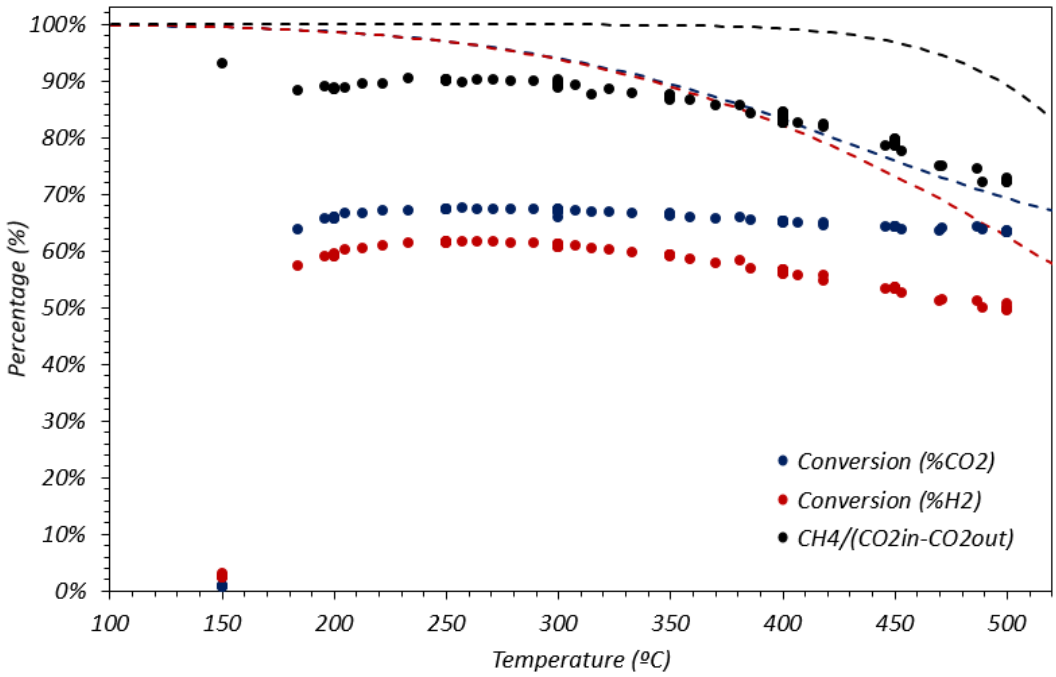

Figure 13. Catalytic performance vs. temperature of Ni-Ce/BC catalyst for CO_2 methanation. Dashed lines represent equilibrium values.

The catalytic performance evaluated over Ni-Ce/BC catalyst at different temperature of reaction was illustrated in the Figure 13. From 150 °C to 250 °C the conversion of CO_2 and H_2 increases and gradually diminished after this temperature. The maximum conversion of CO_2 and H_2 as well as the CH_4 selectivity was achieved at 250 °C which was distinct with what has occurred in Ni-Mg/BC and Ni-MgCe/BC catalysts. Apparently, according to [46], the addition of promoter Ce on the Ni based catalyst enhanced the catalytic performance of the catalyst by showing high conversion of CO_2 at lower temperature. Hence, it is noteworthy that the high loading of Ce (46 wt%) in this catalyst improve the nickel dispersion on the surface of carbonaceous support and as a consequence improve the catalytic performance at lower temperature.

3.2.4 Comparison of catalytic performance of the synthesized Ni-Me/BC catalysts

Figure 14 shows comparison of the conversion of CO_2 and H_2, CH_4 selectivity and yield for the synthesized catalysts as a function of reaction temperature in order to determine which catalyst shows a better performance for the CO_2 methanation reaction.

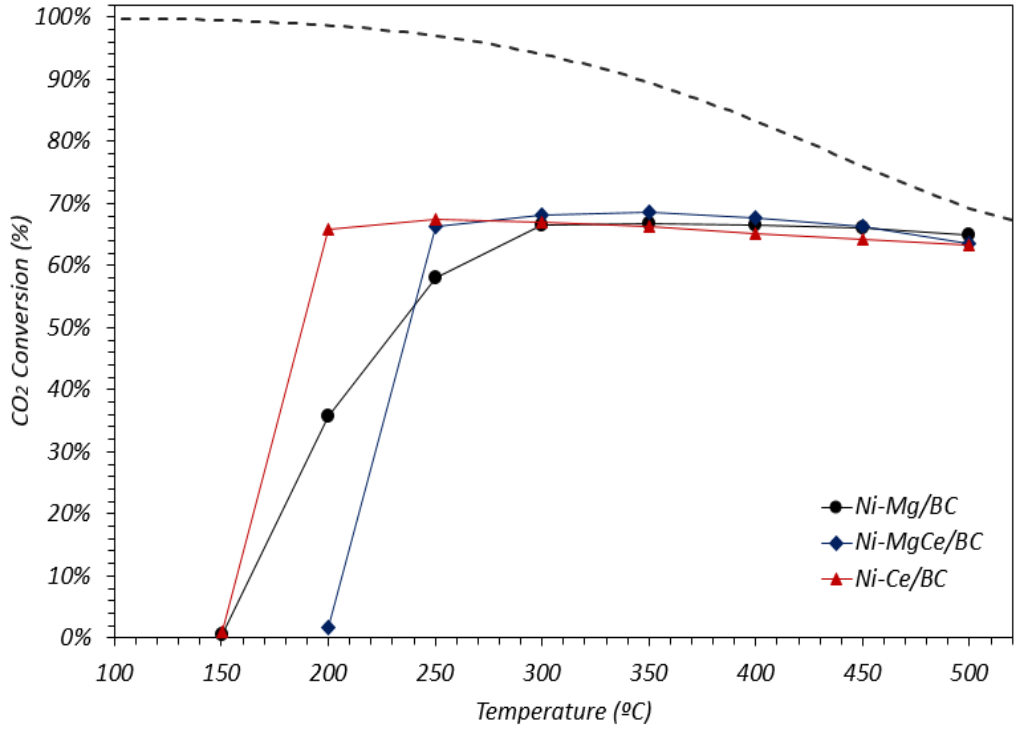
100%
90%
80%
70%
60%
50%
40%
30%
20%
10%
0%
CO2 Conversion (%)
100
150
200
250
300
350
400
450
500
Temperature (ºC)
Ni-Mg/BC
Ni-MgCe/BC
Ni-Ce/BC

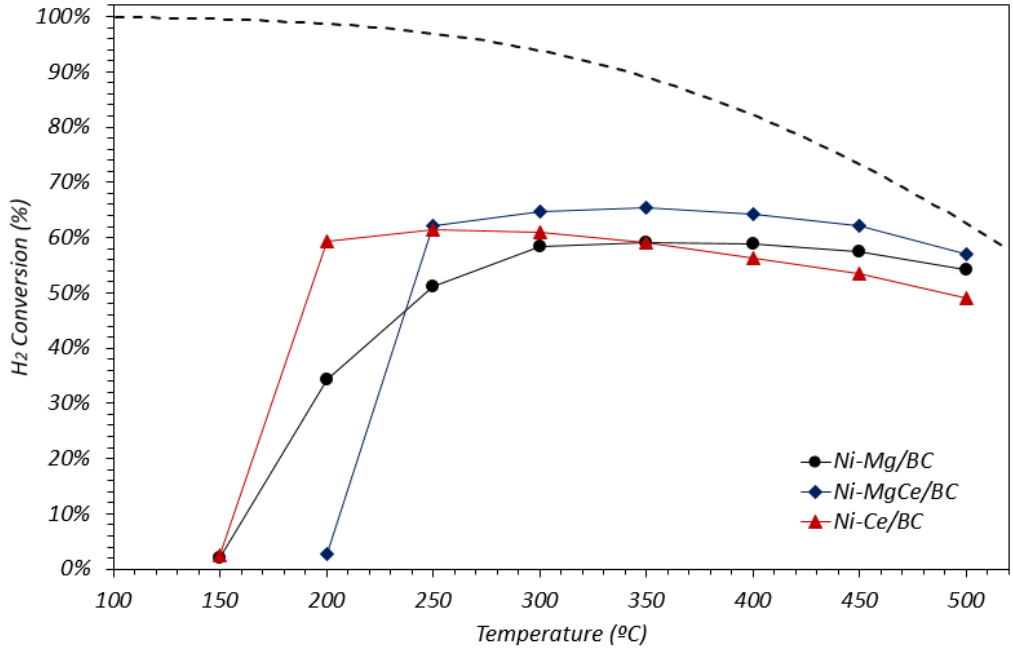
100%
90%
80%
70%
60%
50%
40%
30%
20%
10%
0%
H2 Conversion (%)
100
150
200
250
300
350
400
450
500
Temperature (ºC)
Ni-Mg/BC
Ni-MgCe/BC
Ni-Ce/BC

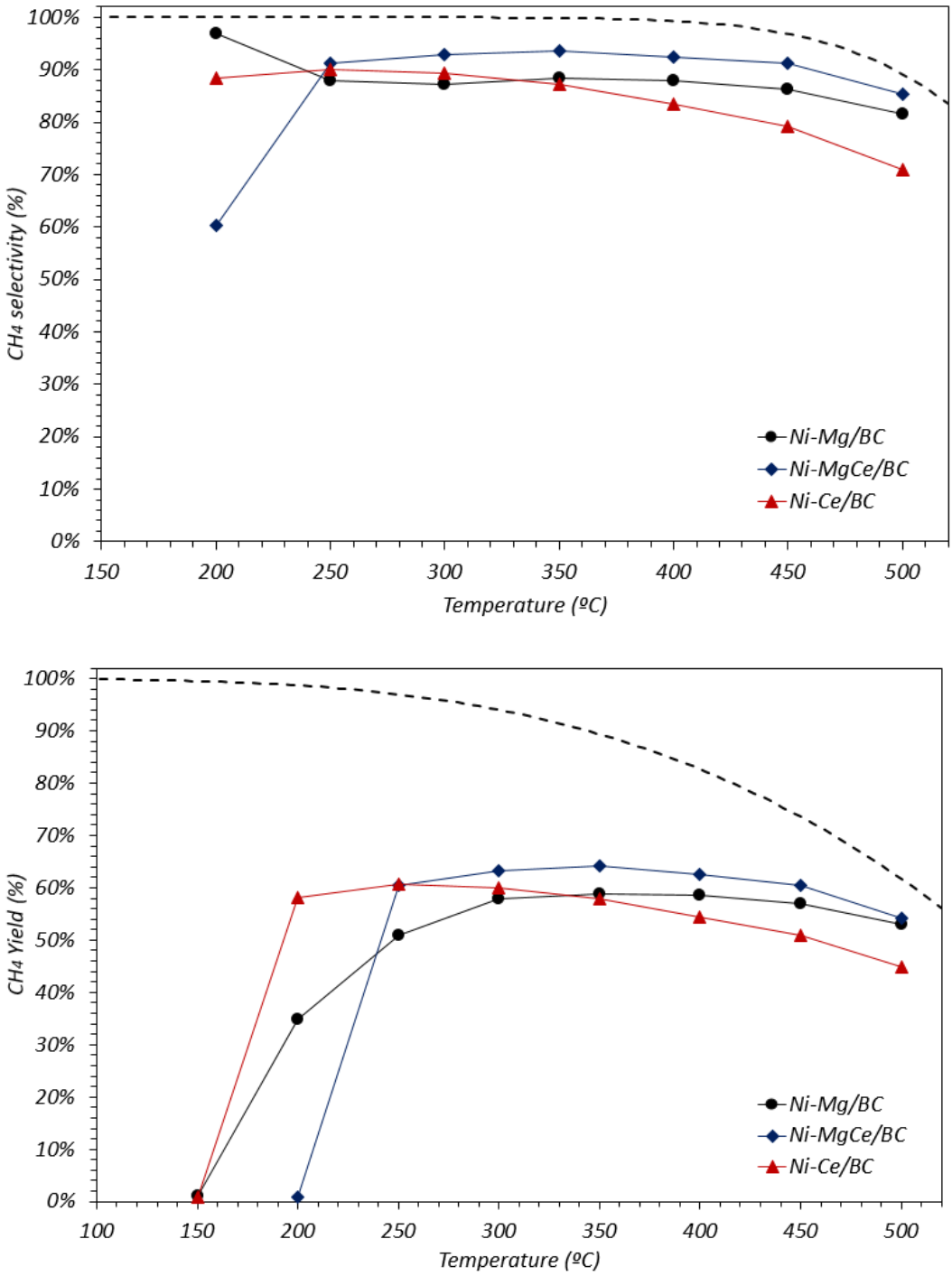

Figure 14. Comparison of catalytic performance for CO_2 methanation of synthesized Ni-Me/BC catalysts. Dashed lines represent equilibrium values.

The conversion of CO_2 achieved by these three catalysts within temperature 300 °C to 500 °C shows no huge difference. Nevertheless, the highest CO_2 conversion (68.7%) obtained was by Ni-MgCe/BC catalyst at 350 °C. As can be seen in the figure, the selectivity of desired CH_4 attained by Ni-MgCe/BC was very close to the equilibrium values compared to the others with the maximum value of 93.5% at 350 °C. In addition, the maximum CH_4 yield (64.2%) achieved also by Ni-MgCe/BC at the temperature of 350

ºC. The overall catalytic performance for these three catalyst followed the general ordering Ni-MgCe/BC > Ni-Ce/BC > Ni-Mg/BC, which can be seen clearly in the Figure 15. As expected, the Ni-MgCe/BC catalyst exhibit the highest catalytic activity owing to the largest surface area of BET and high micropore volume as characterized by N_2 adsorption-desorption isotherm technique.

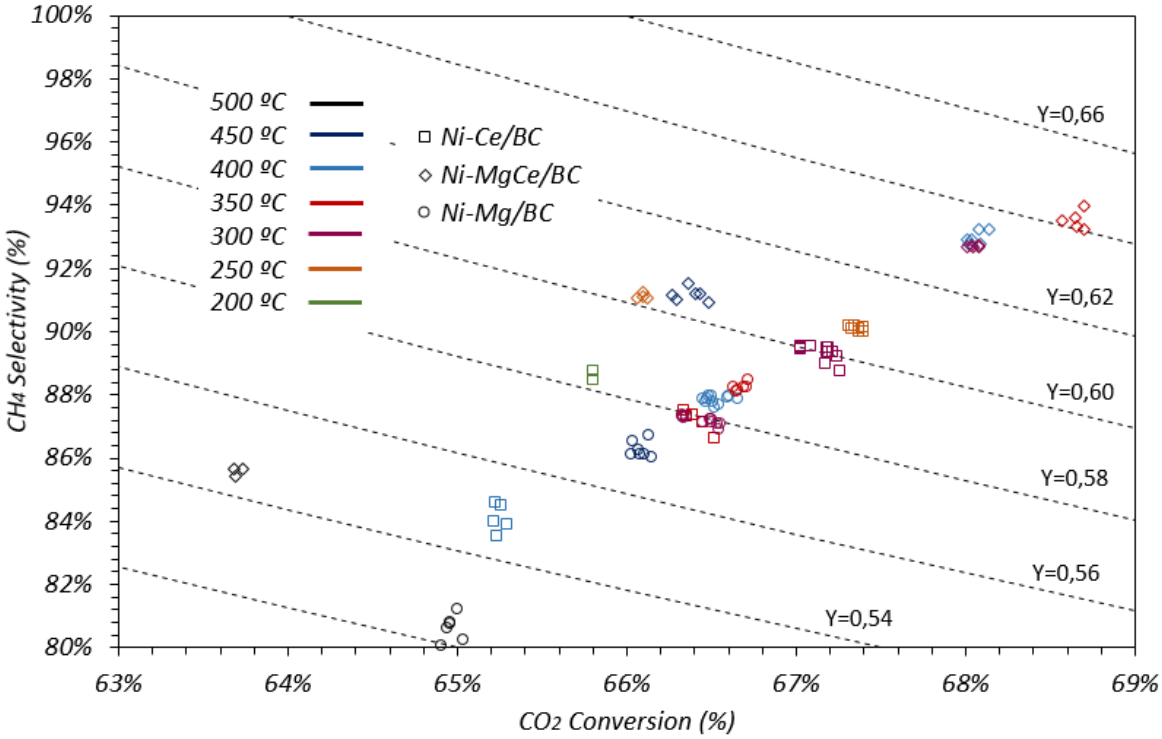

Figure 15. Summary of catalytic performance of Ni-Me/BC catalysts.

3.3 Study on the catalyst stability

Additional catalytic test has been performed on Ni-Me/BC catalysts to study the catalytic behaviour in terms of stability and activity at constant temperature of 325 ºC for 8h on stream. Prior to reaction, the synthesized catalyst was reduced in the reducing atmosphere (50% H_2, 50% N_2) at 500 °C for 10 minutes. Then, constant flow of 700 mL/min of mixed gases was introduced in the reactor with stoichiometric ratio of H_2/CO_2 to start the stability test for the reaction.

3.3.1 Comparison of catalyst stability of the synthesized Ni-Me/BC catalysts

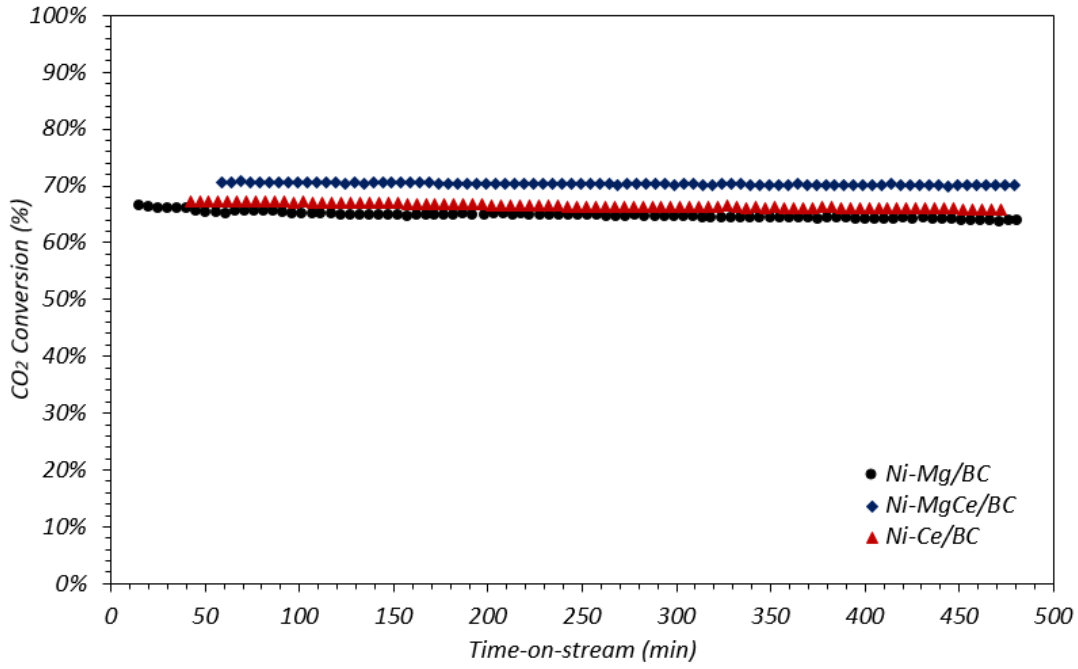

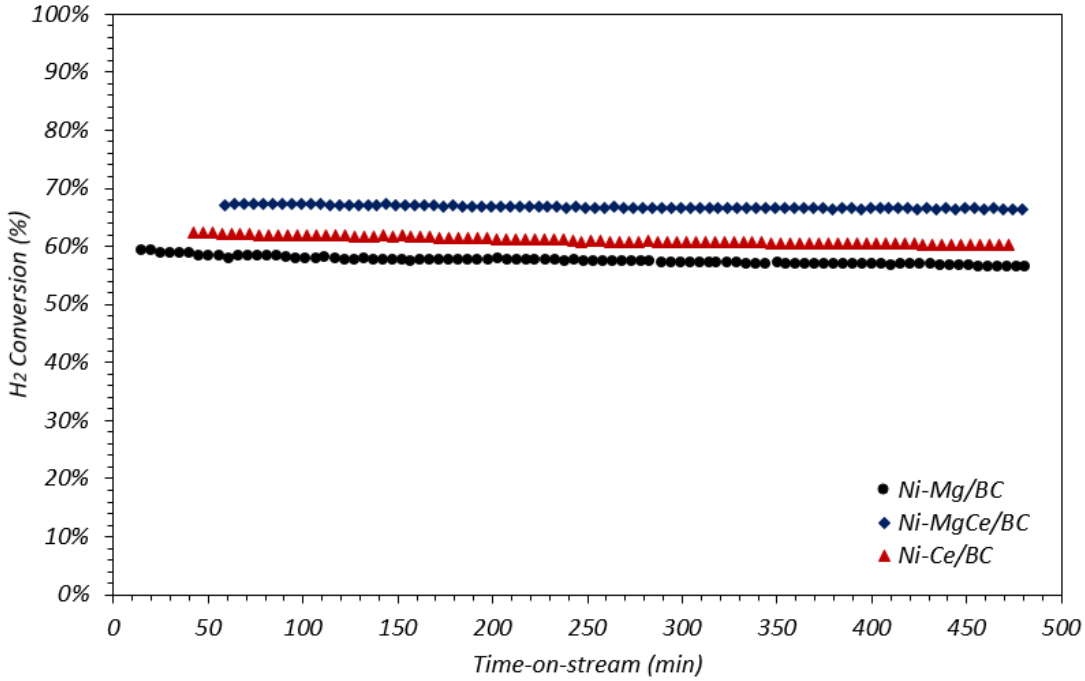

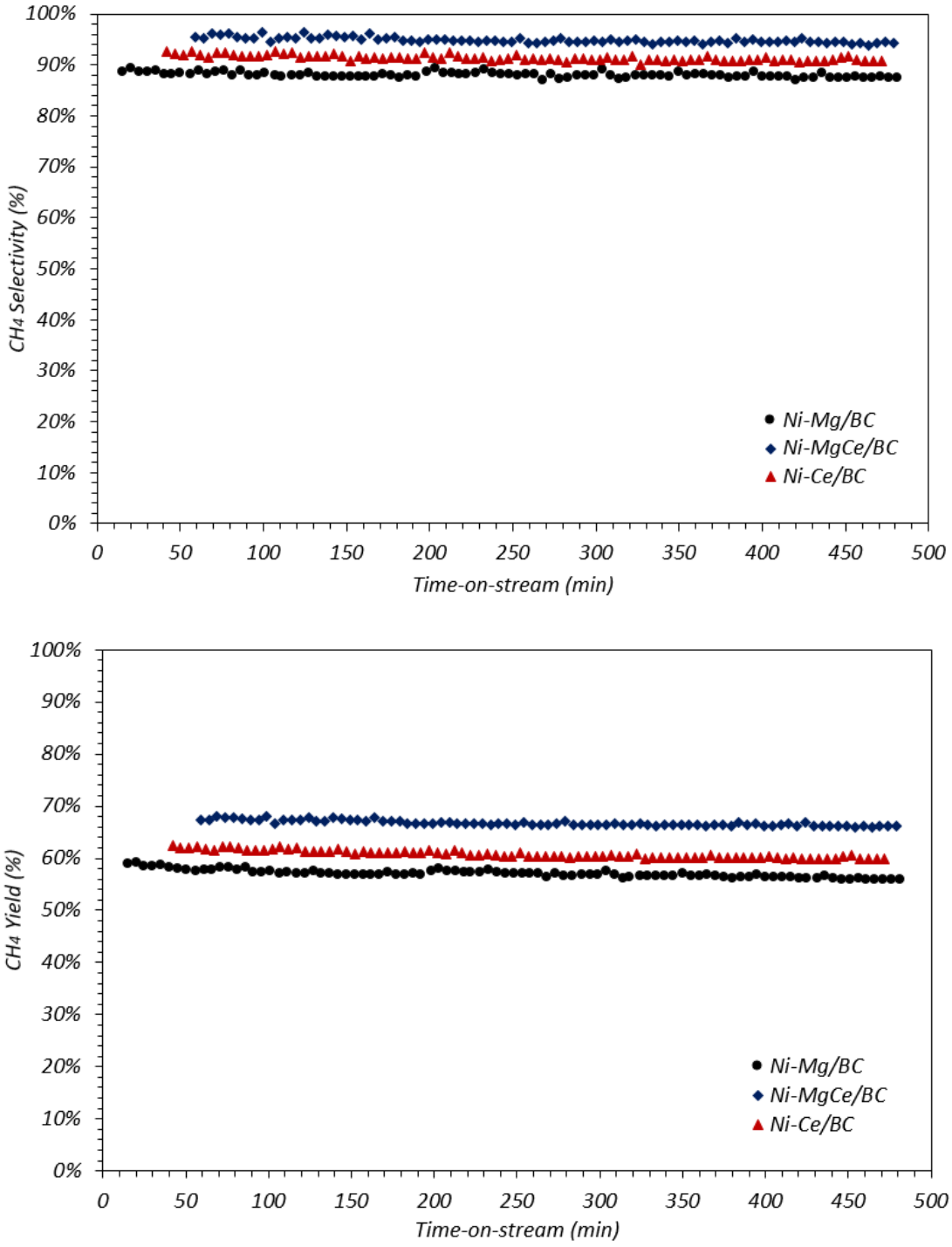

Figure 16. Stability test of catalysts in the reaction performed at 325 °C for 8h on stream.

Figure 16 shows the results of stability studies of catalysts in CO_2 methanation reaction. As can be observed, no significant changes detected in the values of CO_2 and H_2 conversion, selectivity and yield of desired CH_4, which indicates that all the catalysts were very stable within 8h on stream. In spite of having the same values of CO_2 and H_2 conversion, selectivity and yield of desired CH_4 before and after 8h on stream, there was a slight changes detected on the Ni-Mg/BC (about 4%), Ni-Ce/BC (about 1%) catalysts and no changes has been detected on the values obtained by Ni-MgCe/BC. Such

decreases occurred in the performance of the catalysts was due to the sintering of particles on the surface of carbonaceous support. As predicted, the stability of catalysts decreases in the following order: Ni-MgCe/BC > Ni-Ce/BC > Ni-Mg/BC, can be seen clearly in the Figure 17.

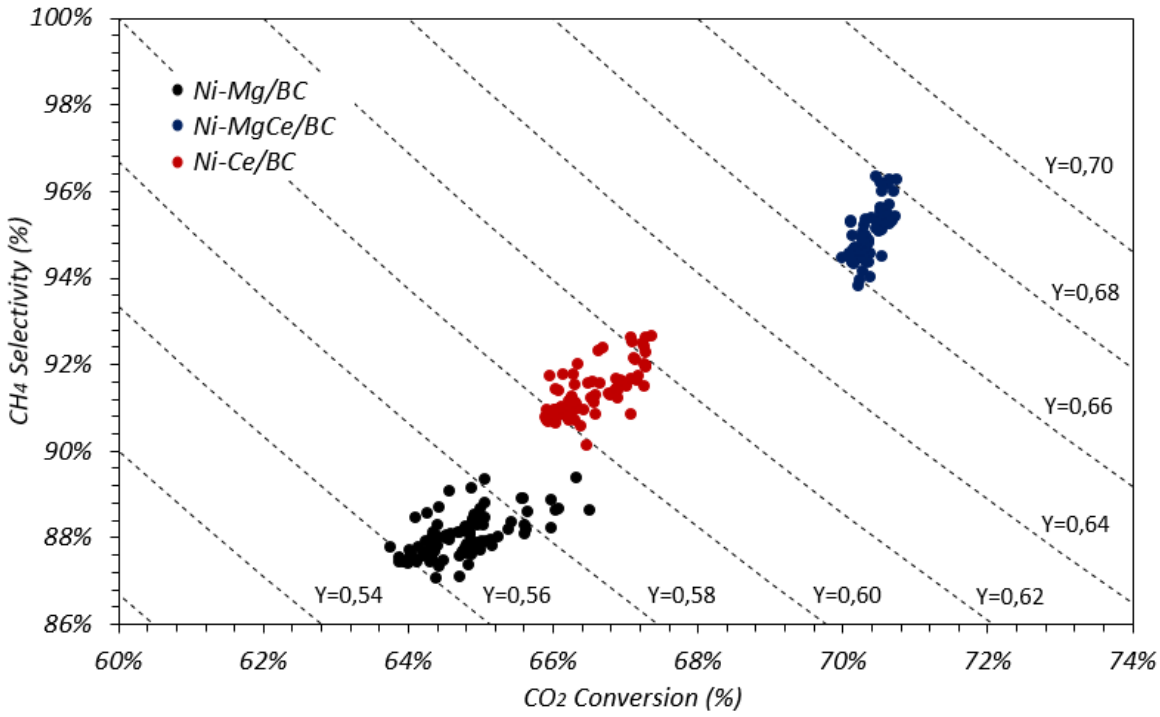

Figure 17. Summary of the stability of Ni-Me/BC catalysts for 8h on stream.

3.4 Study on the variation of molar ratio of H_2:CO_2 on the catalytic performance of Ni-MgCe/BC catalyst

In the catalytic activity and stability test that been performed previously proved that Ni-MgCe/BC catalyst is the most active catalyst among the three catalysts. Hence, this experiment was carried out to examine the performance of the catalyst at the stoichiometric ratio below and above the equilibrium. It is also to determine the ideal concentration of H_2 and CO_2 gas in the feed gas and the temperature of reaction. Before the reaction, the catalyst was reduced at 500 °C for 10 minutes. After that, constant flow of 700 mL/min of mixed gases was introduced in the reactor.

3.4.1 Comparison of catalytic performance of the various concentration of inlet H2 gas at constant temperature

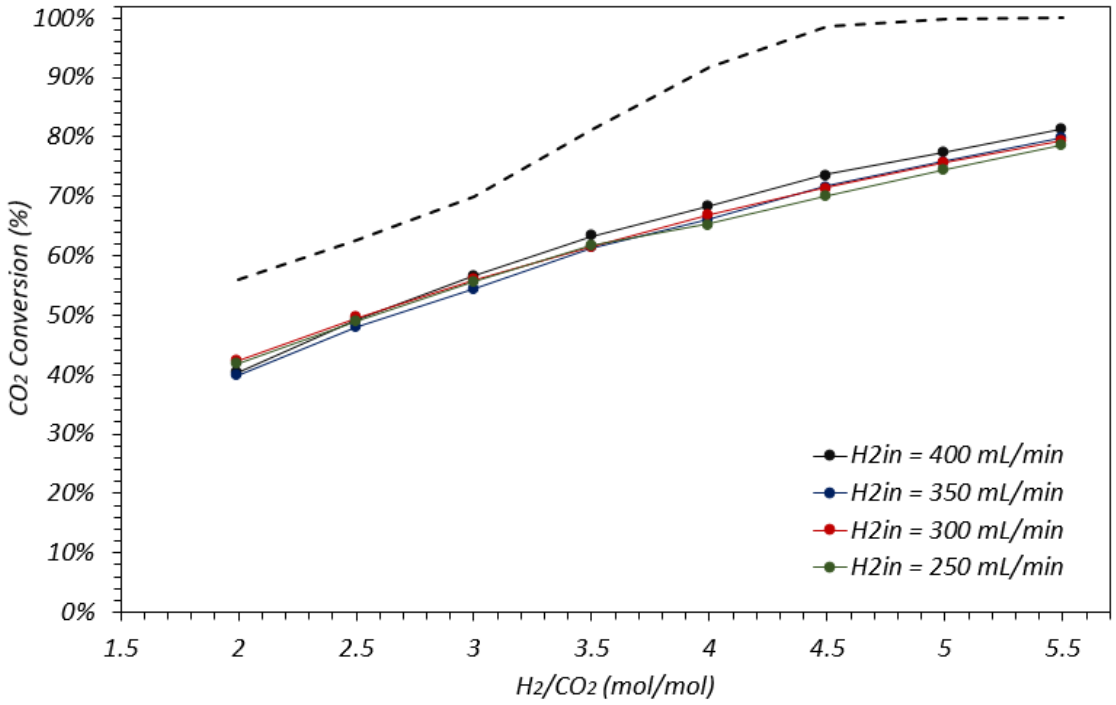

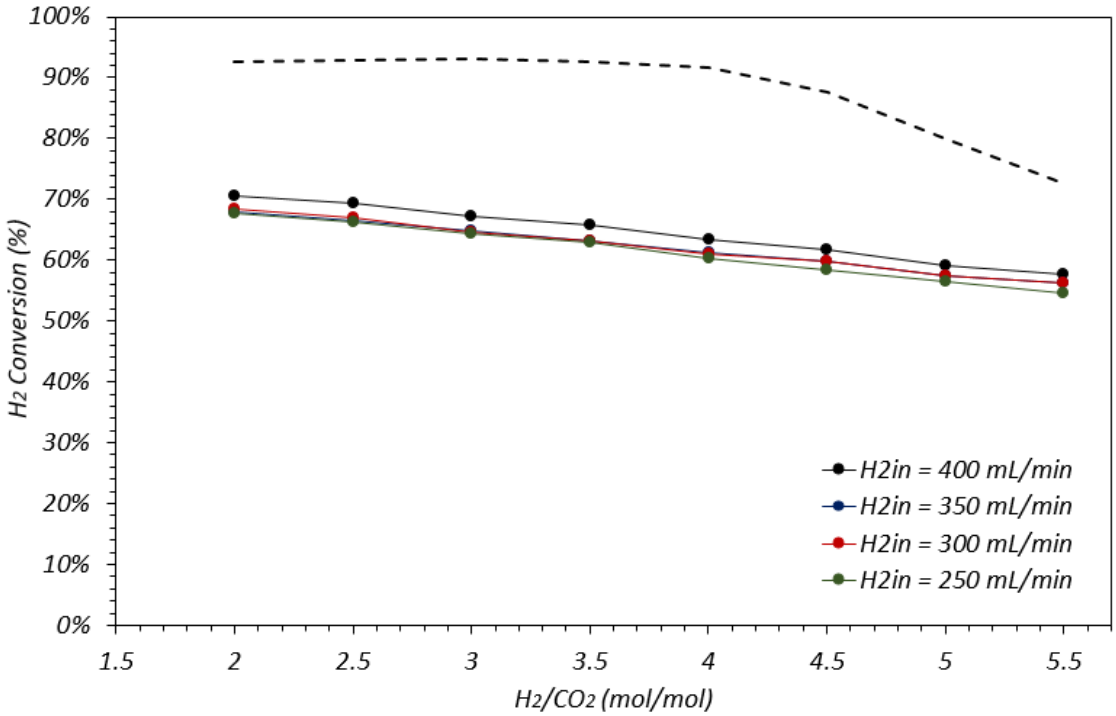

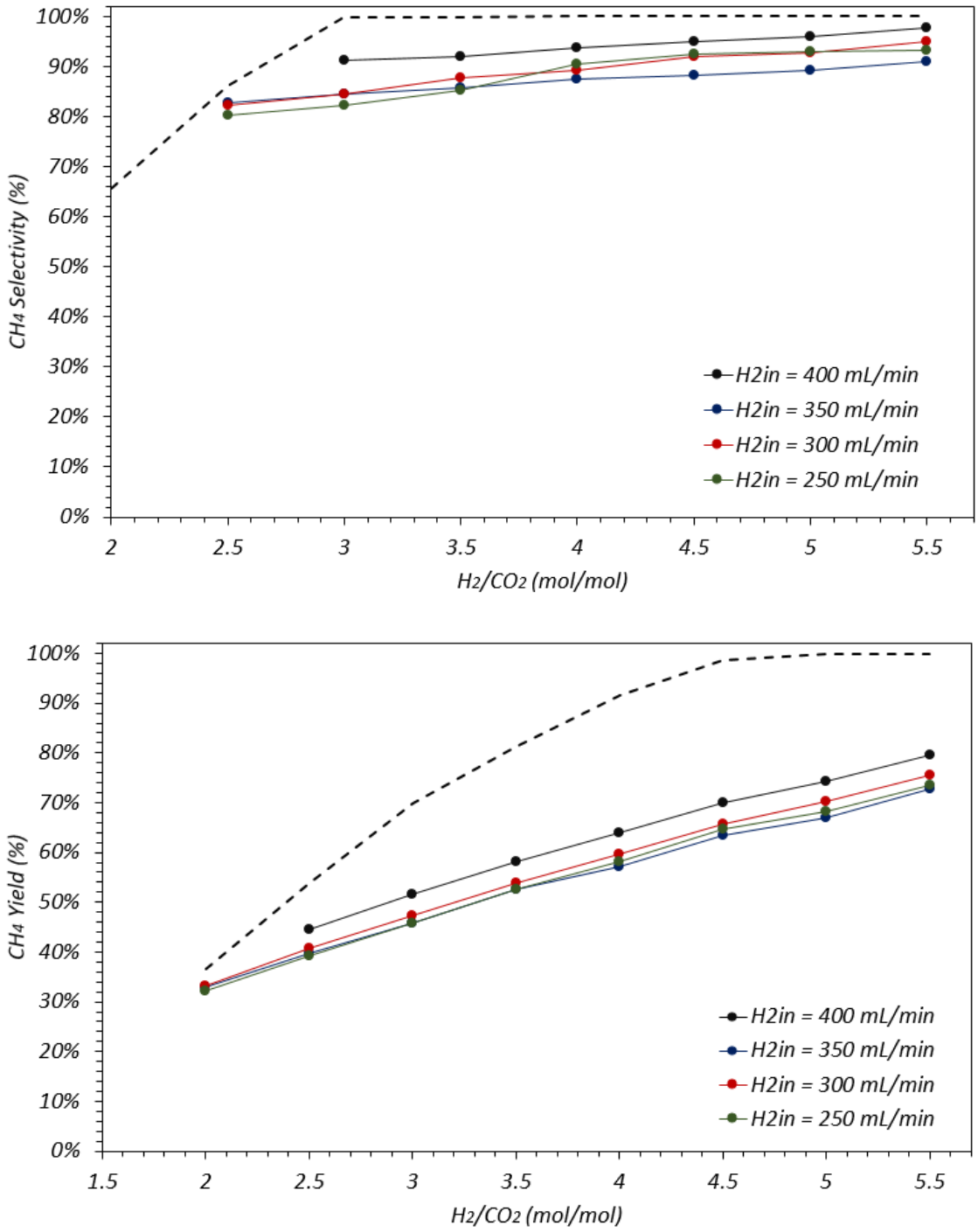

Figure 18. Catalytic performance of different concentration inlet of H_2 as a function of H_2/CO_2 molar ratio at constant 325 °C.

Figure 18 shows the catalytic performance of the different concentration of inlet H_2 gas as a function of H_2:CO_2 molar ratio at constant temperature of 325 °C; the equilibrium values also reported for comparison. No notable difference observed in the result of CO_2 conversion for the various inlet concentration of H_2. However, in the selectivity and yield of desired CH_4, the performance of the catalyst with inlet H_2 concentration of 400 mL/min was much closer to the equilibrium values. Interestingly,

the catalyst performance with various inlet concentration of H_2 decreases in the following order: 400 mL/min > 300 mL/min > 250 mL/min > 350 mL/min.

For the molar ratio of H_2/CO_2 below the stoichiometric value, whereas the CO_2 was in excess, the CO_2 conversion, CH_4 selectivity and yield were decreased. In contrast, at molar ratio above the stoichiometric, by which the CO_2 became the limiting reactant, the aforementioned values were increased. It is worthy to be mentioned that thermodynamically, the production of desired CH_4 was favoured at higher molar ratio of H_2/CO_2, as can be seen in the figure.

3.4.2 Comparison of catalytic performance of the various concentration of inlet CO_2 gas at constant temperature

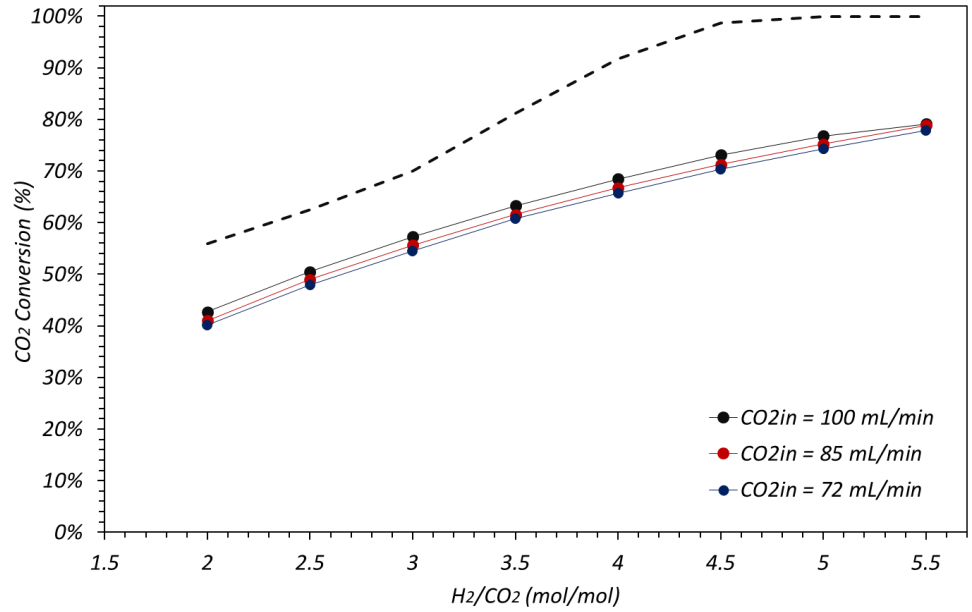

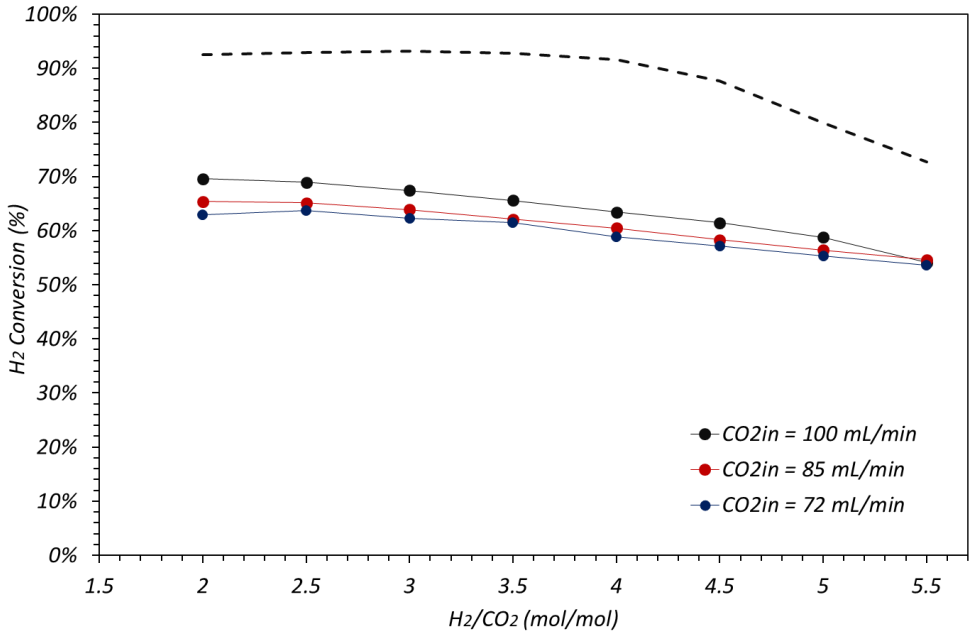

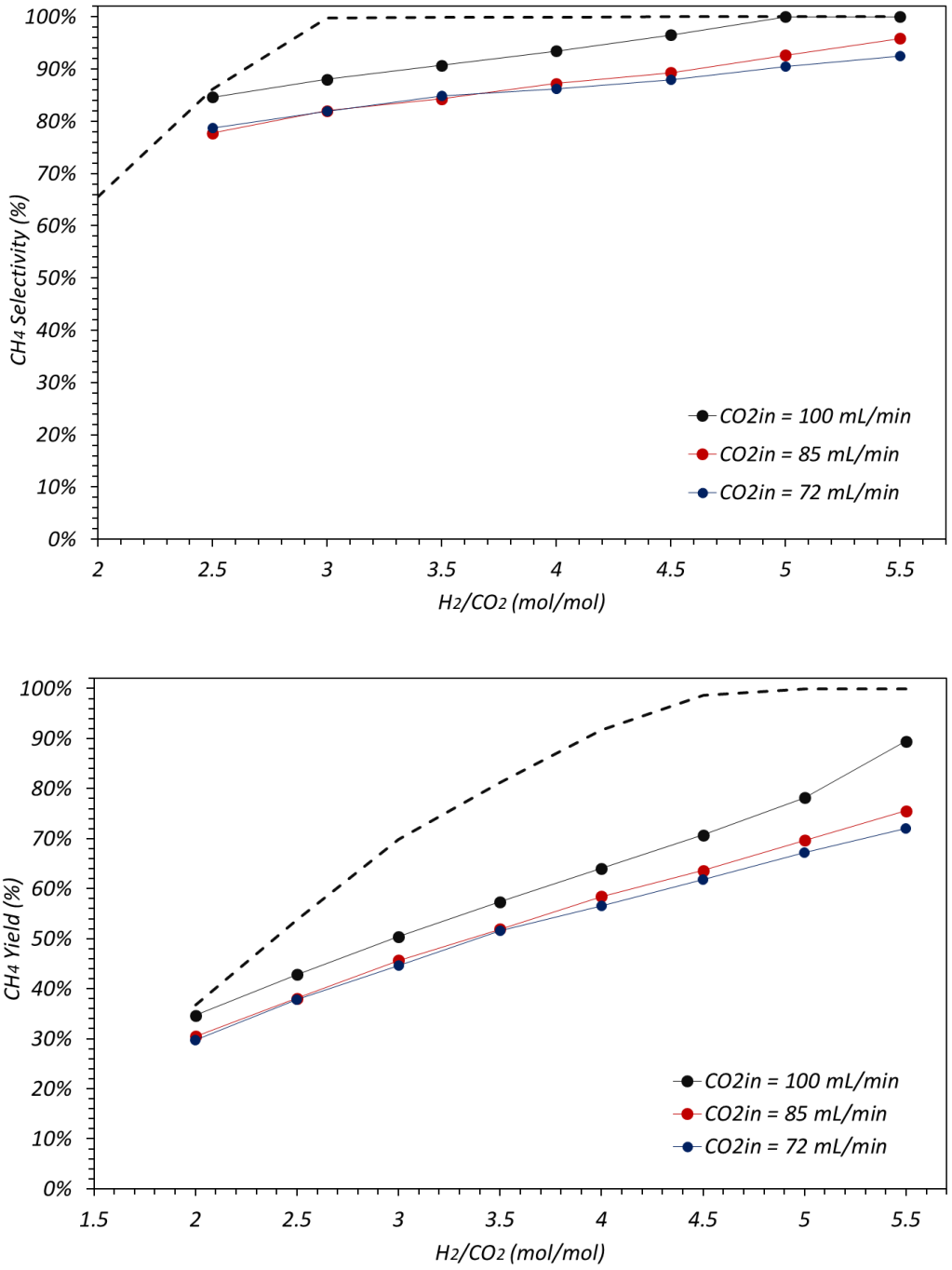

Figure 19. Catalytic performance of different inlet concentration of CO_2 as a function of H_2/CO_2 molar ratio at constant 325 °C.

Figure 19 shows the catalytic performance of different inlet concentration of CO_2 gas as a function of H_2/CO_2 molar ratio at constant temperature of 325 °C; the equilibrium values also reported for comparison. Excellent catalytic performance of the Ni-MgCe/BC catalyst can be seen in this figure with the 100 mL/min of CO_2 concentration in the feed gas. It is worth noting that the selectivity of desired CH_4 obtained, with the aforementioned CO_2 concentration in the feed gas shows crucial difference compared to the rest, by which the thermodynamic equilibrium was achieved at molar ratio of 5

and also at lower molar ratio of 2.5. Hence, the optimum catalytic performance achieved by this catalyst was with 100 mL/min of CO_2 concentration in the feed gas followed by 85 mL/min and 72 mL/min.

Therefore, with the 400 mL/min concentration of H_2 and 100 mL/min concentration of CO_2 in the feed gas, an excellent catalytic performance especially in the selectivity of desired CH_4 performed by Ni-MgCe/BC catalyst at constant temperature of 325 °C was obtained. Coincidentally, such concentration of gases in the feed gas was the stoichiometric molar ratio of H_2/CO_2 for the methanation of CO_2 and one of the operational condition used for the stability and catalytic activity test.

3.4.3 Comparison of catalytic performance of the various temperature of reaction at constant concentration of inlet H_2 gas

By maintaining the concentration of H_2 gas in the feed gas, which is 400 mL/min, the results of catalytic performance carried out over different temperature of reaction as a function of molar ratio of H_2/CO_2 were shown in the Figure 20. The dashed lined that represent the equilibrium values also reported for comparison.

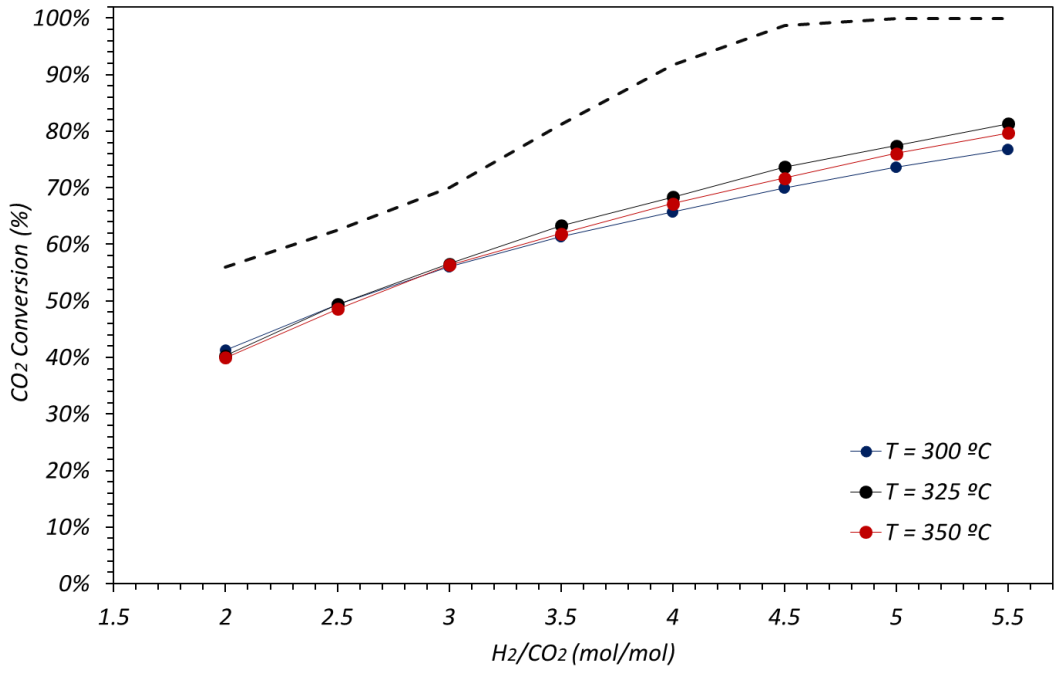

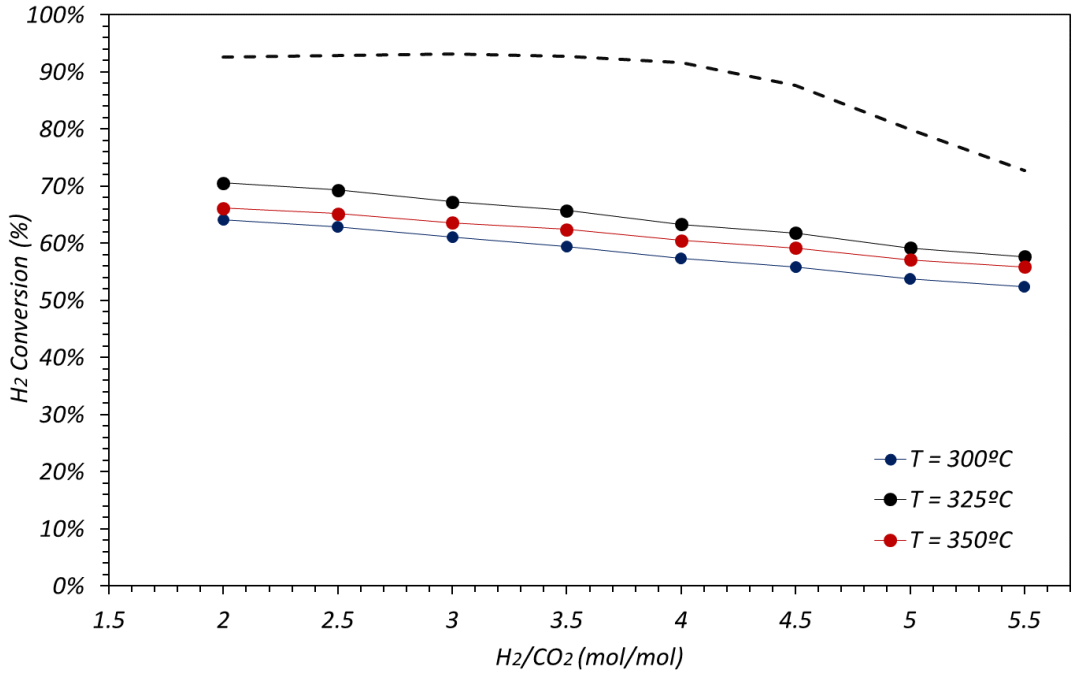
100%
90%
80%
70%
60%
50%
40%
30%
20%
10%
0%
H2 Conversion (%)
1.5
2
2.5
3
3.5
4
4.5
5
5.5
H2/CO2 (mol/mol)
T = 300ºC
T = 325ºC
T = 350ºC

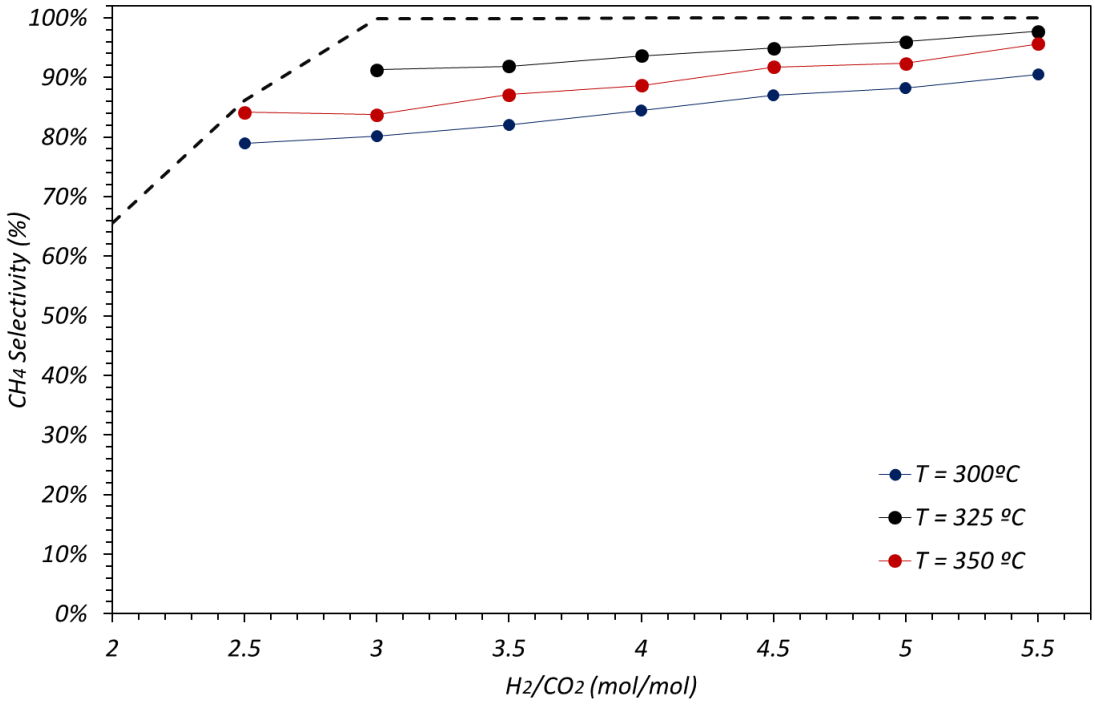
100%
90%
80%
70%
60%
50%
40%
30%
20%
10%
0%
CH4 Selectivity (%)
2
2.5
3
3.5
4
4.5
5
5.5
H2/CO2 (mol/mol)
T = 300ºC
T = 325 ºC
T = 350 ºC

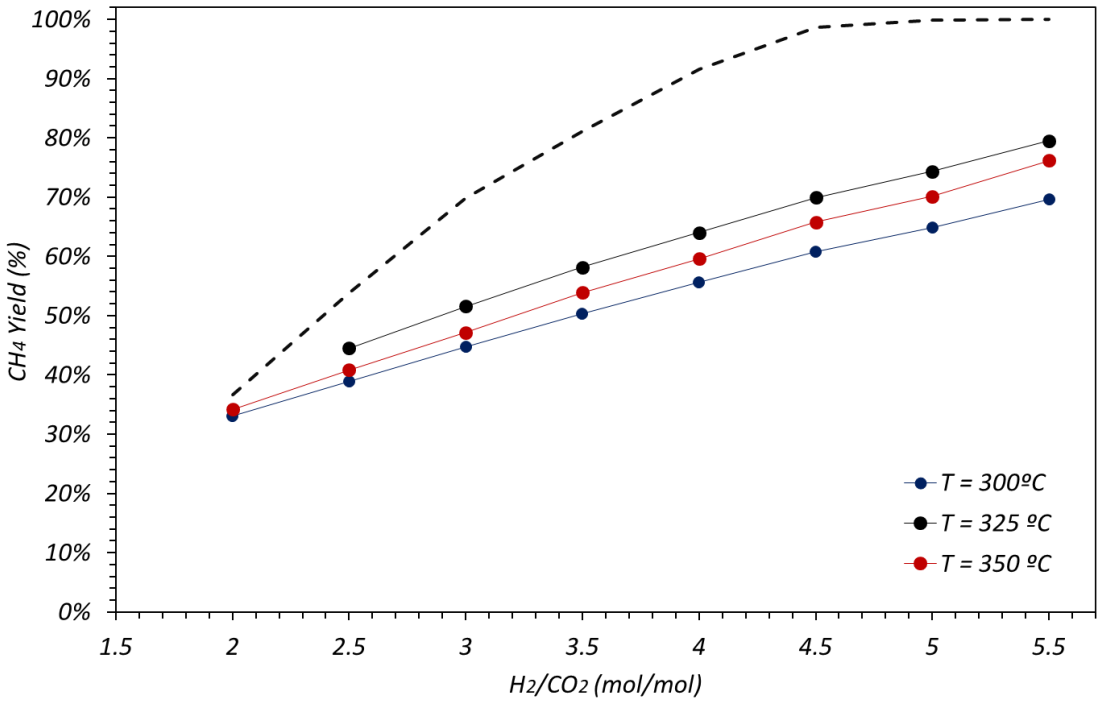

Figure 20. Catalytic performance of different temperature of reaction as a function of H_2/CO_2 molar ratio at constant 400 mL/min of inlet H_2.

At the molar ratio below the stoichiometric value, the CO_2 conversion achieved at 300 °C, 325 °C and 350 °C were approximately identical, however above the stoichiometric value, highest CO_2 conversion obtained was at 325 °C. For the case of CH_4 selectivity and yield, the highest experimental values obtained were also at the temperature of 325 °C. Hence, to be conclude, better temperature of reaction for the methanation reaction was at 325 °C followed by 350 °C and 300 °C.

3.4.4 Comparison of catalytic performance of the various temperature of reaction at constant concentration of inlet CO_2 gas

Figure 21 shows the results of performance of the catalyst carried out with the function of molar ratio of H_2/CO_2 at different temperature of reaction. The dashed lines that represent the equilibrium values also reported for comparison. The concentration of the H_2 gas was varied with the correspondent molar ratio and the concentration of CO_2 gas in the feed gas was maintained at 100 mL/min.

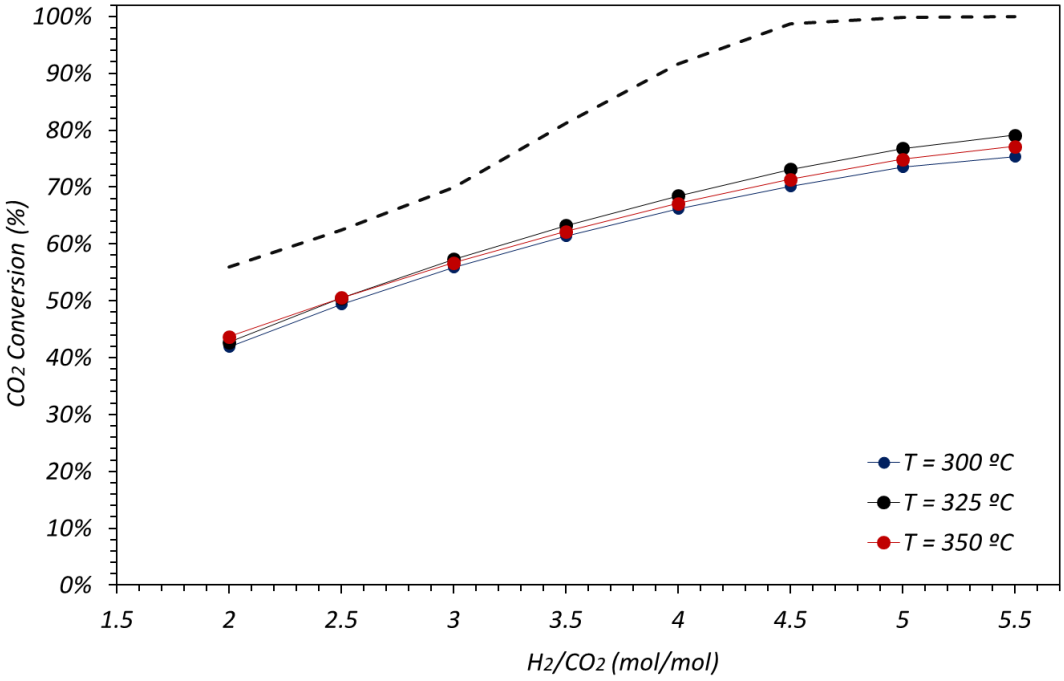
100%
90%
80%
70%
60%
50%
40%
30%
20%
10%
0%
CO2 Conversion (%)
1.5
2
2.5
3
3.5
4
4.5
5
5.5
H2/CO2 (mol/mol)
T = 300 ºC
T = 325 ºC
T = 350 ºC

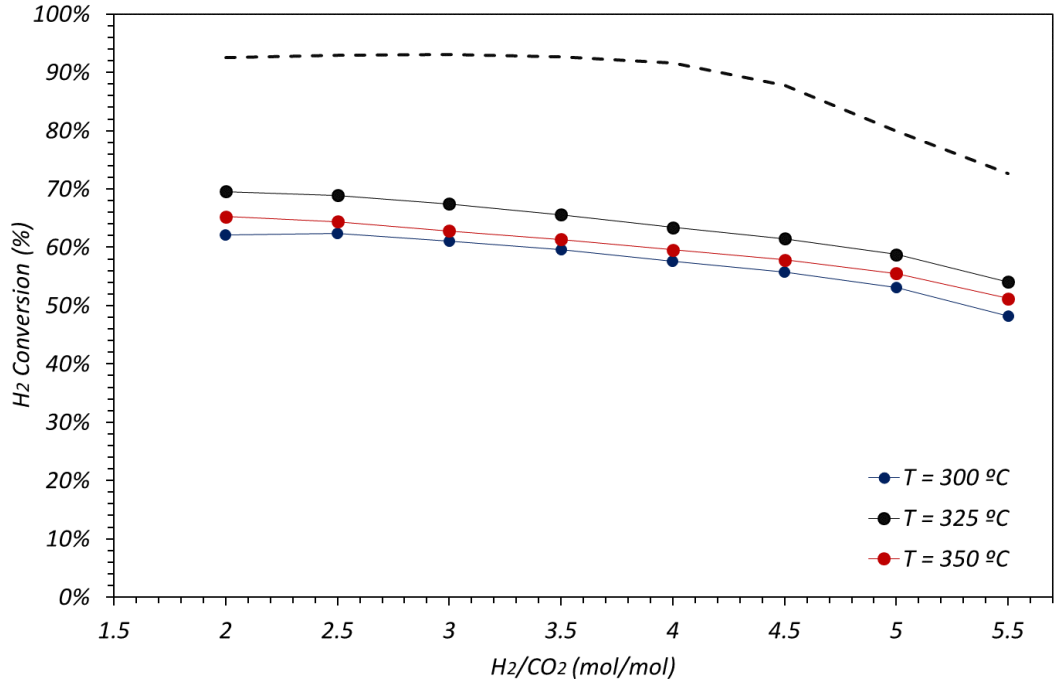
100%
90%
80%
70%
60%
50%
40%
30%
20%
10%
0%
H2 Conversion (%)
1.5
2
2.5
3
3.5
4
4.5
5
5.5
H2/CO2 (mol/mol)
T = 300 ºC
T = 325 ºC
T = 350 ºC

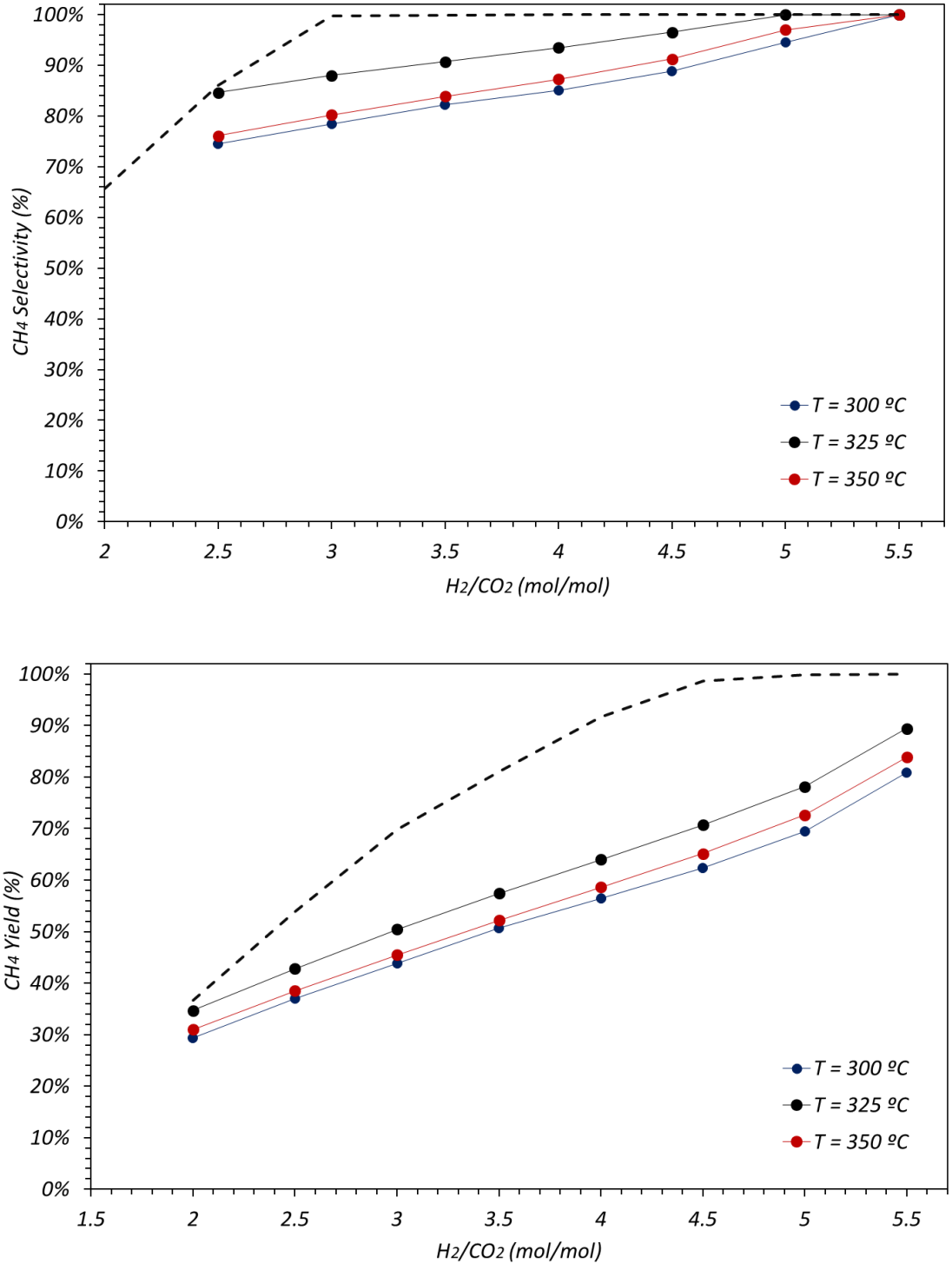

Figure 21. Catalytic performance of different temperature of reaction as a function of H_2/CO_2 molar ratio at constant 100 mL/min of inlet CO_2.

The results of experimental CO_2 conversion obtained was similar with the previous experiment, noting that at higher molar ratio the catalyst was performed the best at the temperature of 325 °C. The highest values of conversion of H_2, selectivity and yield of desired CH_4 also achieved at the temperature of 325 °C. Worth to be mentioned that at the temperature of 325 °C, the CH_4 selectivity approached the equilibrium at the molar

ratio of 5 and later on the temperature of 300 °C and 350 °C also approached the equilibrium but at the highest molar ratio of 5.5.

In this experiment and the previous one (section 3.4.3), the Ni-MgCe/BC catalyst works the best at the temperature of 325 °C. It is worth the note that the stability test that has been carried out previously (section 3.3.1) was at the optimum operational condition (i.e. temperature of reaction of 325 °C and with the stoichiometric molar ratio of H_2/CO_2) for 8h on stream.

4 CONCLUSIONS

Biomorphic mineralization technique is an easy and appropriate method for preparing catalysts based on biomorphic carbon. The catalysts synthesis procedure includes a stage of thermal decomposition in a reductive atmosphere of cellulose previously impregnated with the metallic (nitrates) precursors.

The characterization results indicate that the addition of promoter Ce has increased the BET surface area and microporosity of the catalysts. Besides, it also increased the dispersion of Ni particles on the surface of the catalysts by decreasing the crystallite size of the Ni. The weight percentage of Ni, MgO and CeO_2 were increased in the final catalysts compared to the initial amount on the raw cellulose due to the loss of carbonaceous material during the decomposition stage.

The characterization results show that the Ni-MgCe/BC catalyst has larger BET surface area and high micropore volume. It is proven in the CO_2 methanation reaction, that this catalyst was the most active and selective at temperature of 350 ºC.

Ni-MgCe/BC catalyst also shows great performance in the stability test. After 8h on stream at 325 ºC, the CO_2 and H_2 conversion as well as CH_4 selectivity and yield remained constant. The results of catalyst characterization after the reaction has proven that the sintering of catalyst occurred in Ni-Mg/BC and Ni-Ce/BC; however, in Ni-MgCe/BC no significant sintering of particles has been found.

Due to the great performance achieved by Ni-MgCe/BC in the catalytic activity and stability test, the additional study on the effect of different feed composition and reaction temperature as a function of H_2/CO_2 molar ratio was carried out. The results indicate that the optimal reaction temperature to produce CH_4 was 325 ºC where the conversion and selectivity were maximum. On the other hand, the optimal ratio H_2/CO_2 was 4 confirming the results found in bibliography.

Finally, and as a future work, the wide-ranging set of kinetic data obtained in this work, will allow the proposal and evaluation of rigorous kinetic models and the calculation of the corresponding parameters.

5 REFERENCES

[1] Martins F., Felgueiras C., Smitková M. Fossil Fuel Energy Consumption in European countries. *Energy Procedia*. 2018; 153: 107-111.

[2] Bette N., Thielemann J., Schreiner M., Mertens F. Methanation of CO_2 over a $(Mg,Al)O_x$ Supported Nickel Catalyst Derived from a (Ni,Mg,Al)-Hydrotalcite-like Precursor. ChemCatChem Communications. 2016; 8:1-5.

[3] World Resource Institute. Which Countries Use the Most Fossil Fuels? Emily Cassidy; [Last accessed: 3rd May 2019]. doi: https://cleantechnica.com/2019/05/03/which-countries-use-the-most-fossil-fuels/

[4] Worldwatch Institute. Global Fossil Fuel Consumption Surges. Washington: [Last accessed: 9th August 2019]. doi: http://www.worldwatch.org/global-fossil-fuel-consumption-surges

[5] Kibria A., Akhundjanov SB., Oladi R. Fossil Fuel Share in the Energy Mix and Economic Growth. International Review of Economics & Finance. 2019;59:253-264. doi: https://doi-org.cuarzo.unizar.es:9443/10.1016/j.iref.2018.09.002

[6] Zerrahn A., Schill W., Kemfert C. On the Economics of Electrical Storage for Variable Renewable Energy Sources. European Economic Review. 2018; 108: 259-279.

[7] International Renewable Energy Agency (IRENA). Renewable Energy Now Accounts for a Third of Global Power Capacity. Abu Dhabi, United Arab Emirates: [Last accessed: 2nd April 2019]. doi: https://www.irena.org/newsroom/pressreleases/2019/Apr/Renewable-Energy-Now-Accounts-for-a-Third-of-Global-Power-Capacity

[8] Ghaib K., Nitz K., Ben-Fares F. Chemical Methanation of CO_2: A review. ChemBioEng Reviews. 2016; 3(6): 266-275.

[9] Thema M., Bauer F., Sterner M. Power-to-gas: Electrolysis and Methanation Status Review. Renewable and Sustainable Energy Reviews. 2019; 112: 775-787.

[10] Wang L., Rao M., Diethelm S., Lin T., Zhang H., Hagen A., et al. Power-to-methane via Electrolysis of H_2O and CO_2: The Effects of Pressurized Operation and Internal Methanation. Applied Energy. 2019; 250: 1432-1445. doi: https://doi-org.cuarzo.unizar.es:9443/10.1016/j.apenergy.2019.05.098

[11] Gondal IA. Hydrogen Integration in Power-to-gas Networks. International Journal of Hydrogen Energy. 2019; 44(3): 1803-1815. doi: https://doi-org.cuarzo.unizar.es:9443/10.1016/j.ijhydene.2018.11.164

[12] Ghaib K., Ben-Fares F. Power-to-methane: A state-of-the-art review. Renewable and Sustainable Energy review. 2018; 81: 433-446.

[13] Bär K., Mörs F., Götz M., Graf F. Vergleich der biologischen und katalytischen Methanisierung für den Einsatz bei PtG-Konzepten. Gwf-Gas|Erdgas. 2015; 157(7): 73-466.

[14] Wang W., Gong J. Methanation of Carbon Dioxide: an overview. Frontiers of Chemical Science. And Engineering. 2011; 5(1): 2-10.

[15] Tomsett AD., Hagiwara T., Miyamoto A., Inui T. Highly Active Catalysts for CO_2 Methanation to Provide the Second Reactor of Two Stage Process for High BTU SNG Synthesis. Applied Catalysis. 1986; 26: 391-394.

[16] Gao J., Wang Y., Ping Y., Hu D., Xu G., Gu F., et al. A Thermodynamic Analysis of Methanation Reactions of Carbon Oxides for the Production of Synthesis Natural Gas. RSC Advances. 2012; 2: 2358-2368.

[17] Wang W., Wang S., Ma X., Gong J. Recent Advances in Catalytic Hydrogenation of Carbon Dioxide. Chemical Society Reviews. 2011; 40: 3703-3727.

[18] Agnelli M., Kolb M., Mirodatos C. CO Hydrogenation on a Nickel Catalyst: 1. Kinetics and Modelling of a Low-temperature Sintering Process. Journal of Catalysis. 1994; 148(1): 9-21.

[19] Alrafei B., Polaert I., Ledoux A., Azzolina-Jury F. Remarkably Stable and Efficient Ni and Ni-Co Catalysts for CO_2 Methanation. Catalysis Today. Available online: 12th March 2019. In Press, Corrected Proof. doi: https://doi-org.cuarzo.unizar.es:9443/10.1016/j.cattod.2019.03.026

[20] Tan J., Wang J., Zhang Z., Ma Z., Wang L., Liu Y. Highly Dispersed and Stable Ni Nanoparticles Confined by MgO on ZrO_2 for CO_2 Methanation. Applied Surface Science. 2019; 481: 1538-1548. doi: https://doi-org.cuarzo.unizar.es:9443/10.1016/j.apsusc.2019.03.217

[21] Bacariza M., Graça I., Bebiano S. Magnesium as Promoter of CO_2 Methanation on Ni-based USY Zeolites. Energy Fuel. 2017; 31: 9776-9789.

[22] Aziz MAA., Jalil MAA., Triwahyono S., Ahmad A. CO_2 Methanation over Heterogeneous Catalysts: Recent Progress and Future Prospects. Royal Society of Chemistry. 2015;1 7: 2647-2663.

[23] Liu J., Li C., Wang F., He S. Enhanced Low-temperature Activity of CO_2 Methanation over Highly-dispersed Ni/TiO_2 Catalyst. Catalysis Science & Technology. 2013; 3: 2627-2633.

[24] Sepehri S., Rezaei M. Ce Promoting Effect on the Activity and Coke Formation of Ni Catalysts Supported on Mesoporous Nanocrystalline Y-Al_2O_3 in Autothermal

Reforming of Methane. International Journal of Hydrogen Energy. 2017;4 2: 11130-11138.

[25] Wu H., Wang L. Shape Effect of Microstructured CeO_2 with Various Morphologies on CO Catalytic Oxidation. Catalysis Communications. 2011; 12: 1374-1379.

[26] Wang X., Zhu L., Liu Y., Wang S. CO_2 Methanation on the Catalyst of Ni/MCM-41 Promoted with CeO_2. Science of The Total Environment. 2018; 625: 686-695. doi: https://doi-org.cuarzo.unizar.es:9443/10.1016/j.scitotenv.2017.12.308

[27] Li D., Zeng L. Li X., Wang X., Ma H., Assabumrungrat S., et al. Ceria-promoted Ni/SBA-15 Catalysts for Ethanol Steam Reforming with Enhanced Activity and Resistance to Deactivation. Applied Catalysis B: Environmental. 2015; 176-177: 532-541.

[28] Matos I., Bernardo M., Fonseca I. Porous Carbon: A Versatile Material for Catalysis. Catalysis Today. 2017; 285: 194-203. doi: https://doi-org.cuarzo.unizar.es:9443/10.1016/j.cattod.2017.01.039

[29] Pérez-Mayoral E., Calvino-Casilda V., Soriano E. Metal-supported Carbon-based Materials: Opportunities and Challenges in the Synthesis of Valuable Products. Catalysis Science & Technology. 2016; 6: 1265-1291.

[30] Lam E., Luong JHT. Carbon Materials as Catalyst Supports and Catalysts in the Transformation of Biomass to Fuels and Chemicals. ACS Catalysis. 2014; 4(10): 3393-3410.

[31] Will J., Zollfrank C., Kaindl A., Sieber H., Greil P. Biomorphic Ceramics: Technologies Based on Nature. Keramische Zeitschrift. 2010; 62(2): 114-120.

[32] Azuara M., Latorre N., Villacampa JI., Sebastian V., Cazaña F., Romeo E., et al. Use of Ni Catalysts Supported on Biomorphic Carbon Derived from Lignocellulosic Biomass Residues in the Decomposition of Methane. Frontiers in Energy Research. 2019; 34(7). doi: https://doi.org/10.3389/fenrg.2019.00034

[33] Fan TX., Chow SK., Zhang D. Biomorphic Mineralization: From Biology to Materials. Progress in Materials Science. 2009; 54(5): 542-659. doi: https://doi.org/10.1016/j.pmatsci.2009.02.001

[34] Cazaña F., Jimaré MT., Romeo E., Sebastián V., Irusta S., Latorre N., et al. Kinetics of Liquid Phase Cyclohexene Hydrogenation on Pd-Al/Biomorphic Carbon Catalysts. Catalysis Today. 2015; 249: 127-136. doi: https://doi-org.cuarzo.unizar.es:9443/10.1016/j.cattod.2014.11.022

[35] Lowell S., Shields JE., Thomas MA., Thommes M. Characterization of Porous Solids and Powders: Surface Area Pore Size and Density. Vol. 16. Particle Technology Series. Dordrecht: Springer; 2004.

[36] Thommes M., Kaneko K., Neimark AV., Olivier JP., Rodriguez-Reinoso F., Rouquerol J., et al. Physisorption of Gases, with Special Reference to the Evaluation of Surface Area and Pore Size Distribution (IUPAC Technical Report). Pure and Applied Chemistry. 2015; 87: 1051-1069.

[37] Gregg SJ., Sing KSW. Adsorption, Surface Area and Porosity. London: Academic Press; 1982.

[38] Subhashish D., Dhal GC., Prasad R., Mohan D. Effect of Nitrate Metal (Ce, Cu, Mn and Co) Precursors for the Total Oxidation of Carbon Monoxide. Resource-Efficient Technologies. 2017; 3: 293-302.

[39] Atzori L., Gutrufello MG., Meloni D., Cannas C.,Gazzoli D., Monaci R., et al. Highly active NiO-CeO_2 catalysts for Synthetic Natural Gas Production by CO_2 Methanation. Catalysis Today. 2018; 299: 183-192.

[40] Guilera J., Valle J., Alarcón A., Díaz JA., Andreu T. Metal-oxide Promoted Ni/Al_2O_3 as CO_2 Methanation Micro-size Catalysts. Jourbal of CO_2 Utilization. 2019; 30: 11-17. doi: https://doi-org.cuarzo.unizar.es:9443/10.1016/j.jcou.2019.01.003

[41] Cazaña F., Galetti A., Meyer C., Sebastián V., Centeno M.A., Romeo E., Monzón A. Synthesis of Pd-Al/Biomorphic Carbon Catalysts using Cellulose as Carbon Precursor. Catalysis Today. 2018; 301: 226-238. doi: https://doi-org.cuarzo.unizar.es:9443/10.1016/j.cattod.2017.05.026

[42] Xie X., Goodell B., Zhang D., Nagle D. C., Qian Y., Peterson M. L., Jellison J. Characterization of Carbons Derived from Cellulose and Lignin and their Oxidative Behaviour. Bioresource Technology. 2009; 100(5): 1797-1802. doi: https://doi-org.cuarzo.unizar.es:9443/10.1016/j.biortech.2008.09.057

[43] Zwinkels M. F M., Jaras S.G., Menon P. G., Griffin T.A. Catalytic Materials for High-temperature Combustion. Catalysis Reviews. 1993; 35(3): 319-358.

[44] Cazaña F., Latorre N., Tarifa P., Labarta J., Romeo E., Monzón A. Synthesis of Graphenic Nanomaterials by Decomposition of Methane on a Ni-Cu/Biomorphic Carbon Catalyst. Kinetic and characterization results. Catalysis Today. 2018; 299: 67-79. doi: https://doi-org.cuarzo.unizar.es:9443/10.1016/j.cattod.2017.03.056

[45] Montoya J. A., Romero-Pascual E., Gimon C., Del angel P., Monzón A. Methane Reforming with CO_2 Over Ni/ZrO_2-CeO_2 Catalysts Prepared by Sol-gel. Catalysis Today. 2000; 63(1): 71-85. doi: https://doi-org.cuarzo.unizar.es:9443/10.1016/S0920-5861(00)00447-8

[46] Gac W., Zawadzki W., Rotko M., Słowik G., Greluk M. CO_2 Methanation in the Presence of Ce-promoted Alumina Supported Nickel Catalysts: H_2S Deactivation Studies. Topics in Catalysis. 2019; 62(5-6): 524-534.

[47] The LibreTexts. BET Surface Area Analysis of Nanoparticles. Barron AR., Raja PM; [Last access: 22nd June 2019]. doi:

https://chem.libretexts.org/Bookshelves/Analytical_Chemistry/Book%3A_Physical_Methods_in_Chemistry_and_Nano_Science_(Barron)/02%3A_Physical_and_Thermal_Analysis/02.3%3A_BET_Surface_Area_Analysis_of_Nanoparticles

[48] Nguyen C., Do DD. The Dubinin-Radushkevich equation and the underlying microscopic adsorption description. Carbon. 2001; 39(9): 1327-1336. doi: https://doi-org.cuarzo.unizar.es:9443/10.1016/S0008-6223(00)00265-7

[49] Dombrowski RJ., Lastoskie CM., Hyduke DR. The Horvath-Kawazoe method revisited. Colloids and Surfaces A: Physicochemical and Engineering Aspects. 2001; 187-188: 23-39. doi: https://doi-org.cuarzo.unizar.es:9443/10.1016/S0927-7757(01)00618-5

[50] Kohli R., Mittal KL. Developments in Surface Contamination and Cleaning. Vol. 1. 2nd edition. Norwich, NY: William Andrew; 2012. (pages: 107-178).

[51] Patterson AL. The Scherrer Formula for X-Ray Particle Size Determination. Physical Review. 1939; 56(10): 978.

[52] Williams DB., Carter CB. Transmission Electron Microscopy. New York: Springer cop.; 1996.

[53] Bergeret G., Gallezot P., Ertl G., Knozinger H., Weitkamp J. Handbook of Heterogeneous Catalysis. Vol. 3. Weinheim: Wiley-VCH; 1997. (Page: 738).

ANNEX

ANNEX A. CALIBRATION OF GAS CHROMATOGRAPHY

This section shows the results obtained from the gas chromatography analysis that have been performed on each gases involved in this methanation reaction. The calibration curve obtained (i.e. a curve that relates the areas of the peaks on the chromatograms to the mixture composition) will be used to analyse the gases produced during the methanation reaction. This calibration curve is obtained by introducing the desired molar flow of each gas into the gas chromatography with known composition. Hence, it is necessary to carried out the calibration analysis within the range of value that will be used in the experiment.

The chromatography analysis is performed by injecting known composition of mixture H_2, CO_2, CH_4 and inert gas (N_2) into the gas chromatography. The mixture of gases was then injected with different composition to obtain different area of peaks and the area under these peaks can be used to quantify the partial pressure and mole fraction of each gases. This analysis was performed on various samples and the calibration curve of each gases was shown in the Figure A.1, A.2, A.3, A.4 and A.5.

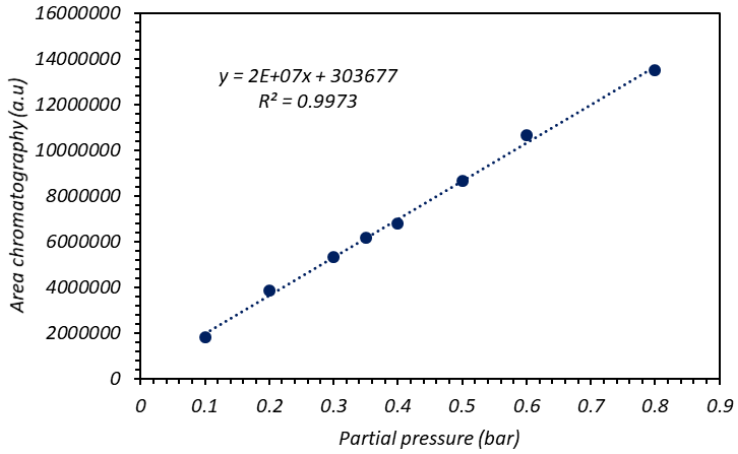

Figure A.1. Calibration curve of N_2.

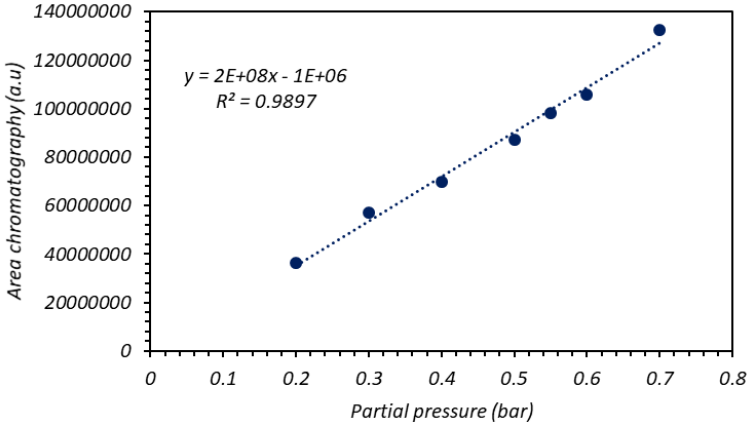

Figure A.2. Calibration curve of H_2.

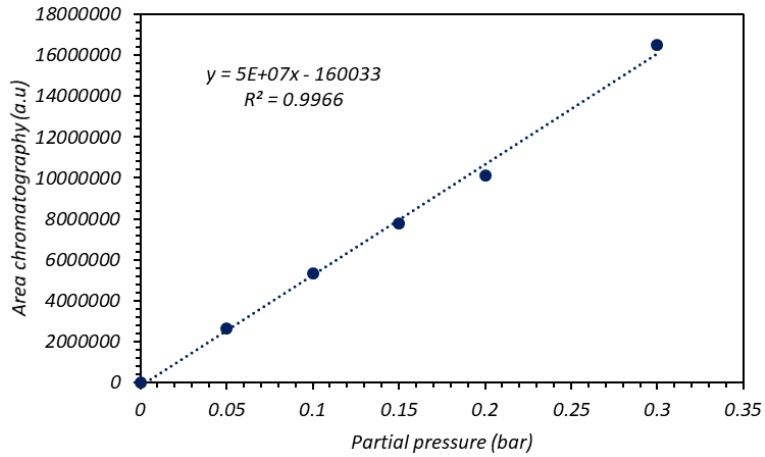

Figure A.3. Calibration curve of CO_2.

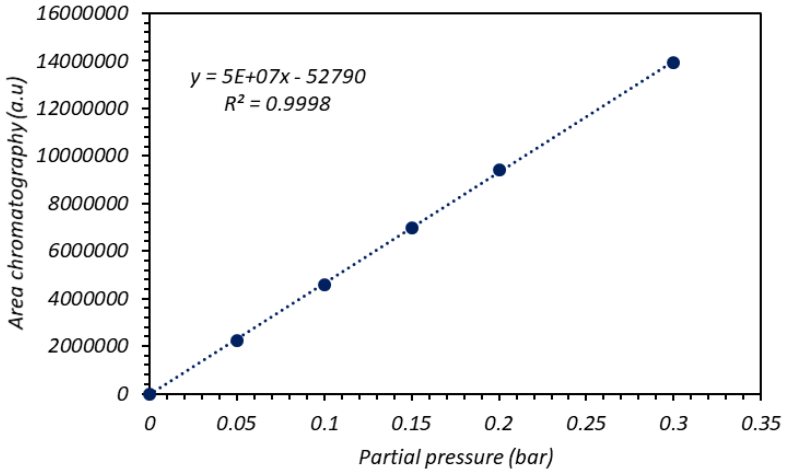

Figure A.4. Calibration curve of CH_4.

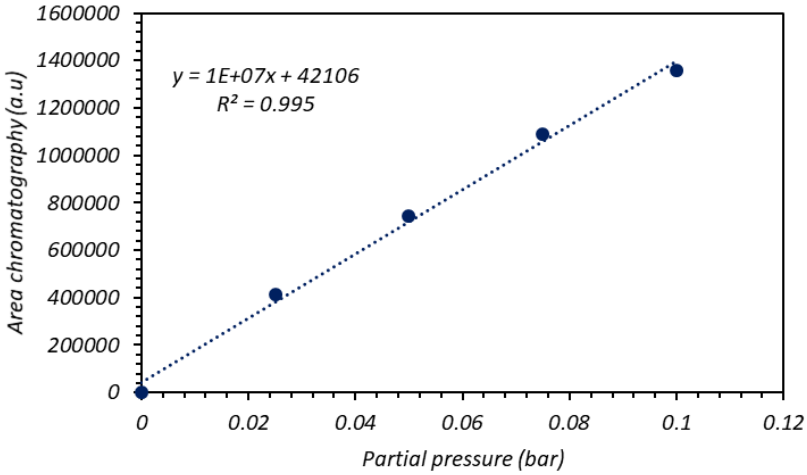

Figure A.5. Calibration curve of CO.

ANNEX B. CALCULATIONS OF CATALYST SYNTHESIS

The calculation for the preparation of Ni based catalysts supported on biomorphic carbon will be shown in this section. All the catalysts have similar Ni loading of 3.5 wt% with different molar ratio of Ni:Mg and/or Ce. The molar ratio for Ni-Mg/BC, Ni-Ce/BC and Ni-MgCe/BC were Ni:Mg = 1:1, Ni:Ce = 1:1 and Ni:Mg:Ce = 1:0.5:0.5 respectively. In the following steps, the calculation for the preparation of Ni-Mg/BC catalyst can be seen. The Ni-MgCe/BC and Ni-Ce/BC were also prepared with the same steps.

At first place, in order to calculate the amount of biomorphic carbon (i.e. cellulose) support needed [Eq. 8] in the 10 g of total amount of catalyst with minimal Ni loading 3.5 wt%, amount of metal precursor needed was calculated with respect to the correspondent relation molar ratio, in this case amount of metallic Mg needed to load in the 10 g of catalyst [Eq. 7].

$$3.5\ wt\%\ of\ Ni\ for\ 10\ g\ of\ catalyst = 0.35\ g \quad \text{[Eq. 6]}$$

$$Mass\ of\ Mg\ neccesary = [Eq.\ 6] \times \frac{P_m\ Mg}{P_m\ Ni} \times \frac{1\ mol\ of\ Mg}{1\ mol\ of\ Ni} \quad \text{[Eq. 7]}$$

$$Mass\ of\ cellulose\ necessary = 10\ g - [Eq.\ 6] - [Eq.\ 7] \quad \text{[Eq. 8]}$$

Next, for the desire 12 g of raw cellulose in the synthesis catalyst, the total amount of the catalyst was calculated [Eq. 9]. With the known amount of metallic Nickel needed to load in the catalyst [Eq. 10], the mass of metallic Nickel nitrate can be determined [Eq. 11]. The amount of Magnesium nitrate also can be quantified with the correspondent atomic relation [Eq. 13]. Lastly, the 12 g of cellulose need to be impregnated with the metallic nitrates precursor, hence the double amount of distilled water with respect to the amount of cellulose support need to be added to dissolve the metallic nitrates. However, the presence of water in the metallic nitrates need to be taken into account, as calculated in the [Eq. 14].

$$Total\ amount\ of\ catalyst = \frac{12\ g\ of\ cellulose \times 10\ g\ of\ catalyst}{[Eq.\ 8]} \quad \text{[Eq. 9]}$$

$$3.5\ wt\%\ of\ Ni = 3.5\% \times [Eq.\ 9] \quad \text{[Eq. 10]}$$

$$Mass\ of\ Ni(NO_3)_2{\cdot}6H_2O\ necessary = \frac{[Eq.\ 10] \times P_m\ Ni(NO_3)_2{\cdot}6H_2O}{P_m\ Ni} \quad \text{[Eq. 11]}$$

$$Mass\ of\ Mg = [Eq.\ 10] \times \frac{P_m\ Mg}{P_m\ Ni} \times \frac{1\ mol\ of\ Mg}{1\ mol\ of\ Ni} \quad \text{[Eq. 12]}$$

$$Mass\ of\ Mg(NO_3)_2{\cdot}6H_2O\ necessary = \frac{[Eq.12] \times P_m\ Mg(NO_3)_2{\cdot}6H_2O}{P_m\ Mg} \quad \text{[Eq. 13]}$$

$$H_2O \text{ in the solute} = \left[[Eq.\ 11] \times \frac{6 \text{ moles } H_2O \times P_m\ H_2O}{P_m\ Ni(NO_3)_2{\cdot}6H_2O}\right] + \left[[Eq.\ 13] \times \frac{6 \text{ moles } H_2O \times P_m\ H_2O}{P_m\ Mg(NO_3)_2{\cdot}6H_2O}\right] \quad \text{[Eq. 14]}$$

$$H_2O \text{ added} = 24\ mL - [Eq.\ 14] \quad \text{[Eq. 15]}$$

Table 7 shows the amount of support and metallic nitrates precursors need to be added for the preparation of Ni-Mg/BC, Ni-MgCe/BC and Ni-Ce/BC catalysts.

Table 7: The amount of support and precursors added for the catalyst synthesis.

	Ni-Mg/BC	**Ni-MgCe/BC**	**Ni-Ce/BC**
Cellulose (g)		12	
$Ni(NO_3)_2{\cdot}6H_2O$ (g)	2.189	2.271	2.359
$Mg(NO_3)_2{\cdot}6H_2O$ (g)	1.930	1.001	-
$Ce(NO_3)_2{\cdot}6H_2O$ (g)	-	1.696	3.524
H_2O added (mL)		22	

ANNEX C. DESCRIPTION OF CHARACTERIZATION TECHNIQUE

C.1 N_2 adsorption/desorption isotherm

To determine the textural properties of the prepared catalysts, the method of adsorption/desorption of nitrogen at 77 K was used. The equipment used was a TriStar 3000 instrument (Micromeritics Instrument Corp.). Nitrogen adsorption has been used for many years and generally accepted as the standard method in the analysis of micropore and mesopore size. Nitrogen is usually use in the BET surface area analysis due to its availability in high purity and its strong interaction with most solids [47].

The physisorption occurs when the nitrogen gas (adsorbate) is brought into contact with the surface of a solid (adsorbent). The amount of gas adsorbed depends on the exposed surface area but also on the temperature, gas pressure and strength of interaction between the adsorbate and adsorbent [47]. In the case of porous adsorbents, the surface can be divided into an external surface and an internal surface. In general case, the external surface is defined as the surface outside the pores, while the internal surface is the surface of all pore walls. However, in the presence of microporosity, the external surface is defined as the non-microporous surface [36].

Specific surface areas of porous (expressed in m^2/g) were measured from the adsorption branches in the relative pressure range of 0.01 – 0.10 using the BET method (*Brunauer, Emmett, Teller*). Under certain carefully controlled conditions, the BET surface area of a non-porous, macroporous or a mesoporous solid can be regarded as

the effective area available for the adsorption of adsorptive. In addition, it is customary to apply the BET equation in the linear form as the following:

$$\frac{\frac{P}{Po}}{n\left(1-\frac{P}{Po}\right)} = \frac{1}{n_m C} + \frac{C-1}{n_m C}\left(\frac{P}{Po}\right) \qquad \text{[Eq. 16]}$$

where *n* is the specific amount adsorbed at the relative pressure P/Po, n_m is the specific monolayer capacity and according to the BET theory, the parameter C is exponentially related to the energy of monolayer adsorption.

The micropore volume estimation was made by means of the Dubinin-Radushkevich method. Originally, the equation is based on the assumption of a change in the potential energy between the adsorbate and adsorbed phases, and has a semi-empirical origin. The adsorption macroscopic behaviour loading for a given pressure was yielded by this equation [48].

In order to determine the pore-size distribution in a microporous material, the method proposed by Horvath-Kawazoe (HK) method was used. In this method, the mean free energy change of adsorption was calculated when an adsorbate molecule is transferred from the bulk gaseous phase to the condensed phase in a slit pore, and from that an analytic pore filling correlation can be obtained [49]. The HK method is known as one of the simplest adsorption model with some quantitative accuracy on the prediction of pore filling pressure.

C.2 X-Ray diffraction (XRD)

X-ray diffraction (XRD) is a non-destructive technique commonly used to study the structural properties of materials. This technique also used to measure crystallite size and to calculate lattice strain, chemical composition and to determine phase diagrams as well. The areas under the peak are related to the amount of each phase present in the sample. The X-Ray diffraction patterns were recorded within the range of 5 - 90° (2θ) with a Rigaku D/Max 2500 apparatus operated at 3.2 kW (40 kV, 80 mA) and with a rotatory anode of Cu using Cu Kα radiation.

For the XRD analysis, fine powder samples that consist of randomly oriented crystallites were placed on the sample holder. A beam of X-rays is then projected into the sample and interact with electrons in atoms and elastically get scattered. The monochromatic beam of X-rays that scattered at specific angles from each set of lattice planes in a samples can interfere with each other and the waves that are in phase interfere constructively [50]. The conditions of the constructive interference need to satisfy Bragg's Law [Eq. 17]. These diffracted X-rays are then detected, processed and counted. Thus, the information regarding the electron distribution in materials can be obtained from the generated x-ray diffraction pattern. In order to identify the crystalline formed, the x-ray diffraction pattern need to be compared with the standard reference patterns and measurements.

$$n\lambda = 2d\ sin\ \theta \quad \text{[Eq. 17]}$$

where, λ is the wavelength of the x-ray, θ is the scattering angle and n is an integer representing the order of the diffraction peak. In addition, the crystallite sizes of the catalysts also can be determined using the Scherrer equation [51], as follows:

$$L = \frac{K \cdot \lambda}{B \cos \theta} \quad \text{[Eq. 18]}$$

where L denotes the average particle size, K is a constant (K = 0.9), B is the full width at half maximum (FWHM) of the peak, λ is the wavelength of the X-ray radiation (0.15406 nm) and θ is the angle between the beam and the normal on the reflection plane.

C.3 Thermogravimetric analyses in air (TGA-Air)

Thermogravimetric analyses in air (TGA-Air) was carried out to determine the amount of Ni, MgO and CeO_2 deposited on the biomorphic carbon support after the thermal decomposition step during the catalyst preparation. In addition, TGA also represents a useful tool to obtain information regarding the thermal stability of the carbonaceous component in the samples. TGA-Air technique was carried out with a Mettler Toledo TGA/SDTA 851 analyser, using 50 mL/min.

This technique shows the evolution of the weight of the sample with temperature in the presence of oxygen. The weight loss in the samples was due to the decomposition of the carbonaceous material and the oxidation of metals in the catalysts. After the decomposition step in TGA-Air, the remained materials consist of ashes, NiO, MgO and/or CeO_2. The percentage of ashes and the amount of Ni oxidized to NiO was calculated by the difference of initial and final weight of the samples. The Ni, Mg and Ce content was estimated by multiplying the NiO, MgO and CeO_2 with the correspond molecular weight of the metals and divided by the molecular weight of the metal oxide. The stoichiometry of metals loaded on the carbonaceous support also need to be taken into account.

C.4 Transmission electron microscopy (TEM)

Transmission electron microscopy (TEM) micrograph images were recorded by a FEI Tecnai T-20 microscope, operated at 200 kV. This technique was used to study the morphology of the synthesized catalysts.

For the analysis of TEM, a high energy beam of electrons is stroked through a very thin sample and parts of it are transmitted depending upon the thickness and electron transparency of the sample. This transmitted portion is focused by the objective lens into an image on phosphor screen or charge couple device (CCD) camera. The image then passed down the column through the intermediate and projector lenses, is magnified all the way. The darker areas of the image represent those area of the sample that fewer electron are transmitted through while the lighter areas of the image

represent those areas of the sample that more electrons were transmitted through [52]. In this studied case, the darker areas portray the dispersed metals meanwhile the lighter areas illustrate the carbonaceous support in the catalyst.

In addition, other characteristic than can be obtained from the TEM images was the particle size distribution and the average size of the particles. For that purpose, more than 500 particles were measured, which confers an important statistical relevance. The average diameter of the Ni contained particles was calculated using the following expression [18]:

$$\overline{d_p} = \frac{\sum(n_i \cdot {d_i}^3)}{\sum(n_i \cdot {d_i}^2)} \quad \text{[Eq. 19]}$$

where $\overline{d_p}$ is the average diameter of Ni particles and n_i is the number of particles with d_i diameter.

ANNEX D. RESUMEN EXTENDIDO EN ESPAÑOL

D.1 INTRODUCCIÓN

D.1.1 Generación de energía renovable

Tradicionalmente, se han utilizados los combustibles fósiles como el principal recurso en la producción de energía tanto en los países desarrollados como en los desarrollos [1]. En la actualidad, la energía y el calor generados se utilizan para el transporte, la producción industrial y los hogares privados [2]. Como la consecuencia, el consumo mundial de los combustibles fósiles aumenta enormemente en las últimas décadas. Los combustibles fósiles se consumen casi 15 mil millones de toneladas métricas cada año. Estados Unidos, China e India se han propuesto como el mayor consumidor de petróleo del mundo, debido al hecho de que aproximadamente el 54% de los combustibles fósiles del mundo han consumidos por estos tres países [3].

Por otro lado, el riesgo del cambio climático global ha aumentado debido al aumenta del consumo mundial de combustibles fósiles. Uno de los factores detrás del aumento de la concentración de CO_2 en la atmósfera y la temperatura global es la emisión de carbono que ha generada por la combustión de los combustibles fósiles [4]. Según la Administración de Información de Energía de Estados Unidos (2016), las emisiones de CO_2 relacionadas con la energía mundial se estima aumentarán de 32,3 mil millones de toneladas métricas en 2012 a 35,6 mil millones de toneladas métricas en 2020, y alcanzarán 43,2 mil millones de toneladas métricas en 2040 [5].

Por lo tanto, debido al efecto negativo del uso continuado de combustibles fósiles en nuestro planeta y al agotamiento de estos recursos, la utilización de fuentes de energía renovables puede ser necesaria.

Una estrategia importante para mitigar el cambio climático como ha estado de acuerdo del mundo es la utilización de las fuentes de energía renovables. En los últimos años, el desarrollo y la utilización de la generación de energía renovable ha crecido rápidamente en todo el mundo. La energía eólica y la solar fotovoltaica (PV) juegan un papel fundamental en la aceleración del crecimiento de la generación de energía renovable, ya que el potencial de la energía hidroeléctrica, de biomasa o geotérmica es limitado en muchos países [6].

Según [7], la capacidad total de generación de energía renovables en todo el mundo ha alcanzado 2.351 GW a fines de 2018, que es alrededor de un tercio de la capacidad total de eléctrica instalada, ver Figura 1. El aumento anual del 7,9% se vio reforzado por la nueva incorporación de energía solar y eólica, que ha representado el 84% del crecimiento. Mientras tanto, la capacidad de generación no renovable se ha expandido en aproximadamente 115 GW por año (en promedio) desde 2000, sin una tendencia perceptible hacia arriba o abajo. La Agencia Internacional de Energía renovable también ha informado que, la capacidad de generación no renovable ha disminuido en Europa, América del Norte y Oceanía aproximadamente 85 GW desde 2010, pero ha aumentado tanto en Asia como en Medio Oriente durante el mismo período.

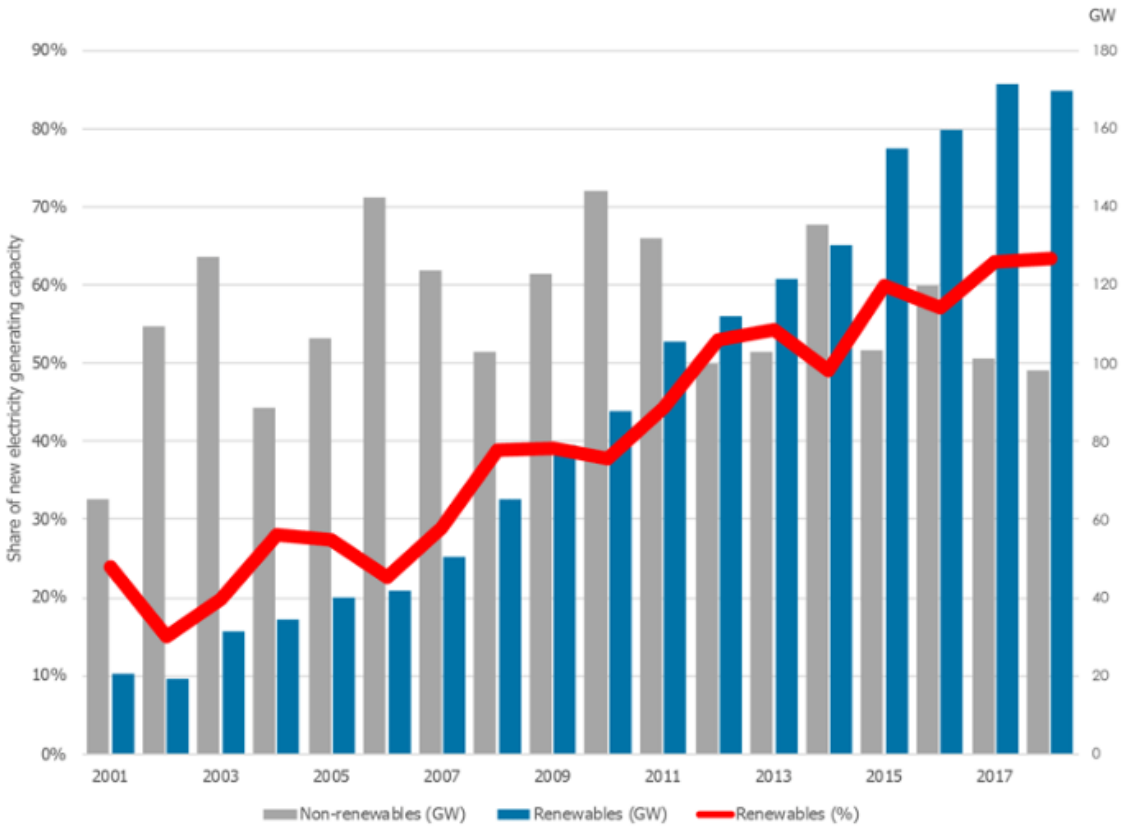

Figura 1. Comparación del crecimiento en la capacidad de generación de energía renovable y no renovable. (Fuente: [7]).

Sin embargo, un problema importante relacionada con estas fuentes renovables es el desajuste de la demanda de carga y el suministro de energía, ya que las fuentes dependen directamente por las condiciones climáticas, la hora del día, la estación y la ubicación. Para solucionar estas dificultades, se necesitan tecnologías eficientes de almacenamiento de energía [2].

Hasta ahora, existen diversas tecnologías de almacenamiento de energía que vienen en muchas formas. El almacenamiento de este tipo de energía a corto plazo solo es posible con el uso de condensadores y bobinas electromagnéticas. No obstante, una forma más económica de almacenar la energía a largo plazo es mediante la conversión de la energía eléctrica a otra forma de energía con el almacenamiento posterior. La transformación de la energía eléctrica en tiempos de generación de energía excesiva por el sol o el viento en compuestos químicos se parece como una alternativa más adecuada para el almacenamiento a largo plazo. Por lo tanto, una tecnología técnicamente realizable que puede resolver el problema mencionado y que se ha demostrado en varios países es el "*Power to Gas*" [8].

D.1.2 Tecnología "***Power to Gas***"

La tecnología "*Power to Gas*" parte de la conversión del exceso de energía eléctrica producida en forma de hidrógeno o metano. Esta tecnología se considera útil porque es la opción de almacenamiento a largo plazo más rentable para la energía. Por otro lado, esta tecnología también se apoyó la descarbonización intersectorial y la sustitución de los recursos energéticos fósiles [9].

El almacenamiento de metano es particularmente ventajoso debido al gran almacenamiento de electricidad a una escala más de 10 GWh y también la existencia de una infraestructura de gran escala, que incluye redes de tuberías, instalaciones de almacenamiento y estaciones de servicio sin coste adicional [2,10]. La conversión de electricidad a metano se lleva a cabo principalmente mediante la combinación de electrólisis y metanación. "*Power-to-methane*" se puede dividir en tres procesos principales, como se muestra en la Figura 2.

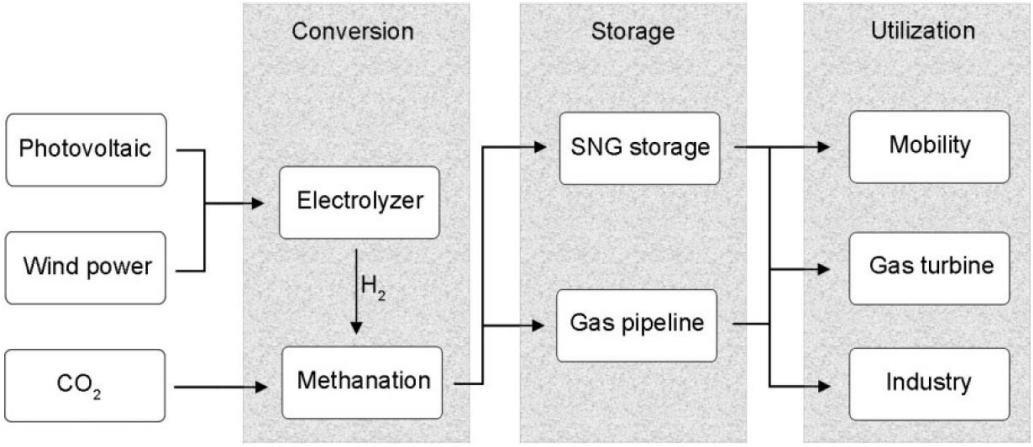

Figura 2: Esquema de flujo del proceso de "Power-to-methane". (Fuente: [8]).

Los inagotables recursos de energía renovable (principalmente recursos de energía eólica y solar) se utilizan para alimentar el electrolizador. Este dispositivo se utiliza para realizar la electrólisis del agua, lo que resulta en la descomposición del agua en hidrógeno y oxígeno [11]. En segundo paso de la cadena del proceso "*power-to-methane*", el H_2 se reacciona con CO_2 para formar CH_4. El CO_2 utilizado en este proceso en cadena se puede obtener de plantas de biomasa, plantas de generación de energía, procesos industriales y aire ambiente; así, al mismo tiempo puede contribuir a la disminución de la emisión de gases de efecto invernadero [12]. El gas natural sintético (SNG) generado por el proceso de metanación que es similar al gas natural puede inyectarse directamente en la tubería de gas natural sin restricción. El proceso de metanación de CO_2 puede llevarse a cabo químicamente o biológicamente [13].

La principal desventaja del concepto de "*power-to-methane*" es la baja eficiencia debido a la larga cadena de procesos. Aparte de eso, la eficiencia disminuirá aún más si no se utiliza el calor producido en el proceso. No obstante, el "*power-to-methane*" promete un almacenamiento a largo plazo y un aceptor de excedente energía procedente de recursos renovables, ya que autoriza la posibilidad de interconectar el mercado de electricidad con lo de calor y combustible [8].

D.1.3 Hidrogenación de CO_2

La hidrogenación catalítica de dióxido de carbono a metano, también se conoce como la reacción Sabatier, es un proceso catalítico importante de interés académico fundamental con potencial aplicación comercial [14,15].

$$CO_2 + 4H_2 \rightarrow CH_4 + 2H_2O \qquad \Delta H_{298K} = -252.9\ kJ\ mol^{-1} \qquad \text{[Eq. 20]}$$

La metanación de CO_2 es fuertemente exotérmica; según la termodinámica, la reacción está favorecida a baja temperatura, alta presión y relaciones H_2/CO_2 superiores a 4. Debido al fuerte carácter exotérmico de la metanación de CO_2, se puede lograr un alto rendimiento de CH_4 a presión atmosférica y a una temperatura de reacción no superiores de 300 °C. Esta reacción es termodinámicamente favorable (ΔG_{298K} = -130.8 kJ/mol); sin embargo, la reducción del CO_2 completamente oxidado a metano es un proceso de ocho electrones con limitaciones significativas, que requiere catalizadores de alta actividad para obtener velocidades de reacción y selectividad al metano adecuadas [16].

D.1.4 Catalizadores

En las últimas décadas, varios metales han sido investigados para la metanación de CO_2. Se ha demostrado que muchos metales del grupo VIIIB en la tabla periódica pueden catalizar la metanación de CO_2 y se encontró que los metales como Rh, Ru, Ni y Co son muy activos para esta reacción [17]. Sin embargo, los catalizadores de níquel soportados siguen siendo los materiales más ampliamente estudiados debido a su bajo coste y fácil disponibilidad. Los catalizadores de Ni presentan gran actividad solo a altas temperaturas 300 – 450 °C. A las temperaturas inferiores de 300 °C, la interacción entre

Ni y CO puede conducir a la formación de subcarbonilos de níquel móviles; que es muy tóxico para los organismos humanos y al mismo tiempo responsable en la desactivación de los catalizadores [18]. Por lo tanto, la conversión y rendimiento de los catalizadores de Ni que se vaya a obtener en la metanación de CO_2 depende de varios parámetros, como el efecto del soporte, la carga de Ni, la presencia del segundo metal y el método de preparación del catalizador.

A pesar de alta actividad de los catalizadores de Ni, este tipo de catalizadores son propensos a la desactivación por deposición de coque y sinterización de los metales a altas temperaturas de reacción [19]. Una solución interesante para superar este problema, que ha sido ampliamente estudiado en los últimos años, es la adición de promotores de metales.

La adición de aditivos alcalinos, especialmente MgO, puede mejorar efectivamente la alcalinidad de la superficie por aumentando la capacidad de adsorción de CO_2 y acelerando la activación de CO_2. Además, la cantidad apropiada de aditivo de MgO en catalizadores basados en Ni soportados fue beneficiosa para el rendimiento de la metanación de CO_2 debido al incremento en la dispersión de especies de Ni y la activación efectivamente de CO_2 sobre la superficie del MgO [20,21,22]. Según [23], las nanopartículas de Ni que altamente dispersas pueden aumentar la actividad a baja temperatura para la metanación de CO_2 al facilitar la disociación de H_2, generando abundante el hidrógeno disociado en superficie para la eliminación de los carbonilos de níquel formados.

El empleo de metales adecuados y/o sus óxidos como promotores es una estrategia común para mejorar la actividad y estabilidad de los catalizadores basados en Ni. La extensa utilización de Ce en el campo de la catálisis ha llamado mucho la atención debido a sus altas propiedades de redox [24]. Ceria tiene un buen potencial de reducción-oxidación de Ce^{4+}/Ce^{3+}, acompañada de una alta capacidad de almacenamiento de oxígeno y la presencia de vacantes de oxígeno [22,25,39]. Recientemente, los estudios han encontrado que la adición de material que contiene CeO_2 al catalizador basados en Ni podría promover efectivamente la adsorción y la activación de CO_2 en la reacción de metanación [26]. Además, la incorporación de CeO_2 podría aumentar la interacción entre el soporte y el componente activo de metal y también controlar el crecimiento de partículas de Ni, entonces como la consecuencia, se puede mejorar la prestación catalítica de los catalizadores basados en Ni [27].

D.1.5 El soporte carbonoso biomórfico

La naturaleza del soporte tiene una influencia significativa sobre la morfología, dispersión y reducibilidad de la fase activa y las propiedades catalíticas de los catalizadores. En los últimos años, se ha prestado atención a los materiales carbonosos, un material versátil y muy respetuoso con el medio ambiente. Algunas de las características de este material como una gran superficie específica, alta porosidad, excelente conductividad electrónica, presencia de una gran variedad de grupos funcionales de superficie y la relativa inercia los hacen interesantes para ser utilizados como catalizadores o soportes catalíticos [28,29]. Una ventaja de los materiales

carbonosos es que pueden prepararse a partir de desechos de biomasa, particularmente desechos lignocelulósicos [30].

El proceso basado en la descomposición de materiales lignocelulósicos utilizando una atmósfera reductora o inerte a altas temperaturas y altas velocidades de calentamiento se denomina mineralización biomórfica. Esta novedosa técnica es una herramienta poderosa que permite convertir estructuras formadas por un proceso biológico, por ejemplo, madera y biomasa lignocelulósica en materiales inorgánicos que pueden ser útiles en una amplia gama de aplicaciones [31]. Además, si la materia prima (e.g. celulosa) se impregna previamente con una solución de precursores metálicos, se puede obtener el catalizador en un solo paso [32]. A través de esta técnica, se puede obtener el catalizador formado por las nanopartículas metálicas altamente dispersas sobre el soporte carbonoso biomórfico (BC) [33]. Este método ha demostrado su versatilidad mediante la cual se pueden utilizar diferentes materias primas de lignocelulosa para sintetizar catalizadores de gran variedad de composiciones y contenidos metálicos [34].

D.1.6 Objetivos

El objetivo general de esta tesis de fin de grado ha sido el estudio del rendimiento catalítico de catalizadores de Ni soportados sobre carbono derivado de celulosa, modificado con la adición de óxidos de Ce y/o Mg.

En este trabajo, una serie de catalizadores bimetálicos: Ni-Mg y Ni-Ce; y un catalizador multi-metálico: Ni-MgCe soportado sobre carbono derivado de celulosa, también denominado carbono biomórfico, se han preparado mediante la técnica de mineralización biomórfica, con relaciones molares nominales de Ni/Mg o Ce y Ni/Mg/Ce de 1/1 y 1/0,5/0,5, respectivamente. Los catalizadores sintetizados se han caracterizado por la isoterma de adsorción de nitrógeno, difracción de rayos X (XRD), análisis termogravimétrico en aire (TGA-Aire) y microscopía electrónica de transmisión (TEM). La metanación de CO_2 se ha investigado en un reactor de flujo continuo de lecho fijo, a presión atmosférica, a temperatura de 325 °C, con elevada velocidad espacial de 60.000 h^{-1} y a relación molar estequiométrica de H_2/CO_2. Para optimizar los resultados obtenidos en la reacción de metanación de CO_2, así como la estabilidad de los catalizadores se ha estudiado el efecto de las principales condiciones de operación (e.g. temperatura de reacción y relación molar de H_2/CO_2) sobre la prestación catalítica de los catalizadores.

D.2 RESULTADOS Y DISCUSIÓN

En esta sección, se discuten los resultados experimentales obtenidos de la caracterización de los catalizadores y el estudio de la metanación de CO_2 utilizando tres catalizadores diferentes basados en Ni soportados sobre carbono biomórfico. El objetivo es determinar la influencia de diversas variables del proceso, como la composición de los catalizadores, la temperatura de la reacción y la composición de la alimentación sobre la actividad catalítica, la estabilidad y la selectividad del metano deseado.

D.2.1 Caracterización de los catalizadores

D.2.1.1 Isoterma de adsorción-desorción de N_2

El efecto de la textura en la adición de Mg y Ce sobre el soporte carbonoso se estudió mediante adsorción de N_2. La Figura 3 muestra la isoterma de adsorción/desorción de N_2 de los catalizadores sintetizados: Ni-Mg/BC, Ni-Ce/BC y Ni-MgCe/BC con un contenido nominal de 3,5% en peso de Ni respecto a la cantidad inicial de celulosa.

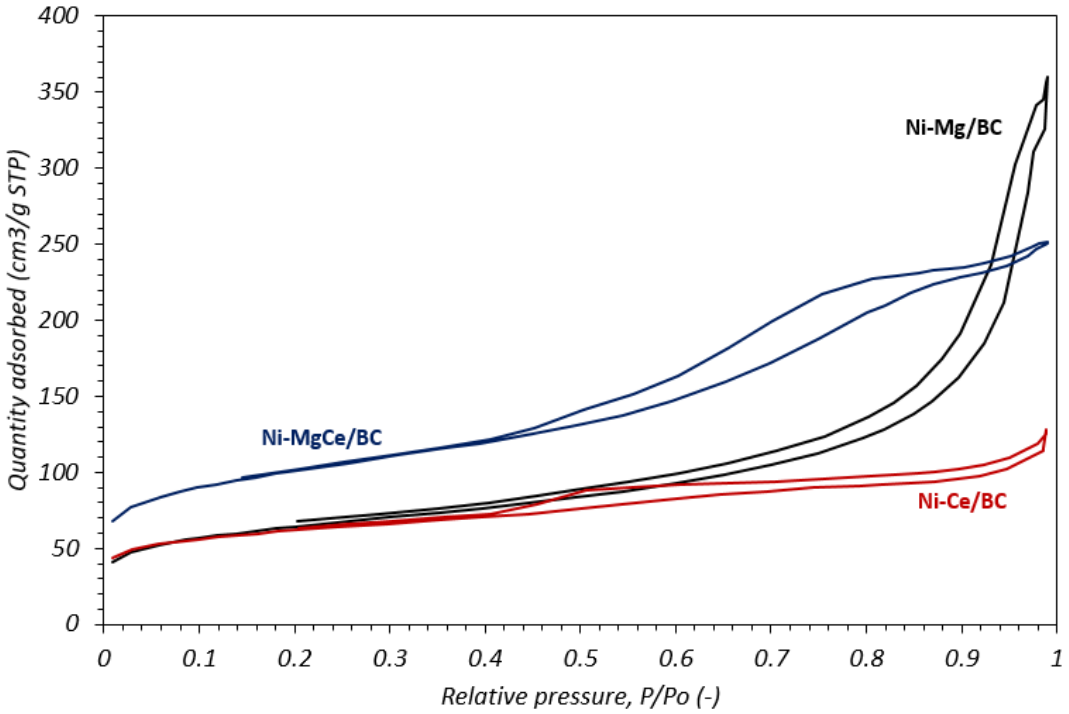

Figura 3. Isoterma de adsorción/desorción de N_2 obtenida para los catalizadores Ni-Me/BC.

Según la clasificación IUPAC, la isoterma corresponde al tipo II con un ciclo de histéresis de tipo H3 o H4. Estas isotermas de tipo II son el resultado de la adsorción sin restricciones de monocapa y multicapa. En la región de baja presión relativa, donde tiene lugar el llenado de microporos, que se considera como un proceso primario de fisisorción, se ha observado una curvatura más gradual que indica que hubo una

cantidad significativa de superposición de la cobertura monocapa y el inicio de la adsorción multicapa [35,36]. Mientras tanto, el llenado de mesoporos anchos comienza a ocurrir a alta presión relativa [37]. El comportamiento de la fisisorción en los mesoporos es distinto de los fenómenos de adsorción que ocurren en los microporos. La adsorción monocapa y la adsorción multicapa que pueden conducir a la condensación de poros muy probablemente puede ocurrir en los mesoporos. El grosor de la multicapa adsorbida en los mesoporos generalmente aumenta con la presión relativa [36]. En el caso de Ni-Mg/BC, se observó la presencia de multicapa adsorbida gruesa y después de la adición de Ce, se ha modificado la textura del catalizador. La formación de adsorción multicapa menos gruesa se puede ver claramente en el catalizador de Ni-MgCe/BC. Para el caso de Ni-Ce/BC, el espesor de la multicapa adsorbida apenas aumenta con la presión relativa.

En la Tabla 3 se muestra los valores del área de superficie BET, el volumen total de poro, el volumen de microporos y el diámetro promedio de poro de los catalizadores sintetizados. Se descubrió que el área de superficie BET de Ni-Mg/BC era de 228 m^2/g con un 21% de volumen de microporos. Por otro lado, el área de superficie BET para los catalizadores de Ni-MgCe/BC y Ni-Ce/BC fue de 359 m^2/g y 357 m^2/g con un porcentaje de volumen de microporos del 46% y 57%, respectivamente.

Tabla 3. Las propiedades de textura de los catalizadores Ni-Me/BC.

Catalizadores	**Superficie BET (m^2/g)**	**Volumen de poro (cm^3/g)**	**Volumen de microporo (cm^3/g)**	**Diámetro promedio de poro (nm)**
Ni-Mg/BC	228	0.556	0.116	28.3
Ni-MgCe/BC	359	0.389	0.177	3.3
Ni-Ce/BC	357	0.179	0.102	1.4

Tras la incorporación de Ce, se ha mejorado el área de superficie BET. Este efecto puede atribuirse a la formación de pequeños cristalitos de CeO_2, que introducen algún efecto geométrico que provoca el desarrollo de una nueva estructura mesoporosa. La distribución del tamaño de poro para los catalizadores Ni-Mg/BC y Ni-MgCe/BC se indica un carácter mesoporoso (2-50 nm, según clasificación IUPAC) mientras que el catalizador Ni-Ce/BC se muestra el carácter microporoso (<2 nm). Claramente, la adición del promotor Ce crea poros más pequeños y aumenta la microporosidad de los catalizadores. Sin embargo, la otra consecuencia de la adición del promotor Ce conduce a la reducción del volumen de poros. Las diferencias entre el volumen de poros y el comportamiento del área de superficie se atribuyeron al hecho de que las partículas metálicas contribuyeron con un área de superficie adicional pero no con un volumen de poro adicional [40].

D.2.1.2 Difracción de rayos X (XRD)

Los patrones XRD de las diferentes muestras de catalizadores de Ni-Mg/BC, Ni-MgCe/BC y Ni-Ce/BC se muestran en la Figura 4. El estudio de XRD en las muestras de catalizador se ha realizado para determinar el tamaño cristalino e identificar la presencia de la fase de material cristalino sobre la capa superficial de catalizadores.

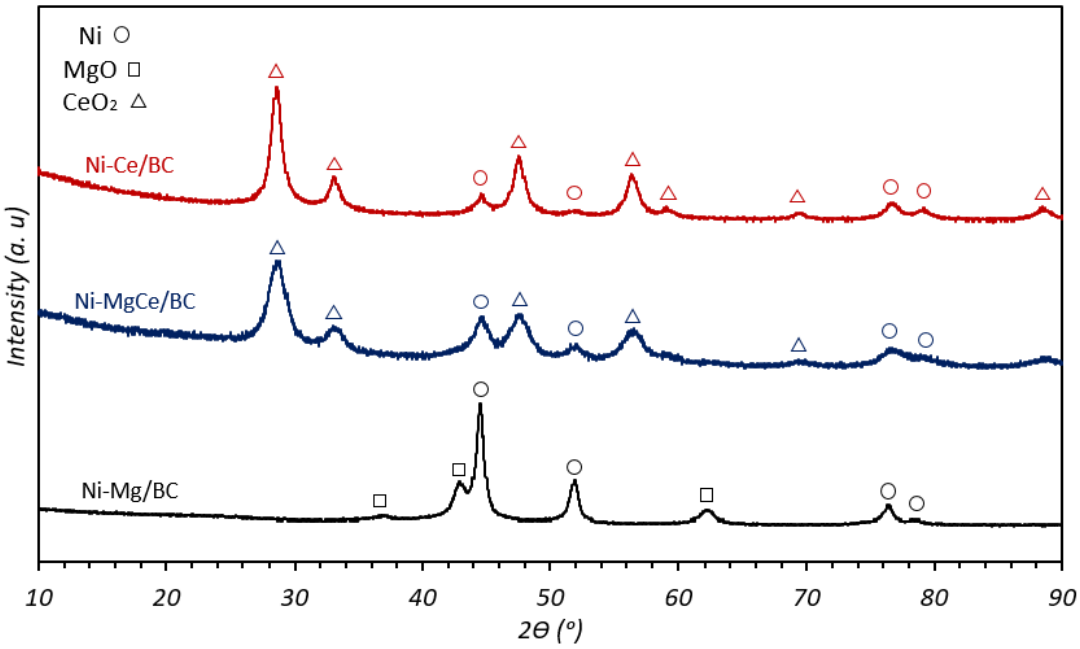

Figura 4. Los patrones XRD de catalizadores de Ni-Mg/BC, Ni-MgCe/BC y Ni-Ce/BC.

En todos los casos estudiados, los picos obtenidos corresponden solo a Ni metálico. No hubo picos asociados a NiO. El pico agudo de Ni se detectó a 2-Theta (2θ) alrededor de 44.5° en el catalizador de Ni-Mg/BC con un tamaño promedio de cristalito de aproximadamente 17 nm. En los catalizadores Ni-MgCe/BC y Ni-Ce/BC, se encontró que el pico identificado de Ni era menos intenso, lo que indica menos contenido de la presencia de Ni después del paso de descomposición durante la preparación. El tamaño promedio de cristalito de las partículas de Ni en los catalizadores Ni-MgCe/BC y Ni-Ce/BC fue de 8 nm y 10 nm, respectivamente. Como se esperaba, la adición del promotor Ce disminuyó el tamaño promedio de cristalito de las partículas de Ni.

Los patrones XRD muestran la reflexión típica de CeO_2 a valores de 2-Theta (2θ) de 28.5°, 33.1°, 47.5°, 56.5° y 69.3° en catalizadores Ni-MgCe/BC y Ni-Ce/BC. Se observó un pico más intenso de CeO_2 en el catalizador Ni-Ce/BC con un tamaño de cristalito promedio de 9 nm mientras que en lo del catalizador Ni-MgCe/BC es igual a 6 nm.

Además, se observaron tres picos de difracción relacionados con MgO en el catalizador de Ni-Mg/BC con un tamaño de cristalito promedio de 8 nm, mientras que en el catalizador de Ni-MgCe/BC no se detectaron picos de cristal. El tamaño de partícula de MgO en el catalizador de Ni-MgCe/BC no se puede estimar, debido a baja

concentración de estos óxidos metálicos que se dispersó altamente sobre la superficie del catalizador y no es detectable por análisis XRD.

La caracterización de las muestras gastadas se realizó para dilucidar las razones por las cuales la actividad de los catalizadores basados en Ni cambió durante la prueba de estabilidad. Las muestras utilizadas se eliminaron de la configuración experimental para poder caracterizar por XRD y TEM (ver sección D.2.1.4). La comparación de los patrones XRD de los catalizadores Ni-Mg/BC, Ni-MgCe/BC y Ni-Ce/BC usados con las muestras frescas se puede observar en la Figura 5.

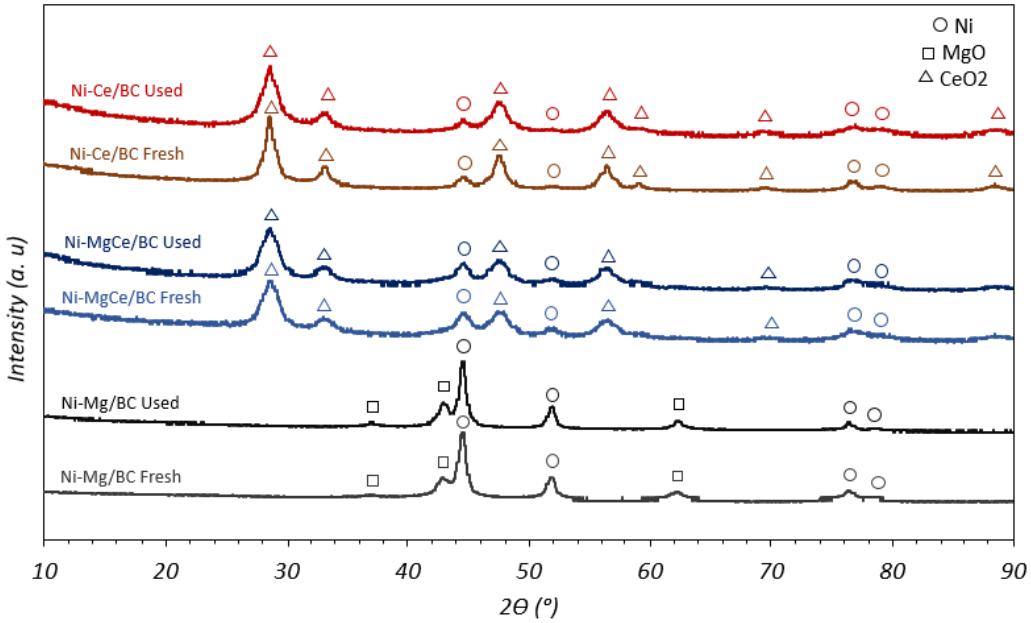

Figura 5. Comparación del patrón XRD para los catalizadores frescos de Ni-Me/BC y los catalizadores usados en la metanación reacción.

Sorprendentemente, los patrones de XRD para todos los catalizadores sintetizados no detectan la presencia de partículas de NiO, lo que significa que no ocurre la reducción de Ni metal después de la reacción de metanación. Además, no se observaron cambios notables en los picos de cada fase de los catalizadores después de la reacción de CO_2 con hidrógeno a 325 °C a lo largo de 8h. A pesar de eso, hubo un ligero cambio en el tamaño promedio de cristalito de las partículas calculadas por la ecuación de Scherrer [39] como se informa en la Tabla 4.

Tabla 4. Estimación del tamaño cristalito de Ni, MgO y CeO_2 calculados por la ecuación de Scherrer antes y después de la reacción.

	Catalizador fresco			Catalizador usado		
Catalizadores/ dp (nm)	**Ni**	**MgO**	**CeO_2**	**Ni**	**MgO**	**CeO_2**
Ni-Mg/BC	17	9	-	19	11	-
Ni-MgCe/BC	8	-	6	9	-	6
Ni-Ce/BC	10	-	9	12	-	6

Los resultados de los tamaños de cristal de Ni, MgO y CeO_2 después de la reacción, medidos por la ecuación de Scherrer, sugirieron que el aumento en los tamaños de cristalito se debió a la sinterización de las partículas [8]. La presencia de ambos promotores Mg y Ce en el catalizador Ni-MgCe/BC redujo la sinterización de Ni y probablemente puede alargar la vida útil del catalizador. También se encuentra que no se ha producido la sinterización de CeO_2. En el caso del catalizador Ni-Ce/BC, se produjo la sinterización de Ni y aumentó el tamaño del cristalito de 10 nm a 12 nm. En contraste, el tamaño de cristalito de CeO_2 ha disminuido de 9 nm a 6 nm.

D.2.1.3 El análisis termogravimétrico en aire (TGA-Aire)

Los análisis termogravimétrico en el aire (TGA-Aire) se llevan a cabo para determinar la composición cuantitativa de los metales presencia en los catalizadores soportados por carbón biomórficos. La Figura 6 se muestra las curvas TGA-Aire para los catalizadores de Ni-Me/BC sintetizados.

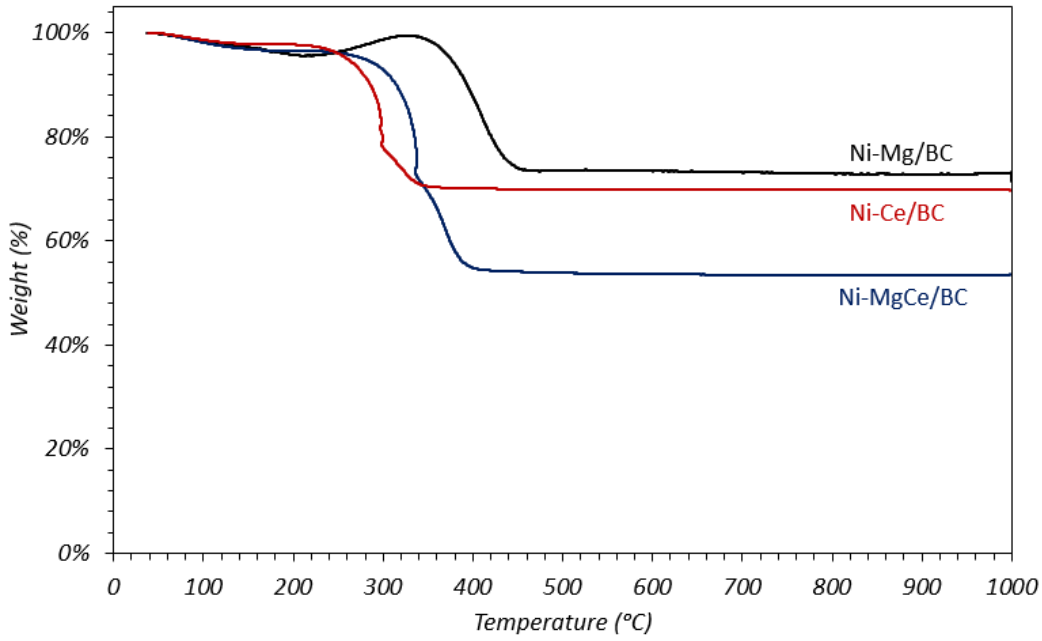

Figura 6. Análisis de TGA-Aire de los catalizadores Ni-Me/BC.

Según [41,42], la combustión de carbón biomórfico se produce en el intervalo de temperatura de 470 °C y 650 °C. Como se muestra en la Figura 6, la curva TGA-Aire para el catalizador Ni-Mg/BC muestra una pérdida de peso que comienza desde aproximadamente 345 °C hasta 460 °C. Mientras tanto, para los catalizadores Ni-MgCe/BC y Ni-Ce/BC, los picos de combustión aparecen a una temperatura de 250 °C y 230 °C, respectivamente. La combustión de carbón biomórfico en estos tres catalizadores sintetizados se ha producido a una temperatura inferior a la mencionada en [41,42] debido al efecto catalítico del Ni durante la combustión [43]. Además, entre la temperatura de 250 °C y 345 °C, se observó un notable aumento de peso en la curva TGA de Ni-Mg/BC. Esta situación probablemente se atribuye a la oxidación de Ni a NiO. No se detectó un aumento de peso significativo en los catalizadores de Ni-MgCe/BC y Ni-Ce/BC debido a la menor presencia de Ni metálico en el soporte de carbón biomórfico en comparación con los catalizadores de Ni-Mg/BC como se muestra en la Tabla 5.

Tabla 5. Porcentaje de Ni, Mg, Ce y BC presentes en los catalizadores Ni-Me/BC.

Catalizadores/ Composiciones (%)	**Ni**	**Mg**	**Ce**	**BC**
Ni-Mg/BC	42%	18%	-	40%
Ni-MgCe/BC	20%	4%	24%	52%
Ni-Ce/BC	19%	-	46%	35%

Según los resultados de XRD, después de la etapa de descomposición durante la preparación, se encontraron partículas de Ni, MgO y CeO_2 en los catalizadores sintetizados correspondientes. Después de la oxidación en los análisis TGA-Aire, los materiales restantes encontrados en Ni-Mg/BC fueron cenizas, NiO y MgO; cenizas, NiO, MgO y CeO_2 en el caso de Ni-MgCe/BC; y cenizas, NiO y CeO_2 en el caso de Ni-Ce/BC. Como se esperaba, los porcentajes en peso de Ni, Mg y Ce aumentaron en los catalizadores finales en comparación con la cantidad inicial en la celulosa bruta debido a la pérdida de material carbonoso en la etapa de descomposición térmica durante la síntesis del catalizador. De hecho, la descomposición térmica es el factor crucial para controlar el contenido final y la dispersión de los metales sobre la superficie del catalizador [44].

D.2.1.4 Microscopía electrónica de transmisión (TEM)

La morfología de los catalizadores sintetizados se investigó utilizando microscopía electrónica de transmisión (TEM). La Figura 7 muestra las imágenes TEM de los catalizadores Ni-Me/BC nuevos y usados.

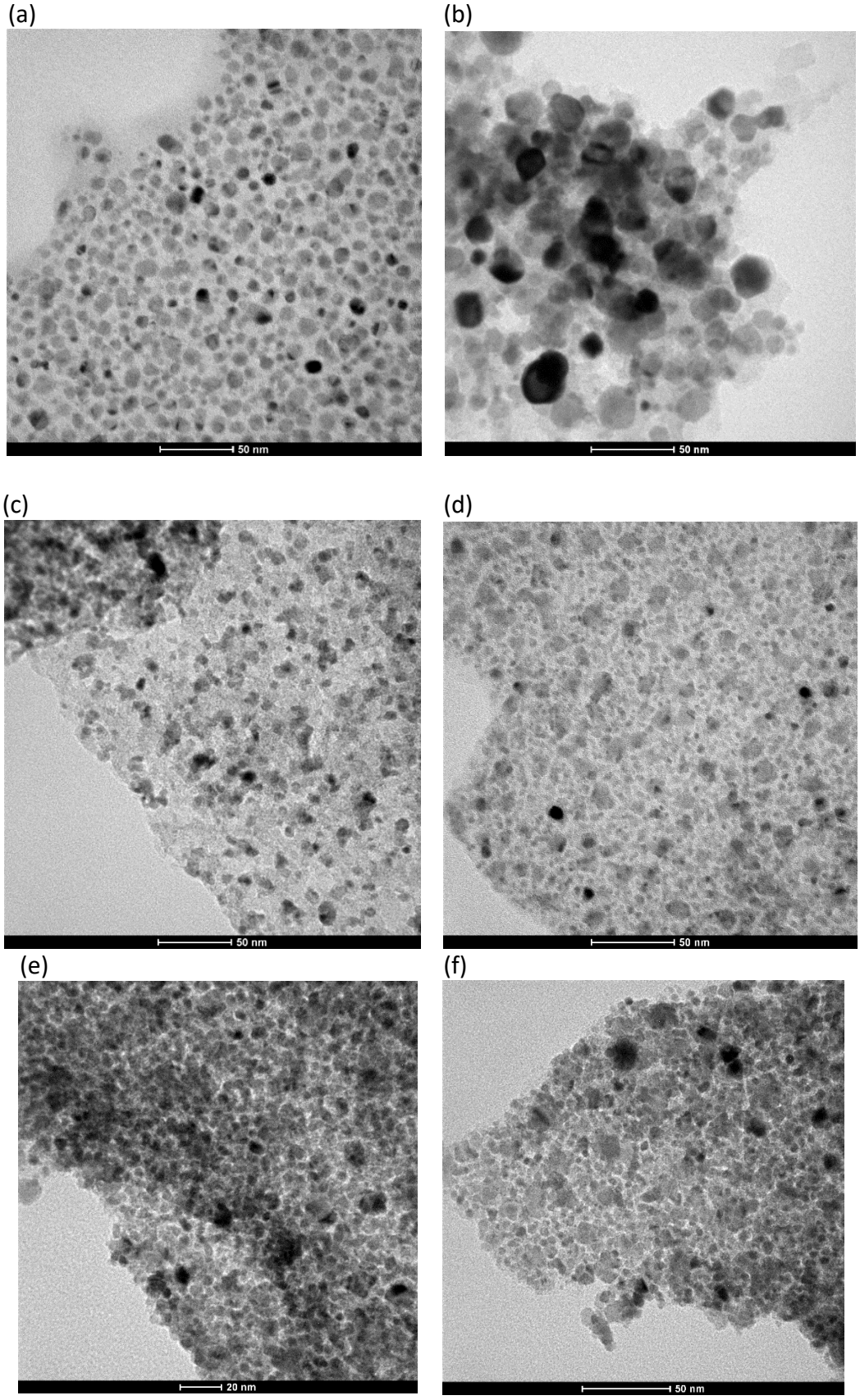

Figura 7. Imágenes obtenidas por TEM del catalizador de Ni-Mg/BC (a) fresco (b) usado, catalizador de Ni-MgCe/BC (c) fresco (d) usado y catalizador de Ni-Ce/BC (e) fresco (f) usado.

Nuevos catalizadores de Ni-Mg/BC (Figura 7a), Ni-MgCe/BC (Figura 7c) y Ni-Ce/BC (Figura 7e), tras la descomposición térmica a 600 °C, parecen tener una alta dispersión de partículas de metales sobre el soporte carbonosos, presentando distribuciones estrechas de 10.7 ± 2.8 nm, 9.6 ± 2.1 nm y 8.9 ± 2.3 nm, respectivamente.

Después de la reacción de CO_2 con hidrógeno a lo largo de 8h, las partículas se mantuvieron bien dispersas, aunque se observaron partículas más grandes. La imagen de TEM para el catalizador de Ni-Mg/BC después de la reacción (Figura 7b) muestra que se ha producido agregación de las partículas. El tamaño medio de partícula es 18.8 ± 6.1 nm.

El tamaño promedio de partícula para los catalizadores sintetizados determinados por la técnica TEM se muestra en la Tabla 6. Asimismo, el tamaño estimado de las partículas calculadas por la ecuación de Scherrer en el método XRD (Tabla 4) parece estar en un acuerdo razonable con los resultados de TEM. Por lo tanto, a partir de los resultados obtenidos para la caracterización por XRD y TEM antes y después de la reacción de metanación, la estabilidad térmica de los catalizadores disminuye en el siguiente orden: Ni-MgCe/BC > Ni-Ce/BC > Ni-Mg/BC [45].

Tabla 6. El tamaño promedio de partícula calculado por la técnica TEM para los catalizadores Ni-Me/BC nuevos y usados.

Catalizadores/dp promedio (nm)	**Nuevo**	**Usado**
Ni-Mg/BC	10.7 ± 2.8	18.8 ± 6.1
Ni-MgCe/BC	9.6 ± 2.1	9.9 ± 2.7
Ni-Ce/BC	8.9 ± 2.3	8.6 ± 2.2

C.2.2 Estudio sobre la actividad catalítica

Para estudiar la actividad catalítica de cada catalizador, se realizó el análisis del efecto de la temperatura de reacción. Después de una reducción in situ del catalizador de 10 minutos, se alimentaron en el reactor 700 mL/min de gases mezclados con relación de H_2:CO_2 = 4:1 y el resto N_2 para la evaluación catalítica. Los datos de actividad en estado estacionario a diferentes temperaturas se midieron durante 30 minutos de reacción para cada temperatura, comenzando desde la temperatura más alta que es 500 °C y se disminuyó hasta que no se detectó más conversión de CO_2.

D.2.2.1 Comparación del rendimiento catalítico de los catalizadores Ni-Me/BC sintetizados

La Figura 8 muestra la comparación de la conversión de CO_2, selectividad y rendimiento de CH_4 para los catalizadores sintetizados en función de la temperatura de reacción para determinar qué catalizador tiene un mejor rendimiento para la metanación de CO_2.

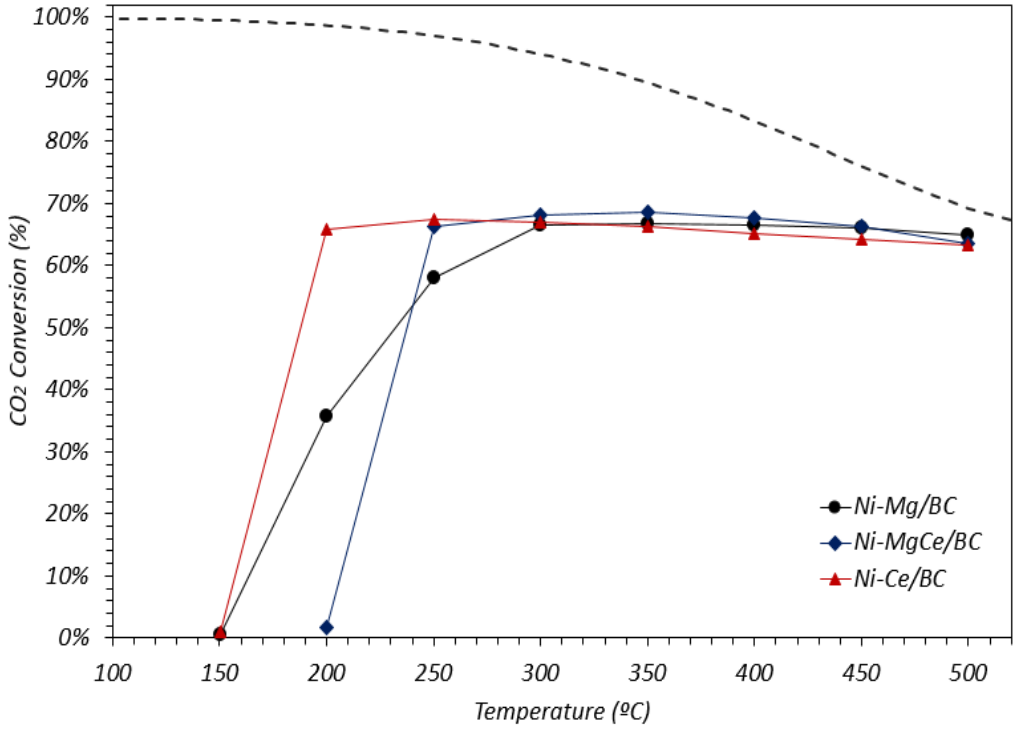
100%
90%
80%
70%
60%
50%
40%
30%
20%
10%
0%
CO2 Conversion (%)
100
150
200
250
300
350
400
450
500
Temperature (ºC)
Ni-Mg/BC
Ni-MgCe/BC
Ni-Ce/BC

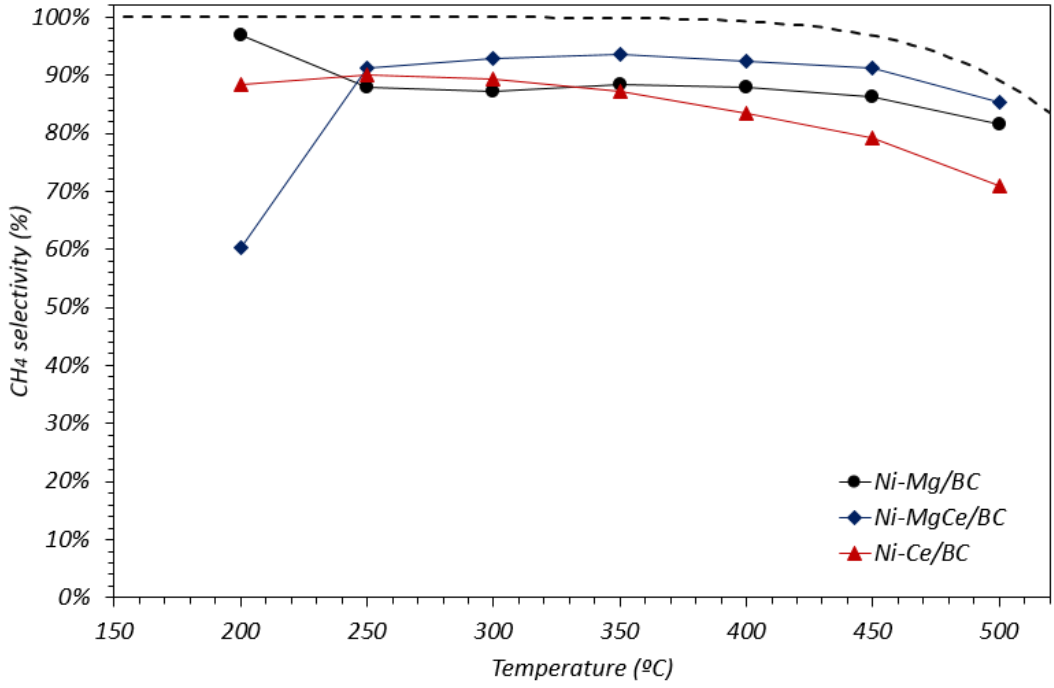
100%
90%
80%
70%
60%
50%
40%
30%
20%
10%
0%
CH4 selectivity (%)
150
200
250
300
350
400
450
500
Temperature (ºC)
Ni-Mg/BC
Ni-MgCe/BC
Ni-Ce/BC

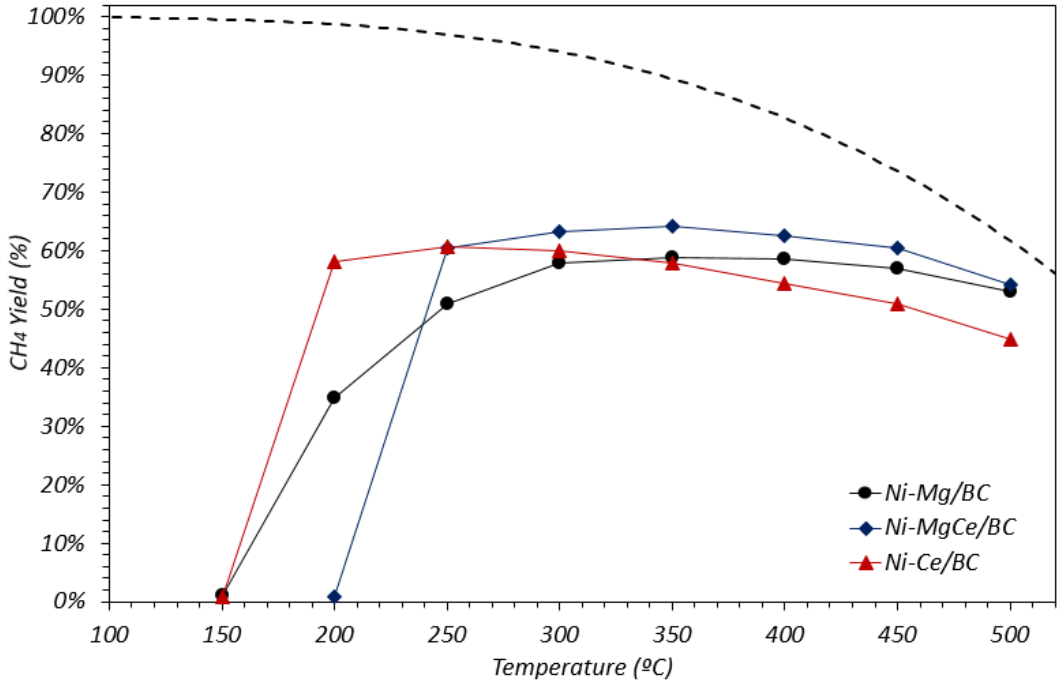

Figura 8. Comparación del rendimiento catalítico para la metanación de CO_2 de catalizadores Ni-Me/BC. Las líneas discontinuas representan los valores de equilibrios.

La conversión de CO_2 lograda por estos tres catalizadores dentro del rango de 300 °C a 500 °C no muestra una gran diferencia. Sin embargo, la mayor conversión de CO_2 (68,7%) obtenida fue por catalizador de Ni-MgCe/BC a 350 °C. Como se puede ver en la figura, la selectividad del CH_4 deseado alcanzado por Ni-MgCe/BC estaba muy cerca a los valores de equilibrio en comparación con los demás con el valor máximo de 93,5% a 350 °C. Además, el rendimiento máximo de CH_4 (64,2%) fue alcanzado también por Ni-MgCe/BC a la temperatura de 350 °C. El rendimiento catalítico general para estos tres catalizadores siguió el orden general Ni-MgCe/BC > Ni-Ce/BC > Ni-Mg/BC, que se puede ver claramente en la Figura 9. Como se esperaba, el catalizador Ni-MgCe/BC exhibe la actividad catalítica más alta debido a la mayor área de superficie de BET y al alto volumen de microporos caracterizado por la técnica de isoterma de adsorción-desorción de N_2.

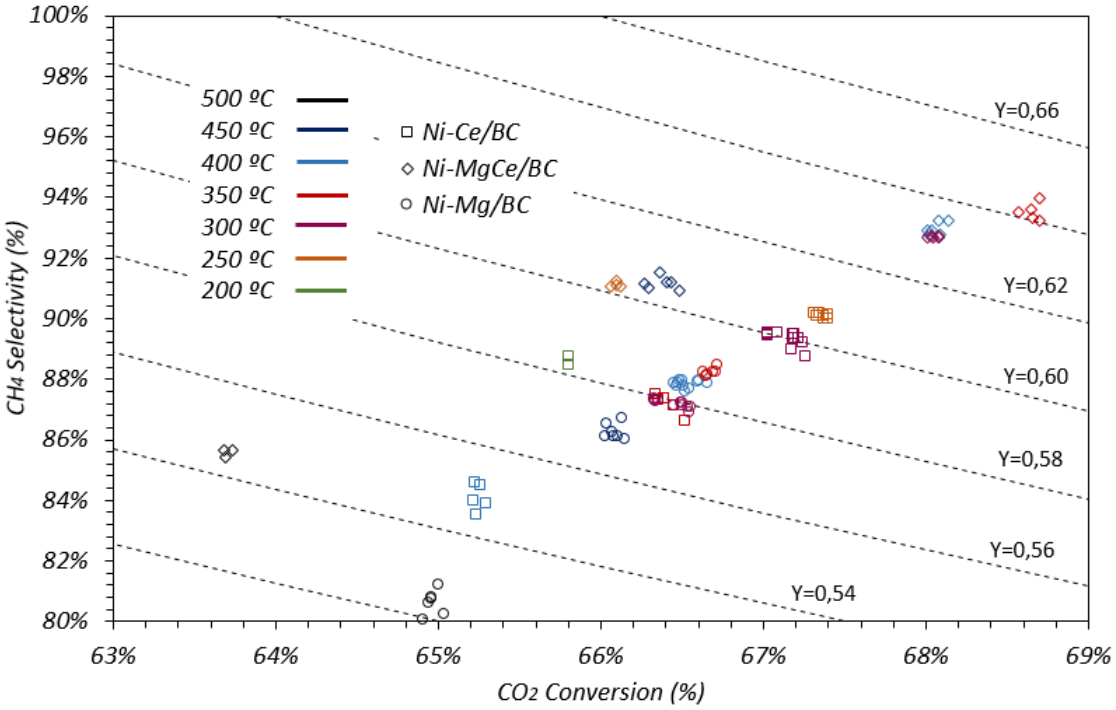

Figura 9. El resumen del rendimiento catalítico de los catalizadores Ni-Me/BC.

D.2.3 Estudio sobre la estabilidad de catalizador

Se ha realizado una prueba catalítica adicional sobre los catalizadores Ni-Me/BC para estudiar el comportamiento catalítico en términos de estabilidad y actividad a una temperatura constante de 325 °C continuamente durante 8h. Antes de la reacción, el catalizador sintetizado se redujo en atmósfera reductora (50% H_2, 50% N_2) a 500 °C por 10 minutos. Luego, se introdujo un flujo constante de 700 mL/min de gases mezclados en el reactor con una relación estequiométrica de H_2/CO_2 para comenzar la prueba de estabilidad.

D.2.3.1 Comparación de estabilidad de los catalizadores Ni-Me/BC sintetizados

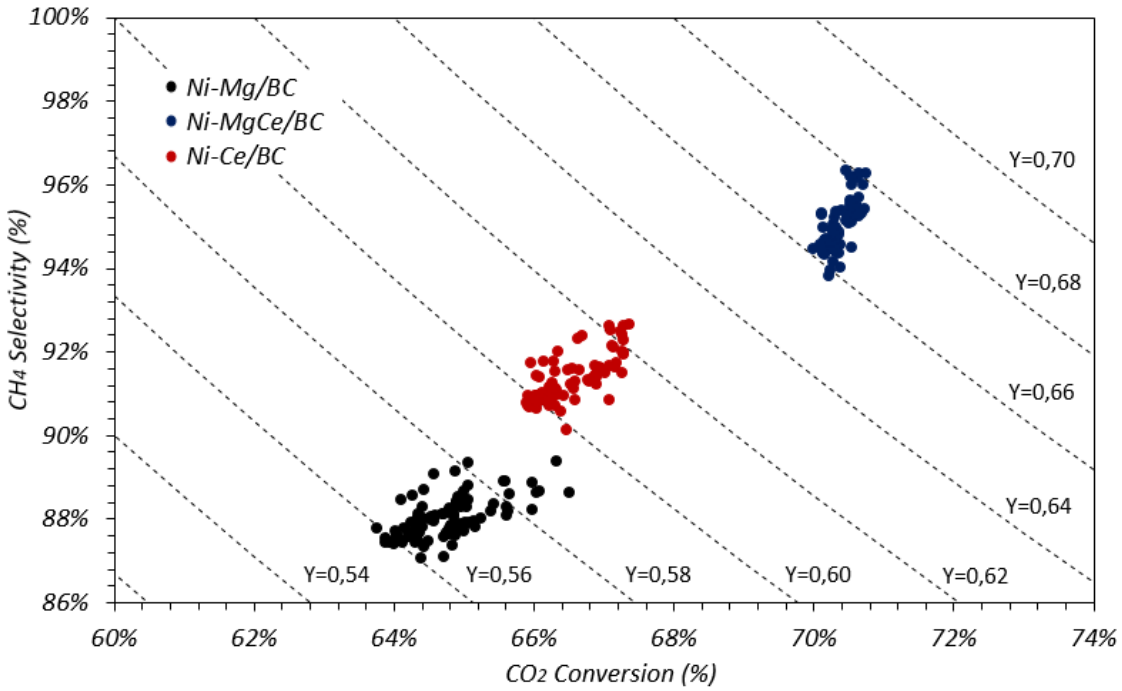

Figura 10. El resumen de estabilidad de catalizadores Ni-Me/BC por 8h en la corriente.

La Figura 10 muestra el resumen de los estudios de estabilidad de catalizadores en la metanación de CO_2. Como se puede observar, no se detectaron cambios significativos en los valores de conversión de CO_2, selectividad y rendimiento del CH_4 deseado, lo que indica que todos los catalizadores fueron muy estables por las 8 horas en la corriente. A pesar de tener los mismos valores de conversión de CO_2 y H_2, selectividad y rendimiento del CH_4 deseado, antes y después de 8h en la corriente, se detectaron ligeros cambios en los catalizadores de Ni-Mg/BC (aproximadamente 4%), Ni-Ce/BC (aproximadamente 1%) y no se detectaron cambios en los valores obtenidos por el Ni-MgCe/BC. Dichas disminuciones ocurridas en el rendimiento de los catalizadores se debieron a la sinterización de partículas sobre la superficie del soporte carbonosos. Como se predijo, la estabilidad de los catalizadores disminuye en el siguiente orden: Ni-MgCe/BC > Ni-Ce/BC > Ni-Mg/BC.

D.2.4 Estudio en la variación de la relación molar de H_2:CO_2 sobre el rendimiento catalítico del catalizador Ni-MgCe/BC

En la prueba de actividad catalítica y estabilidad que se realizó previamente se demostró que el catalizador Ni-MgCe/BC es el más activo entre los tres catalizadores. Por lo tanto, este experimento se llevó a cabo para examinar el rendimiento del catalizador en la relación estequiométrica por debajo y por encima del equilibrio. También es para determinar la concentración ideal de gas H_2 y CO_2 en la alimentación y la temperatura de reacción.

D.2.4.1 Comparación del rendimiento catalítico de las diversas concentraciones de H_2 a temperatura constante

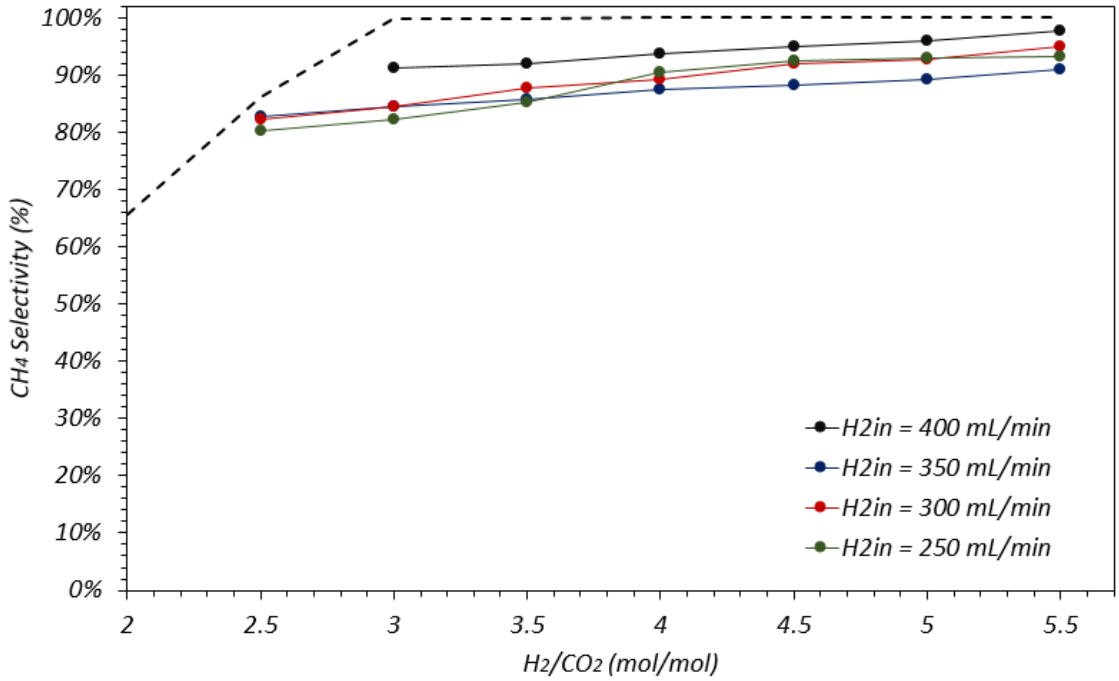

Figura 11. Rendimiento catalítico de diferentes concentraciones de H_2 en función de la relación molar H_2/CO_2 a 325 °C.

La Figura 11 se muestran el rendimiento catalítico de las diferentes concentraciones de H_2 a la entrada en función de la relación molar H_2:CO_2 a una temperatura constante de 325 °C; los valores de equilibrio también se informaron para comparación. No se observaron diferencias notables en el resultado de la conversión de CO_2 para las diversas concentraciones de entrada de H_2. Sin embargo, en la selectividad y rendimiento del CH_4 deseado, el rendimiento del catalizador con una concentración de H_2 de entrada de 400 mL/min fue mucho más cercano a los valores de equilibrio. Curiosamente, el rendimiento del catalizador con varias concentraciones de entrada de H_2 disminuye en el siguiente orden: 400 mL/min > 300 mL/min > 250 mL/min > 350 mL/min.

D.2.4.2 Comparación del rendimiento catalítico de las diversas concentraciones de CO_2 a temperatura constante

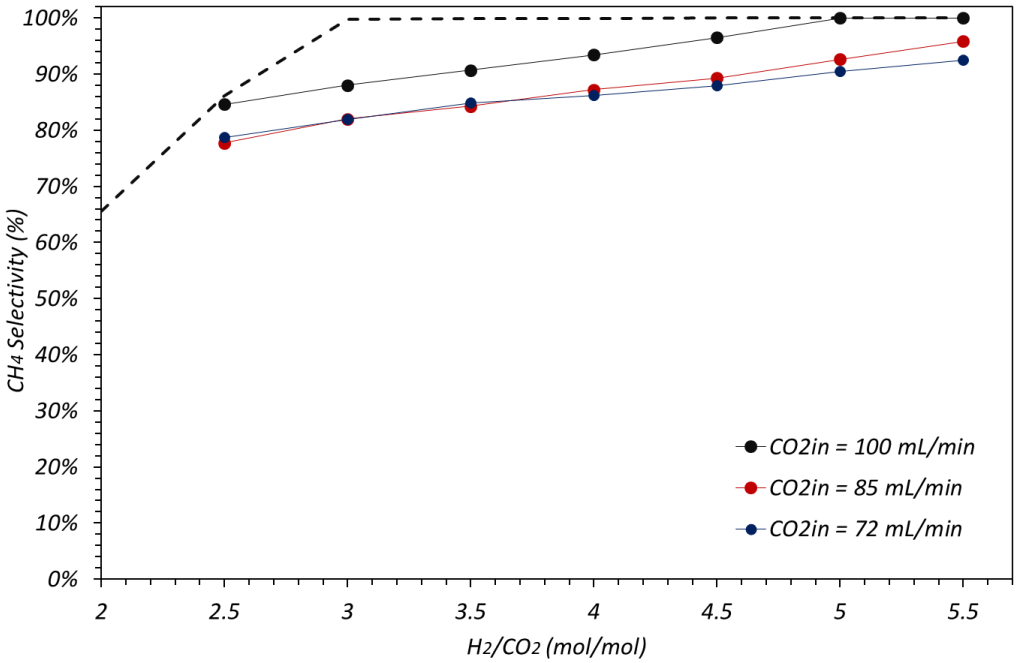

Figura 12. Rendimiento catalítico de diferentes concentraciones de CO_2 en función de la relación molar H_2/CO_2 a 325 °C.

La Figura 12 muestra el rendimiento catalítico de diferentes concentraciones de CO_2 a la entrada en función de la relación molar H_2/CO_2 a una temperatura constante de 325 °C; los valores de equilibrio también se informaron para comparación. En esta figura se puede observar un excelente rendimiento catalítico del catalizador Ni-MgCe/BC con la concentración de 100 mL/min de CO_2 en la alimentación. Vale la pena señalar que la selectividad del CH_4 deseado con la concentración de CO_2 en la alimentación como se menciona muestra una diferencia crucial en comparación con el resto, por lo que el equilibrio termodinámico se logró en una relación molar de 5 y también en una relación molar más baja de 2,5. Por lo tanto, el rendimiento catalítico óptimo alcanzado por este catalizador fue con 100 mL/min de concentración de CO_2 en la alimentación seguido de 85 mL/min y 72 mL/min.

D.2.4.3 Comparación del rendimiento catalítico de las diversas temperaturas de la reacción a concentración constante de H_2

Al mantener la concentración de gas H_2 en la alimentación, que es de 400 mL/min, en la Figura 13 se muestran los resultados del rendimiento catalítico realizado a diferentes temperaturas de reacción en función de la relación molar de H_2/CO_2. Las líneas discontinuas que representan los valores de equilibrio también reportados para comparación.

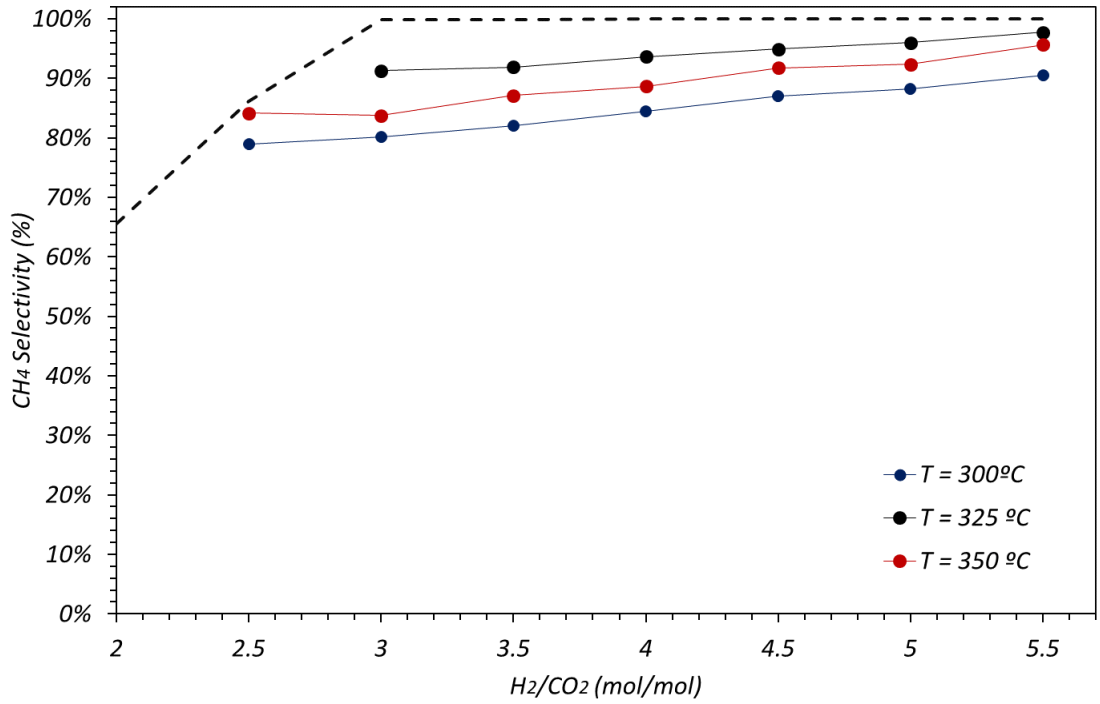

Figura 13. Rendimiento catalítico de diferentes temperaturas de la reacción en función de la relación molar H_2/CO_2 a 400 mL/min de H_2.

A la relación molar por debajo del valor estequiométrico, la conversión de CO_2 lograda a 300 °C, 325 °C y 350 °C fue aproximadamente la misma, sin embargo, por encima del valor estequiométrico, la mayor conversión de CO_2 obtenida fue de 325 °C. Para el caso de selectividad y rendimiento de CH_4, los valores experimentales más altos obtenidos también estaban a la temperatura de 325 °C. Por lo tanto, la mejor temperatura de reacción para la reacción de metanación fue de 325 °C seguido de 350 °C y 300 °C.

D.2.4.4 Comparación del rendimiento catalítico de las diversas temperaturas de la reacción a concentración constante de CO_2

La Figura 14 se muestra los resultados del rendimiento del catalizador llevado a cabo con la función de la relación molar de H_2/CO_2 a diferentes temperaturas de reacción. Las líneas discontinuas que representan los valores de equilibrio también informaron para comparación. La concentración del gas H_2 se varió con la relación molar correspondiente y la concentración de gas CO_2 en el gas de alimentación se mantuvo a 100 mL/min.

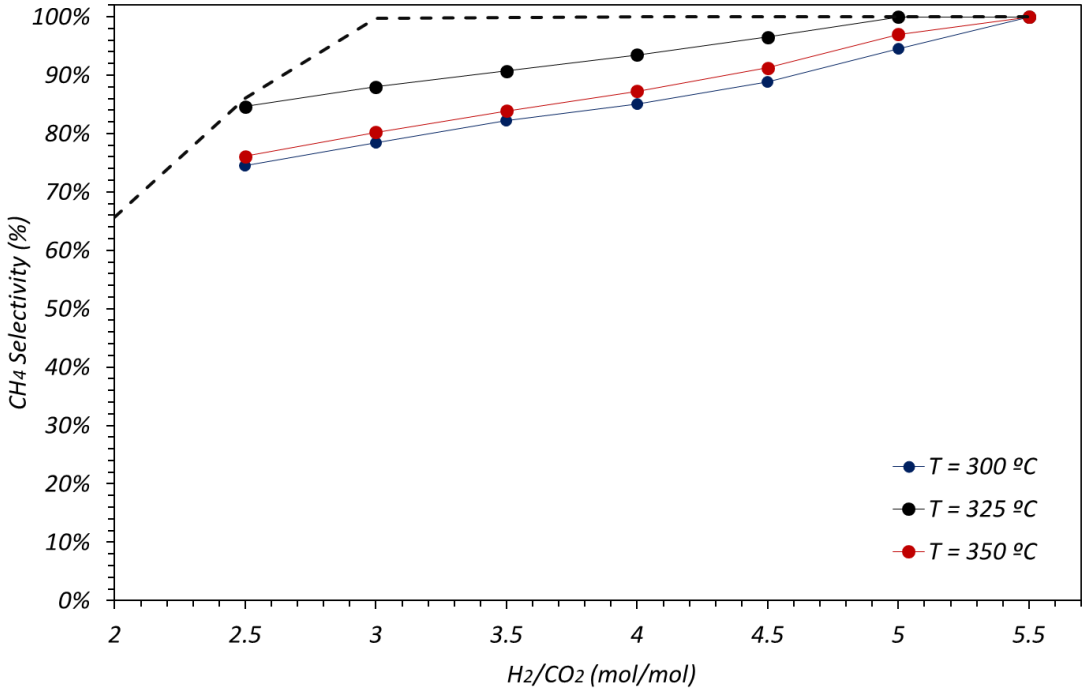

Figura 14. Rendimiento catalítico de diferentes temperaturas de la reacción en función de la relación molar H_2/CO_2 a 100 mL/min de CO_2.

Los resultados de la conversión experimental de CO_2 obtenida fueron similares con el experimento anterior, señalando que, a una relación molar más alta, el catalizador se realizó mejor a la temperatura de 325 ºC. Los valores más altos de conversión de H_2, selectividad y rendimiento del CH_4 deseado también se lograron a la temperatura de 325 ºC. Vale la pena mencionar que a la temperatura de 325 ºC, la selectividad de CH_4 se acercó al equilibrio en la relación molar de 5 y más tarde en la temperatura de 300 ºC y 350 ºC también se acercó al equilibrio, pero en la relación molar más alta de 5,5.

En este experimento y en el anterior (sección D.2.4.3), el catalizador Ni-MgCe/BC funciona mejor a la temperatura de 325 ºC. Vale la pena señalar que la prueba de estabilidad se ha llevado a cabo (sección D.2.3.1) en las mejores condiciones de operación durante 8h en la corriente (i.e. a temperatura de reacción 325 ºC y con la relación molar estequiométrica de H_2/CO_2).

D.3 CONCLUSIONES

La técnica de mineralización biomórfica es un método fácil y apropiado para preparar catalizadores basados en carbón biomórfico. El procedimiento de síntesis de catalizadores incluye una etapa de descomposición térmica en una atmósfera reductora de celulosa previamente impregnada con los precursores de nitratos metálicos.

Los resultados de caracterización indican que la adición del promotor Ce ha aumentado el área de superficie BET y la microporosidad de los catalizadores. Además, también aumentó la dispersión de partículas de Ni sobre la superficie de los catalizadores al disminuir el tamaño de cristalito del Ni. El porcentaje en peso de Ni, MgO y CeO_2 se incrementó en los catalizadores finales en comparación con la cantidad inicial en la celulosa cruda debido a la pérdida de material carbonoso durante la etapa de descomposición.

Los resultados de la caracterización muestran que el catalizador Ni-MgCe/BC tiene un área de superficie BET más grande y un alto volumen de microporos. Está demostrado en la reacción de metanación de CO_2, que este catalizador fue el más activo y selectivo a una temperatura de 350 ºC.

El catalizador Ni-MgCe/BC también muestra un gran rendimiento en la prueba de estabilidad. Después de 8h en la corriente a 325 ºC, la conversión de CO_2 y H_2, así como la selectividad y el rendimiento de CH_4 permanecieron constantes. Los resultados de la caracterización del catalizador después de la reacción han demostrado que la sinterización del catalizador se produjo en Ni-Mg/BC y Ni-Ce/BC; sin embargo, en Ni-MgCe/BC no se ha encontrado una sinterización significativa de partículas.

Debido al gran rendimiento alcanzado por Ni-MgCe/BC en la prueba de actividad catalítica y estabilidad, se realizó el estudio adicional sobre el efecto de diferentes composiciones de alimentación y temperatura de reacción en función de la relación molar H_2/CO_2. Los resultados indican que la temperatura de reacción óptima para producir CH_4 fue 325 ºC, donde la conversión y la selectividad fueron máximas. Por otro lado, la relación óptima H_2/CO_2 fue 4, confirmando los resultados encontrados en la bibliografía.

Finalmente, y como trabajo futuro, el amplio conjunto de datos cinéticos obtenidos en este trabajo, permitirá la propuesta y evaluación de modelos cinéticos rigurosos y el cálculo de los parámetros correspondientes.